Thesis

Bottom-up organisation of metallic nanoparticles for metamaterials applications

CUNNINGHAM, Alastair

Abstract

A study of the self-organisation of metallic nanoparticles into assemblies of interest to the metamaterials community has been conducted. Numerous colloidal nanochemistry techniques were developed to fabricate structures of interest. Spectroscopic techniques were then employed to probe the optical properties and evaluate to what extent they could be used to advance metamaterials research. In particular, large scale planar arrays of metallic nanoparticles fabricated on a variety of functionalised substrates such as glass, silicon and polymers, as well as analogues prepared on microscale spherical substrates were studied. Bottom-up techniques were employed to build up structures into the third dimension, one of the principal challenges currently facing metamaterials researchers and the suitability of the planar structures for SERS applications was investigated. A magnetic resonance, a key building block of a number of metamaterials applications was identified in the spherical structures and the potential of these structures as cloaking devices was studied.

Reference

CUNNINGHAM, Alastair. *Bottom-up organisation of metallic nanoparticles for metamaterials applications*. Thèse de doctorat : Univ. Genève, 2012, no. Sc. 4501

URN : urn:nbn:ch:unige-255797
DOI : 10.13097/archive-ouverte/unige:25579

UNIVERSITÉ DE GENÈVE
FACULTÉ DES SCIENCES

Section de chimie et biochimie
Département de chimie physique

Professeur T. Bürgi

Bottom-up Organisation of Metallic Nanoparticles for Metamaterials Applications

THÈSE

présentée à la Faculté des sciences de l'Université de Genève
pour obtenir le grade de Docteur ès sciences, mention chimie

par

Alastair CUNNINGHAM

de

Glasgow (Écosse)

Thèse N^{o} 4501

GENÈVE

Centre d'impression de l'Université de Genève

2012

UNIVERSITÉ
DE GENÈVE

FACULTÉ DES SCIENCES

Doctorat ès sciences
Mention chimie

Thèse de *Monsieur Alastair CUNNINGHAM*

intitulée :

" Bottom-up Organisation of Metallic Nanoparticles for Metamaterials Applications "

La Faculté des sciences, sur le préavis de Messieurs T. BÜRGI, professeur ordinaire et directeur de thèse (Département de chimie physique), S. STOLL, docteur (Institut F.-A. Forel), P. BAROIS, professeur (Centre de recherche Paul Pascal, Université de Bordeaux, France), autorise l'impression de la présente thèse, sans exprimer d'opinion sur les propositions qui y sont énoncées.

Genève, le 13 décembre 2012

Thèse - 4501 -

Le Doyen, Jean-Marc TRISCONE

N.B. - La thèse doit porter la déclaration précédente et remplir les conditions énumérées dans les "Informations relatives aux thèses de doctorat à l'Université de Genève".

Contents

Curriculum vitae

Rue Cherbuliez 5
Geneva 1207
Switzerland

Date of Birth: 30th December 1982
Nationality: Scottish

Phone: +41 762252553
E-mail: alastair.cunningham@hotmail.co.uk

LANGUAGES

English – mother tongue, French – fluent, German - basic

EDUCATION

Doctoral studies

2010 – Present **University of Geneva**, Department of Physical Chemistry
&
2009 - 2010 **University of Heidelberg**, Physical Chemistry Institute

- Functionalisation and organisation of plasmonic nanoparticles.
- Publication of a book chapter and papers in high impact factor journals.
- Oral and poster presentations at several international conferences.
- Collaboration with a variety of groups of differing disciplines.
- Supervision of numerous Masters and Bachelors student projects.
- Tutorial assistant for undergraduate chemistry lectures.

MSc in Micro and Nanotechnology

2007 - 2008 **University of Neuchâtel**, Institute of Microtechnology

- Specialised in Molecular Sciences, grade average of 5.73 / 6.
- Research projects: photovoltaic cell optimisation; organisation of metallic nanoparticles in liquid crystal and polymer systems.

MSci Chemistry

2000 - 2005 **University of Strathclyde**, Department of Pure and Applied Chemistry

- MSci Chemistry (hons) 2:2
- Masters research project based on an investigation into the optical and electrochemical properties of gold nanowire arrays.
- Class representative on the staff-student council.

PROFESSIONAL EXPERIENCE

2008 **Summer Internship** in Nanosciences Laboratory, University of Neuchâtel

- Development of high thermal conductivity nanofluids to be used in next generation cooling systems.
- Insight into academic and industrial collaborations gained.

2005 - 2007 **Chemical Analyst**, Chivas Brothers Ltd.

- Quality control of distillery products and process development.
- Gained familiarity with a wide range of chemical analytical techniques.
- Achieved grade B pass in industry standard exam.
- Worked to strict deadlines for both internal and external customers.

2003 - 2004 **Industrial Placement**, Merck Chemicals Ltd.

- Worked as part of a multi-disciplinary team on the appliance of liquid-crystal systems in optical devices.
- Gained experience and insight into the research and business practices of a large company

PUBLICATION LIST

Double active control of the plasmonic resonance of a gold nanoparticle array
Luciano De Sio, Alastair Cunningham, Vanessa Verrina, Caterina Maria Tone, Roberto Caputo, Thomas Bürgi and Cesare Umeton *Nanoscale*, **2012**, DOI:10.1039/c2nr31426f

Exciting Bright and Dark Eigenmodes in Strongly Coupled Asymmetric Metallic Nanoparticle Arrays.
Alastair Cunningham, Stefan Mühlig, Carsten Rockstuhl, and Thomas Bürgi *J. Phys. Chem. C*, **2012**, 116, 17752

Self-Assembled Plasmonic Core–Shell Clusters with an Isotropic Magnetic Dipole Response in the Visible Range.
Stefan Mühlig, Alastair Cunningham, Sebastian Scheeler, Claudia Pacholski, Thomas Bürgi, Carsten Rockstuhl, and Falk Lederer *ACS Nano*, **2011**, 5, *6586*

Coupling of Plasmon Resonances in Tunable Layered Arrays of Gold Nanoparticles.
Alastair Cunningham, Stefan Mühlig, Carsten Rockstuhl, and Thomas Bürgi *J. Phys. Chem. C*, **2011**, 115, *8955*

Pigments based on silica-coated gold nanorods: Synthesis, colouring strength, functionalisation, extrusion, thermal stability and colour evolution.
Cyrille Gautier, Alastair Cunningham, Lynda Si-Ahmed, Gilles Robert and Thomas Bürgi *Gold Bulletin* **2010**, 43, *94*

REFEREES

Prof. Thomas Bürgi (PhD supervisor)
Professor in Physical Chemistry
University of Geneva
Phone: +41 223796552
E-mail: thomas.buergi@unige.ch

Dr. Toralf Scharf (PhD project coordinator)
Lecturer
École Polytechnique Fédérale de Lausanne
Phone: +41 327183286
E-mail: toralf.scharf@epfl.ch

Prof. Iain McCulloch (Supervisor at Merck)
Chair in Polymer Materials
Imperial College London
Phone: +44 2075945669
E-mail: i.mcculloch@imperial.ac.uk

Keywords

Bottom-up, self-organisation, plasmonics, metamaterials, metallic nanoparticles, optical properties, polyelectrolytes, layer-by-layer, electromagnetic coupling, substrate functionalisation, electrostatic assembly, large scale nanoparticle arrays, core-shell nanoclusters

List of Acronyms

AFM – Atomic force microscopy

BD – Ballistic deposition

CTAB - cetyltrimethylammonium bromide

EBL – Electron beam lithography

EDL – electrostatic double layer

GISAXS – Grazing incidence small angle X-ray scattering

ITO – Indium tin oxide

LSPR – Localised surface plasmon resonance

PAA – Poly(acrylic acid)

PAH – Poly(allylamine hydrochloride)

PDMS – Poly(dimethylsiloxane)

PE – Polyelectrolyte

PEG – Poly(ethylene glycol)

PSS – Poly(4-sodium styrene sulfonate)

RCF – Relative centrifugal force

RSA – Random sequential adsorption

SEM – Scanning electron microscopy

SERS – Surface enhanced Raman scattering

SNOM – Scanning near-field optical microscopy

SRR – Split ring resonator

TEM – Transmission electron microscopy

Abstract

A study of the self-organisation of metallic nanoparticles into assemblies of interest to the metamaterials community has been conducted. A variety of colloidal nanochemistry techniques were developed to fabricate structures proposed by theoreticians working in the field. Spectroscopic techniques were then employed to fully probe the optical properties of these structures and evaluate the extent to which they could be used to advance metamaterials research.

Large scale planar arrays of metallic nanoparticles were fabricated on a variety of functionalised substrates such as glass, silicon, polymers and transparent conducting oxides, using electrostatic interactions. Several means to control the overall filling fraction were also investigated. Arrays encapsulating a variety of densities, from extremely isolated nanoparticles through to closely packed structures approaching monolayers, were successfully fabricated.

The construction of three-dimensional structures, one of the principal challenges faced by researchers attempting to fabricate metamaterials through more conventional top-down techniques, was then achieved. The deposition concepts referred to above were combined with the layer-by-layer deposition of charged polymer layers to build up multiple arrays of metallic nanoparticles. The distances between arrays could be accurately tuned, with almost nanometre precision, allowing the magnitude of the electromagnetic coupling, and therefore the optical properties, between separate arrays to be controlled. Only limitations of a practical nature restrict the overall number of metallic nanoparticle arrays and their relative separations. Several parameters, including array separation and nanoparticle size, were investigated using this system.

A similar structure was also used to probe asymmetric coupling between gold and silver nanoparticle arrays. The optical properties of these structures were studied as a function of both the angle of incidence of the probing beam and, again using polyelectrolytes, array separation.

Investigations with a view to applying these structures as potential surface enhanced Raman scattering (SERS) substrates were also conducted. The principal mechanism resulting in signal enhancement in SERS originates from the intense electric fields which can be applied to analyte molecules. These ‘hotspots’ exist between nanoparticles and as such the stratified arrays of metallic nanoparticles with tunable separation distances appear to be the perfect system on which to probe these properties.

Studies of nanoparticle structures were not limited to nanospheres. The unique properties of metallic nanorods, which exhibit two plasmon resonances, one corresponding to the oscillation of

electrons along the length of the rod with the other describing the oscillation of electrons across the width of the rod, were also investigated. Coupled pairs of nanorods have been shown to exhibit magnetic resonances and as such deposition and reorganisation techniques were developed to fabricate such structures.

The importance of magnetic resonances to the field of metamaterials also led to research on core-shell nanoclusters. Prepared in an analogous fashion to the planar arrays described above, this research was motivated by several theoretical papers outlining the magnetic dipole moment that such spherical organisations of metallic nanoparticles should exhibit and the importance of this in preparing negative refractive index materials. These assemblies were fabricated both in solution and as large scale arrays on suitably functionalised substrates and were also investigated for their potential cloaking properties.

In conclusion, a variety of techniques have been developed that enable the organisation of metallic nanoparticles into structures of interest to the field of metamaterials. These structures have undergone in-depth characterisation and the relevance of their properties to a diverse range of applications has been highlighted.

Résumé en français

Cette thèse est consacrée à la fabrication de métamatériaux optiques par auto-assemblage de nanoparticules métalliques. Différentes techniques de nano chimie colloïdale ont été mise en œuvre afin de réaliser plusieurs structures choisies pour leur propriétés optiques spécifiques dans le cadre d'une collaboration avec une équipe de théoriciens travaillant dans le domaine des métamatériaux. Leurs propriétés optiques ont été caractérisées par spectroscopie UV-Visible et confrontées à des résultats théoriques pour évaluer leur potentiel dans le champ des métamatériaux.

Dans un premier temps, des monocouches de nanoparticules ont été déposés par adsorption électrostatique sur divers substrats (verre, silicium, polymères et oxydes transparents conducteurs) après modification de leur chimie de surface. Plusieurs méthodes ont été développées pour contrôler la densité de nanoparticules de ces couches et une série d'échantillons allant de nanoparticules extrêmement isolées jusqu'à une monocouche presque complète a été réalisée.

La fabrication de métamatériaux massifs (i.e. tridimensionnelles) reste l'un des défis actuels les plus importants, la plupart des réalisations actuels ayant été fabriquées grâce des approches descendantes. Pour résoudre ce problème, les techniques de dépositions exposées brièvement au-dessus ont été combinées avec la technique de déposition « couche par couche » (Layer-by-Layer) de polyélectrolytes permettant de réaliser un empilement de monocouches de nanoparticules. Cette méthode offre la possibilité de contrôler la distance entre deux couches successives avec une précision de l'ordre du nanomètre, ce qui nous a permis d'étudier précisément l'influence du couplage électromagnétique entre couches de nanoparticules adjacentes sur les propriétés optiques de ces multicouches. D'autres paramètres tels que la taille ou la composition des nanoparticules ont également été étudiés.

Concernant ce dernier point, des structure bicouches alternant nanoparticules d'or et nanoparticules d'argent ont été réalisés afin d'étudier le phénomène de couplage asymétrique entre résonances plasmons de ces deux types de nanoparticules. Les propriétés optiques de ces échantillons ont été mesurées en fonction de l'angle d'incidence d'illumination et de la séparation entre nanoparticules en utilisant les polyélectrolytes comme précédemment

Des études ont également été menées concernant l'utilisation de ces structures comme substrats pour la spectroscopie Raman. L'excitation des résonances plasmon dans ces systèmes s'accompagne d'une importante exaltation du champ optique, fortement localisée dans l'espace séparant deux nanoparticules adjacentes. Ces points chauds (« hot spots ») permettent d'exalter considérablement

l'activité Raman de molécules localisées dans ces régions rendant cette technique d'analyse, généralement peu efficace particulièrement sensible. La possibilité de varier la séparation des nanoparticules, leur composition et leur taille en employant la méthode de déposition décrite précédemment nous a permis d'étudier de manière approfondie l'influence de ces différents paramètres sur le phénomène d'exaltation Raman.

Outre les nanoparticules sphériques, les propriétés particulières des nanobâtonnets d'or qui possèdent deux bandes plasmoniques distinctes ont aussi été examinées. En particulier, nous avons examiné la possibilité de fabriquer des paires de nanobâtonnets selon les même méthodes d'auto-assemblage. Ce type d'arrangement a un intérêt tout particulier pour la réalisation de métamatériaux, plusieurs études ayant démontré leur capacité à supporter des résonances magnétiques aux fréquences optiques. De telles résonances constituent un ingrédient essentiel pour l'obtention d'un indice de réfraction négatif, objectif phare de la recherche dans ce domaine.

L'importance de telles résonances nous a également conduits à étudier un autre type d'arrangement dans lequel les nanoparticules sont organisées selon une géométrie sphérique. Différents travaux théoriques ont montré que, de manière analogue aux paires de nanobâtonnets, le couplage entre nanoparticules sphériques organisées selon cette géométrie conduit à l'émergence d'une activité magnétique importante. Pour obtenir un tel arrangement, nous avons employé la même technique de fonctionnalisation de surface en remplaçant les substrats plats par des substrats sphériques, en l'occurrence des nanospheres de silice. L'étude de leurs propriétés optiques a confirmé l'existence des résonances magnétiques mentionnée précédemment. En collaboration avec des théoriciens nous avons également évalué le potentiel des structures pour des applications de camouflage.

En conclusion un nombre de techniques ont été développés qui permettent l'organisation de nanoparticules métalliques dans les structures d'intérêt dans le domaine des métamatériaux. Ces structures ont subi une caractérisation détaillée et leur rapport à une gamme diverse d'applications a été mise en valeur.

1. Introduction[1]

The work that forms the bulk of this thesis was carried out as part of the Nanogold project – a Framework Programme 7 project funded by the European Commission. The project was extremely interdisciplinary in nature and comprised eight partner groups located throughout Europe, specialising in theory, fabrication and characterisation. The stated aim of the project was the fabrication and application of bulk electromagnetic metamaterials using bottom-up techniques and combined inorganic chemistry, organic macromolecular synthesis, the physics of electromagnetic resonances and liquid crystal technology in order to achieve this. The principal strategy used to accomplish this goal was the self-organisation of, as the title of the project suggests, nanoscale units composed of noble metals such as gold. By embedding and organising small resonant particles in dielectric materials it is possible to obtain materials with unprecedented properties that operate in the correct spectral domain for photonic applications.

The field of metamaterials is, despite incorporating relatively novel concepts, extremely varied. At related congresses it is not uncommon to meet researchers from the disparate worlds of theoretical physics, materials science, organic chemistry, optics, electrical engineering and mechanics and it was as a result of this that the collaborative nature of the project came to the fore. The research conducted for this thesis essentially involved the fabrication and experimental characterisation of structures that were based upon designs proposed by theoreticians working in the field. The areas of research are extremely diverse and as a result the science underpinning this research incorporates a wide variety of concepts which in turn lead to a number of questions. Firstly, and fundamentally, what are metamaterials and why should we be trying to produce them? What structures are capable of producing these unprecedented electromagnetic effects and last but not least, why choose bottom-up methods and nanomaterials to fabricate them? These are questions which will be addressed in this introduction before the specific structures and systems that have been studied are described in more detail.

1.1. What are metamaterials?

The term metamaterial, with the prefix taken from Greek and meaning literally “beyond”, first appeared in literature around the beginning of the century with an early example being in the seminal paper published by Smith et al. which discussed a composite medium with simultaneously

[1] Some passages in this section will be published in the chapter entitled ‘Bottom-up organisation of metallic nanoparticles’ written by Alastair Cunningham and Thomas Bürgi contained in the book ‘Amorphous Nanophotonics’. Edited by Carsten Rockstuhl and Toralf Scharf, the book will be published in 2013 by Springer-Verlag Berlin and Heidelberg GmbH & Co. KG.

negative permeability and permittivity in the microwave range of the electromagnetic spectrum.[1] While the literal definition of the term conjures up vague ideas of properties "beyond" those of normal materials a scientific definition that is universally accepted is harder to pin down. The term is often loosely used to describe materials which possess electromagnetic properties which do not exist in nature. As well as being unclear this has been shown to be untrue. Initially, the term metamaterials was used almost interchangeably with negative refractive index materials[2] as, following on from the work of Smith et al.,[1] this was the major focal point of the research conducted. However, it has since been found that certain natural materials, for example the compound eyes of some lobsters,[3] are able to negatively refract light. In addition, and while this point may be slightly pedantic, it seems somewhat premature to state that certain properties do not exist in nature when there are an abundance of natural materials that are, as yet, unknown to man. The field of metamaterials has exploded since these earlier days and research is no longer focussed solely on producing negative index materials. Cloaking[4] and perfect lensing[5] have become equally important motivating goals, providing three 'Holy Grails' for researchers to pursue. In the intervening period journals dedicated to the topic have come into existence, several monographs[6, 7, 8] have been written and novel pieces of research, which even a decade ago could have been dismissed as science fiction rather than science fact, have surfaced in the popular media.[9] As they become increasingly important within scientific communities and even begin to invade everyday parlance it is necessary to classify exactly what constitutes a metamaterial.

It is generally accepted that metamaterials are artificial structures whose properties depend not only on their composition, as tends to be the case with conventional materials, but also on the organisation of the constituent parts within the structure. Usually, metamaterials are composite structures, constructed from resonant units, also known as metaatoms and typically composed of metals and dielectrics, although some approaches have used other materials such as graphene.[10] While each component element maintains its individual properties it is the properties of the ensemble that are of interest. Whilst the properties of metamaterials are dependent on the organisation of the metaatoms contained within it is not mandatory that they have a periodic structure. Indeed, in many cases amorphous arrangements are often thought of as being highly desirable as they do not pose any problems in terms of spatial dispersion and anisotropy. By definition, the optical response of an amorphous arrangement of metaatoms will be independent of the direction of propagation of light – an obvious advantage for a variety of applications. These properties emerge upon interaction with electromagnetic radiation only when the structural units within the material, as well as their separation, are significantly smaller than the wavelength of the incident radiation – also known as the electrostatic limit. That the inhomogeneity scale is

considerably less than the wavelength of operation serves to separate metamaterials from other artificial structures such as photonic crystals,[11] whose unit cells tend to be on a similar scale to the wavelength of visible light and therefore their optical response is dominated by interference and diffraction. It also sheds light on why the study and use of metamaterials is of interest to such a wide variety of disciplines.

The fact that such a broad range of the electromagnetic spectrum is used by mankind, from radio waves with wavelengths of several hundred metres all the way down to gamma radiation with wavelengths less than the diameter of an atom shows that metamaterials could be applied at a huge variety of scales which necessitate an equally large variety of skills and experience. Taking the relative scale of the inhomogeneities in materials and their interaction with incident electromagnetic fields to be one part of the definition of metamaterials, it can readily be seen that, in all but name, they have been used for several decades in the field of microwave engineering.[6] This only serves to highlight that when discussing metamaterials there are multiple facets that should be considered when seeking to construct an all inclusive definition. Indeed, using the above stipulations as a starting point it could be considered that one of the first metamaterials fabricated was the oft-cited Lycurgus Cup,[12] a Roman cup that dates from the 4th century A.D. and which shows differing optical properties in reflection and in transmission. The properties derive from colloidal dispersions of gold and silver nanoparticles embedded in the glass which are around ten times smaller than the wavelength of light in the optical regime. A more modern example of what could still technically be termed as a metamaterial would be the metallic plate containing an array of holes that is found on the door of all microwave ovens. The holes which are comparatively large when considering the wavelength of visible light make it possible to see inside the oven but are much smaller that the wavelength of the microwave radiation ($\sim$12 cm) used to heat the contents of the chamber and cannot, therefore, penetrate the plate.

That the active inclusions in metamaterials and their spatial organisation are much smaller than the wavelength of the electromagnetic radiation in question means that it is not able to probe any differences between, for example, a dielectric host and a metallic guest. The incident radiation 'sees' a homogeneous material that can be described using effective material parameters and described using approximations such as Bruggeman[6, 13] or Maxwell Garnett[14] theory. While producing architectures that possess unusual or advantageous properties for use in the radio wave regime may pose problems of an engineering nature, it can readily be seen that as the wavelength is reduced through the microwave and infrared regions and down into the visible the fabrication of these structures is fraught with ever increasing challenges of both a technical and scientific nature. As

many of the intriguing effects that have been proposed are most interesting, for obvious reasons, at optical frequencies, novel fabrication solutions should be sought in order to produce structures of ever decreasing size whilst maintaining the ability to achieve well defined geometrical parameters. A succinct overview of the advancements made in pushing metamaterials properties into the visible region through a combination of innovative structure design and down-scaling can be found in Reference 15. Although top-down techniques have made massive inroads into the down-sizing of structures, particularly in the domain of informatics, self-assembly fabrication methods open up a wealth of possibilities that would be otherwise unachievable. The potential contribution that metallic nanoparticle structures fabricated by bottom-up techniques have to make to this field is considerable and is only beginning to be tapped. This potential will be outlined in more detail in the following section.

1.2. Why bottom-up?

The term 'nanotechnology' was first coined in 1974[16] and since then the drive to produce structures of increasingly small dimensions and explore their unique properties has not abated. There are few aspects of modern life that do not rely on, at least in some part, the scientific breakthroughs in fabricating smaller structures that have been made in the last few decades, with nanotechnology now pervading our lives to an extent that very few, with some notable exceptions,[17] could have predicted. As well as being applied to metamaterials, the advances in down-scaling that have been made have been exploited in a wide range of disciplines, and have played a prominent role in the fields of information technology,[18] renewable energy generation[19] and medicine and health care.[20] In general, the approaches to fabricate these structures can largely be divided into two categories; top-down and bottom-up techniques.[21] The fast rate of down-scaling achieved over the last few decades, in some cases advancing at almost exponential rates, can largely be attributed to the top-down techniques, loosely defined as being the fabrication of structures from larger precursors. This can be thought of as being more of a sculpting approach, with typical examples of top-down technologies including lithographic methods, the most technologically advanced of which is arguably electron beam lithography (EBL),[22] and etching methods, which can vary from wet-chemical etches[23] to focused ion beam[24] and laser ablation.[25] While there is still an important role to be played by top-down methods, there are inherent limitations associated and these, if they have not been already, are on the verge of being reached. One notable drawback is the minimum feature sizes that are accessible using such techniques. In addition, such techniques tend to be cumbersome and slow, requiring prohibitively expensive equipment to produce small scale and, often uniquely, two-dimensional structures. This can cause particular problems in the fabrication of metamaterials

where, alongside the downscaling of structures, one of the major challenges currently facing the metamaterials community is the production of truly 3D materials allowing bulk material parameters to be assigned and eventually their incorporation into real devices. None of these disadvantages, on the other hand, are suffered by the more novel and versatile bottom-up techniques which are increasingly being applied to produce structures of even smaller scale and more complex architecture than has previously been achievable. As the name suggests, the bottom-up approach involves the fabrication of structures from smaller units, using the properties that they possess to induce their self-assembly in the desired manner. This building block approach to materials synthesis, often likened to the construction of objects with Lego, is still in its nascent stage and only the surface of what is potentially accomplishable has been scratched.

Evidence for the power and efficacy of these techniques can be gathered through the observation of nature, which is also seen to follow a bottom-up approach. The organisation of molecules to form progressively larger structures, from cells and DNA up to, and including, metre scale biological organisms, in a hierarchical manner show the effectiveness that such approaches can provide. Indeed the entire field of biomimetics seeks to take advantage of structures found in nature which have evolved over a long period of time and, as the name suggests, use them as models or blue-prints which can then be reproduced using innovative chemical methods. Biomimetics also introduces another interesting aspect of structure fabrication. In general, for useful functional structures, for example metamaterials, to be fabricated a degree of organisation must be available at two discrete levels; both at the nanoscale and at the mesoscale. After the initial self-assembly step which results in the formation of a unit, or in the particular case of metamaterials a metaatom, it is then typically necessary to induce, chemically or otherwise, the organisation of these units into an ordered structure which can then be used in applications. A whole host of techniques exist in the ever expanding toolkit of the materials scientist that permits both the fabrication of nanoscale materials and their organisation into larger scale architectures in a controlled manner. An exhaustive list of these is, due to the inter-disciplinary and fast-moving nature of the field, extremely difficult to produce and even more difficult to discuss in great detail. However an effort will be made in Section 2.2.5 to provide an introduction to some of the more important bottom-up methods, with particular attention being paid to the organisation and application of metallic nanoparticle structures. These methods could be, and in some cases are already being, applied to fabricate bulk metamaterials at optical frequencies.

1.3.What structures can give metamaterials properties?

Metamaterials were defined in Section 1.1 as being composite artificial materials that have unusual or advantageous electromagnetic properties which; (i) derive largely from the organisation of ensembles of resonant units embedded in dielectric matrices; (ii) exist in a wavelength range that is considerably larger than the size and separation of these metaatoms; (iii) and are not readily observed in nature. This definition could remain, however, somewhat vague to people who have little or no experience in the field and it would be instructive to introduce several of the structures that researchers target in order to achieve particular electromagnetic effects. Some of these architectures are shown in Figure 1 and will be described in more detail in this section.

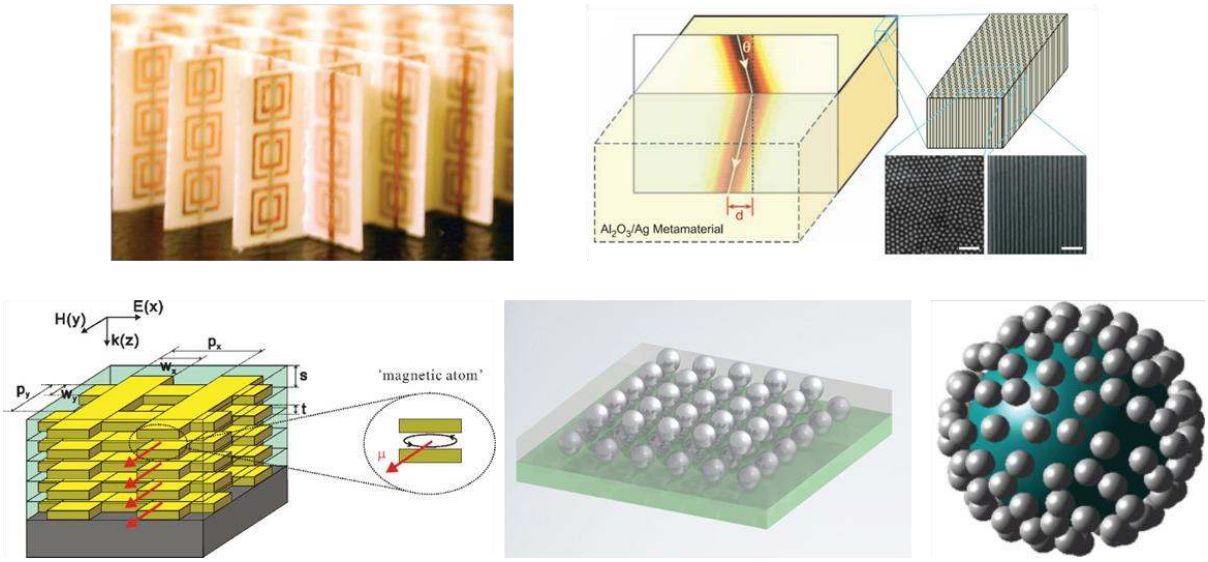

Figure 1 – Examples of metamaterials structures. Clockwise from top left; an array of split ring resonators that exhibit negative refractive indices in the microwave regime;[2] regular arrays of cylindrical metallic structures which have been shown to exhibit optical negative refraction;[26] a core-shell nanocluster that has potential applications as a cloaking device;[27] layered arrays of metallic nanoparticles which have been proposed as facilitating sub-wavelength imaging;[28] and a layered fishnet structure highlighting the magnetic moments (red arrows) associated with the 'magnetic atoms' contained within the structure.[29]

Initial experimental work, developed around the turn of the century by Smith[1, 2] and Pendry,[30] was centred on arrays of split ring resonators (SRRs) - two broken concentric rings rotated in-plane 180° with respect to one another and one of the first structures to bear the name 'metamaterial'. Essentially, the structure is the equivalent of a small capacitor with a specified capacitance and inductance. When embedded in a suitable host, it was proven that both the permittivity and permeability, and therefore the refractive index, of these structures, in some frequency domains at least, can be simultaneously negative. Negative refractive indices had never previously been

observed despite being first proposed several decades previously by Veselago.[31] In addition, the precise optical properties of ensembles of SRRs can be tuned by altering the relative organisation and orientation of the individual structures.[32]

At the outset this work was conducted in the microwave regime, the unit cells being on the order of 5 mm – several times smaller than the wavelength of the incident radiation. Since then technological advances have permitted arrays of smaller SRRs to be produced which allow similar effects to be measured down into the infra-red.[33] However, as outlined in Section 1.2 it becomes extremely challenging to fabricate three dimensional structures, which would be required, for example, to create a prism with which to measure negative refraction, using top-down techniques. In addition, complicated forms such as the SRR are currently outwith the capabilities of colloidal nanochemistry which is generally used to produce the metaatoms used in bottom-up fabricated metamaterials.

Despite this there are alternative structures, not entirely dissimilar to the SRR, which also induce magnetic dipole moments. It can be shown using plasmon hybridisation schemes that when two metallic nanorods approach they couple with one another – the plasmonic modes mixing and splitting into hybridised resonances (for more details see Section 2.2.4). The antisymmetric mode of coupled metallic nanorod pairs in the transverse configuration gives a magnetic response - one of the fundamental building blocks of metamaterials - and provides researchers with a metaatom which is conceivably accessible using bottom-up techniques.[32] This becomes evident when, considering advances in colloidal preparative techniques, it can be seen that metallic nanorods can be readily prepared with a variety of materials and dimensions in a controlled fashion.[34] Several studies, using both top-down[35, 36] and bottom-up[26] fabrication techniques have investigated such systems with a view to producing negative index materials. On the other hand, while some research has been carried out examining the coupling properties between dimers of nanorods produced by colloidal methods[37] very few studies exist where the full potential to construct bulk materials with effective properties using these methods has been tapped.

The concept of using nanorod pairs to induce magnetic resonances was further developed and several studies now exist based on what is known as the ‘fishnet’ structure.[29] As with the work conducted on SRRs, fishnet structures, which are essentially layered structures of metallic wires of differing thickness that intersect at right angles, have undergone a downscaling process which has gradually allowed the effects that they display to be pushed into smaller and smaller wavelength regimes. This design has facilitated higher figures of merit than could previously be achieved using the double wire system[38] The cross-linked structure provides the necessary double wire pairs as part of a large scale array while at the same time consisting of long wires, thus giving rise to the negative

values of permeability and permittivity respectively. In addition there are many geometrical material parameters that can be tuned to give the most efficient structures. As with the SRRs, prisms can be fashioned from these structures and negative refractive indices observed in the optical regime.[39, 40] Despite the advantages afforded by this structure fishnet metamaterials are outwith current bottom-up capabilities and are limited by lithographic technologies.

However, several other structures that incorporate resonant units into dielectric hosts are also accessible using bottom-up colloidal methods. One example, of particular interest to the metamaterials community, are spherical arrangements constructed from smaller plasmonic particles. Several studies, both of a theoretical and experimental nature, have shown that such architectures could be used in, amongst other things, cloaking devices[27] and double negative materials.[41] So called meta-metamaterials, that is spherical arrangements of metallic nanoparticles which have themselves been organised into a three-dimensional bulk material, have been shown to exhibit negative effective permeability in the visible domain.[42] Similarly, other purely theoretical papers discuss spherical arrangements of nanoparticles such as core-shell nanoclusters which were shown to also display artificial resonant magnetism.[41, 43] In addition, they offer an easier route to metamaterials from the perspective of fabrication. It has also been shown that the scattering response of a dielectric sphere at the centre of a core-shell nanocluster can, at least to some extent, be cancelled by a shell of nanoparticles which scatter the incident electric field 180° out of phase relative to the core.[27] While not providing 100% invisibility this could prove to be a first step towards this target and demonstrates why these structures are currently of such interest.

It has also been thought that several practical metamaterials applications could arise from lamellar structures, alternating between arrays of 'active' inclusions and dielectric spacers. Several methods already exist, using for example block copolymers[44] or polyelectrolytes (PEs),[45] that allow structures such as these to be fabricated and allow several material parameters, including particle filling fractions and layer thicknesses to be controlled with a high degree of precision. This in turn allows the optical properties to be tuned for particular applications. Theoretical studies have proposed that stratified structures of metals and dielectrics could be used for sub-wavelength imaging at optical frequencies.[28] Similar principles have also been used to experimentally demonstrate this effect, again in the optical regime.[46] Here, alternating layers of metal and dielectric were organised in a cylindrical fashion to achieve sub-diffraction limit imaging, or hyperlensing. This can be accomplished by the metamaterial which is capable of recovering the evanescent waves that are lost in the far-field – this being the cause of the diffraction limit of light.[46] The colours in objects as diverse as butterfly wings, peacock feathers and gemstones originate from the same mechanism – Bragg

reflection – and it is possible to mimic this mechanism through the production of stratified arrays of small particles.[47] By combining these structures with metallic nanoparticles to give plasmonic-photonic hybrid materials adds an extra degree of complexity that allows optical properties, such as the position and strength of reflection peaks, to be further tuned.[48]

Periodic arrays of metallic nanowires have also proved to possess several advantages over other materials that negatively refract light.[26] Here, silver nanowires were electrodeposited in a porous alumina array resulting in a truly bulk metamaterial that has been shown to negatively refract a broad range of optical frequencies with relatively low losses. Additionally, negative refraction is not confined, as it is in some other materials, to two dimensions and occurs for all angles of incidence. A somewhat similar structure – linear chains of metallic nanoparticles – has also been proposed in the literature as being capable of superlensing.[49] Architectures such as this could be accessible using bottom-up strategies[50] and would open up one possible route to sub-wavelength imaging.

This section has sought to provide a brief overview of some of the principal structures that are currently used to generate interesting electromagnetic properties. Of course, many other structures are used for specific applications and several variations and combinations of those introduced also allow a high degree of flexibility in terms of tuning the optical properties of the end product. The developments illustrated in this section also highlight the importance of collaboration in this field. Advancements in theory and computing power now allow material properties to be successfully predicted before they have been fabricated and some of the major theoretical principles that underpin the interaction of light with matter, with a particular focus on metamaterials, will be made in Section 2.1.1. By working in tandem, a feedback loop can be set up between theoreticians and materials scientists, allowing a balance to be struck between what is desirable from a theoretical point of view and what is technologically possible. One of the several advantages offered by this design process is that problems can be identified and potentially ironed out at an early stage and greater understanding of the structures involved can be attained.

2. Theory[2]

2.1.Metamaterials

At a basic level, the properties of metamaterials can be reduced to, essentially, the interaction of light and matter - something that most of us take for granted in our everyday lives. Despite the field of metamaterials coming to the fore relatively recently, the interaction of light and matter has been studied and understood for well over a century. James Clerk Maxwell pioneered work in this area, describing for the first time the electromagnetic field in what is sometimes known as the second great unification of physics. The famous equations, for which Maxwell is perhaps best remembered, are equally as valid now as they were when first published in 1865 and form the basis of what modern day theoreticians use to predict and design the properties of metamaterials.[51] Full descriptions of the Maxwell equations and their derivations can be found in most physics textbooks however for a more instructive understanding of the reasons why metamaterials possess the extraordinary properties they do it is worthwhile to look at some of the material parameters that appear in the equations in slightly more detail.

2.1.1. Interaction of light and matter

Metamaterials that exhibit negative refraction were discussed at length in the Introduction but what is actually meant by this term? Put simply, the refractive index of a material is the ratio of the speed of light in a vacuum to the speed of light in the material. At the interface, going from a medium of lower refractive index to one of higher refractive index, the incident beam will 'bend' towards the normal according to Snell's Law. This is what causes the perceived location of, for example, a fish in a pond to be closer to the surface of the water than it actually is. The refractive index of a material is dependent on the wavelength of the incident light and this dispersion is what allows us to see the colours of a rainbow when light is reflected from the back of raindrops. In some cases it is perhaps more informative to describe refractive indices in terms of material parameters, such as the relative permittivity (also known as the dielectric constant) and the relative permeability, rather than the velocity of light inside the material. These two quantities appear in Maxwell's equations and describe to what extent a material will interact with the electric and magnetic field components of the electromagnetic field respectively. They are effective material properties that describe the bulk of a material as a whole and while metamaterials are, in general, composite materials which have

[2] Some passages in this section will be published in the chapter entitled 'Bottom-up organisation of metallic nanoparticles' written by Alastair Cunningham and Thomas Bürgi contained in the book 'Amorphous Nanophotonics'. Edited by Carsten Rockstuhl and Toralf Scharf, the book will be published in 2013 by Springer-Verlag Berlin and Heidelberg GmbH & Co. KG.

components with vastly differing properties, the use of effective material parameters is still valid as, as was described in the introduction, the wavelength of incident light is so large, relative to the length scale of the inhomogeneities, that it is unable to probe the difference between the individual components. When combined, these two material parameters also yield the refractive index as shown in Equation 1:

$$n = \sqrt{\varepsilon\,\mu} \qquad [1]$$

where n = refractive index

ε = relative permittivity

μ = relative permeability

Positive values of the relative permittivity (permeability) indicate that the electric (magnetic) fields propagate in the same direction in the material as the incident electromagnetic fields. At optical frequencies the relative permeability of most materials is very close to unity, meaning that the refractive index is essentially equal to the square root of the relative permittivity and it is this parameter that has a greater influence on the overall optical properties of the material. A positive relative permittivity means that both the electric and magnetic fields can propagate in the same direction and a common transparent dielectric will result. A negative value of the relative permittivity, on the other hand, indicates that the direction of the electric field within the material is in the opposite direction to that of the incident field, and the magnetic field, and as such no propagation is possible. Almost all of the incident light will be either absorbed or reflected giving what are commonly known as metals. The relationship between ε, μ and the properties that differing values of these induce is summarised in Figure 2 where a different class of material can be seen in each quadrant of the diagram.

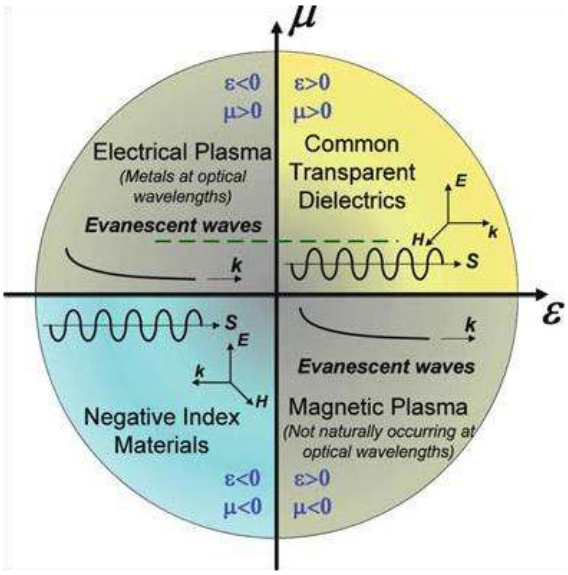

Figure 2 – Parameter space showing classification of materials for differing (real) values of ε and μ.[6]

As explained, most materials used in the world of optics can be placed in either the first or fourth quadrants however it is the third quadrant that most interests metamaterials researchers. That both ε and μ are negative in this quadrant gives rise to the term 'double negative media', one which is now synonymous with negative refraction, as in this quadrant both ε and μ are less than zero. By convention, the negative square root of their product should be taken to give the refractive index resulting in, again, negative values. This would indicate that both the electric field and the magnetic field should propagate in the material in the opposite direction to that of the incident field resulting in what are known as backward waves. It should be noted that in such materials Snell's Law still applies, meaning that the angle of refraction, measured from the normal, remains constant, however the direction of propagation in the material is a mirror image of that which would be expected in a normal dielectric material, as can be seen in Figure 3. In a hypothetical pond containing water with a negative refractive index the perceived location of the fish discussed above would now be above the surface of the water! These materials are sometimes also known as 'left-handed' and, as indicated in the Introduction, have rarely been observed in nature - clearly opening the door to a wide range of potential applications which would otherwise be unobtainable.

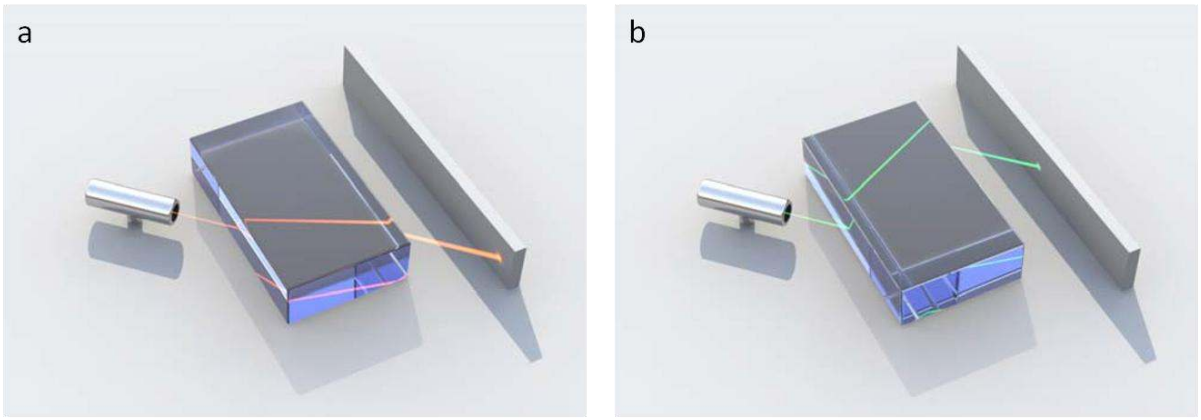

Figure 3 - Diagram showing paths taken by light, incident from a vacuum, in materials of both positive (a) and negative (b) refraction. Images taken from lecture on Plasmonic Metamaterials given by Tobias Utikal on the 19th of July 2011 at the École Polytechnique Fédérale de Lausanne.

As explained, the relative permittivity of metals is negative at optical frequencies – which is one of the major reasons that they are used so prominently in the preparation of double negative media. However, a more significant challenge arises from achieving negative relative permeabilities. This can be attained through taking advantage of the coupling properties of metallic inclusions which occur when the inclusions are arranged in some of the specific geometries introduced in Section 1.3.

Several other classes of materials exist in the parameter space shown in Figure 2. When both ε and μ are close to zero, zero index materials result.[52] Where only one of the parameters is close, or equal, to zero the reflectance of the material tends to be very high. Zero index materials, as with double negative materials, can also be engineered through the combination of suitable components in the correct structure and it has been proposed that such metamaterials could enhance the efficiency of some waveguides by reducing reflections at junctions or bends.[52]

For similar reasons that no wave propagation exists in the fourth quadrant of Figure 2 there is also no wave propagation in the second quadrant (where $\varepsilon > 0$ and $\mu < 0$). No material exists with these properties at optical frequencies and as no propagating waves can be supported the refractive index becomes purely imaginary. Consequently, these materials will not be further considered here.

The refractive index, the relative permittivity and the relative permeability are all complex functions and have real and imaginary parts. Large losses commonly occur for dielectric materials in the infrared and ultraviolet regions of the electromagnetic spectrum. These are as a result of absorption of phonons due to lattice vibrations and interband electron-hole transitions respectively and manifest themselves as peaks in the imaginary part of the relative permittivity. In-between these two peaks – in the visible regime – the imaginary part of the relative permittivity for dielectrics is

close to zero. The real part of the dielectric constant exhibits a Lorentz line shape around each of these resonances, as can be seen in Figure 4, but in the visible region is relatively constant and positive. The extent to which light is reflected or refracted at, for example, the interface between a vacuum and a dielectric is governed by the Fresnel equations. These equations, which depend solely on the refractive index of the two media, the angle of incidence and the polarisation state of the impinging light can also be adapted for use with metals.

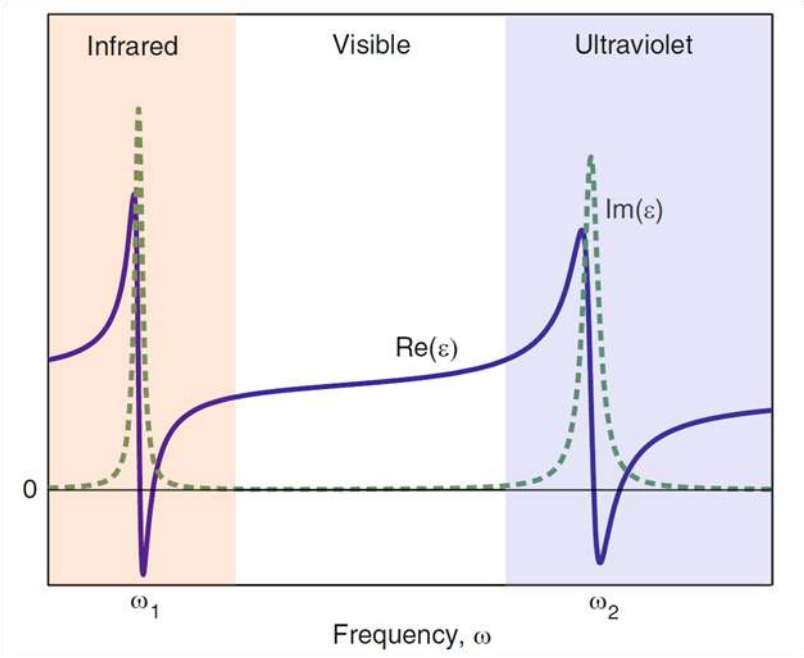

Figure 4 – Real and imaginary parts of the permittivity of a standard dielectric as a function of frequency. Lattice resonance in the infrared and electron transition resonance in the ultraviolet are marked at ω_1 and ω_2 respectively.[6]

Metals are readily identifiable due to their opacity and reflectivity and, as with dielectric materials, these optical properties are largely dependent on their relative permittivity which is in turn a function of the frequency of the incident light. Light which is not directly reflected from the surface of a metal is extremely efficiently absorbed over a very short distance also known as the skin-depth which tends to be on the order of 50 nm. This is because no band gap exists and all photons can transfer their energy to excite electrons. The optical properties of metals are governed largely by the interaction of light with the conduction electrons – a process that is very successfully described by the Drude free electron model[6] which depicts the motion of electrons in metals and treats the free electrons and positive ions in metals as simple harmonic oscillators. However the Drude model does not completely reflect reality in that it only considers free electrons and at optical frequencies it is also possible to promote more tightly bound inner core electrons to higher energy levels. While it is the free electrons that dominate the optical properties of metals these inter-band transitions also

play an appreciable role and are in fact what causes the differences in appearance between silver and gold when exposed to light. These inter-band transitions contribute to the dielectric function, governing the frequencies at which light is absorbed or can be efficiently reflected. In the case of gold, blue and green light is absorbed more than in some other metals such as silver or aluminium and causes it to preferentially reflect longer wavelengths – the origin of its familiar 'golden' hues. As with dielectrics, absorption, or losses are governed by the imaginary part of the relative permittivity. The imaginary part of the relative permittivity for silver is close to zero across the full visible spectrum and, in this respect at least, renders it more attractive for use in metamaterial designs than other metals such as gold which displays much greater losses. The real part of the relative permittivity is negative across the full visible spectrum for metals but becomes positive at higher frequencies. The point at which it becomes positive is known as the plasma frequency, ω_p, a bulk material parameter corresponding to the frequency at which the electron gas oscillates. Neglecting damping and using the Drude model the plasma frequency can be connected to the localised surface plasmon resonance (LSPR) , which will be discussed at length in Section 2.2.3, as in Equation 2:

$$\omega = \frac{\omega_p}{\sqrt{1+2\varepsilon_h}} \qquad [2]$$

where ω = frequency of plasmon resonance

ω_p = plasma frequency

ε_h = relative permittivity of host medium

The optical properties of metals are also extremely size dependent. As the dimensions of metals are reduced into the nanoregime, for example, the movement of electrons within the metal is limited by the physical boundaries presented at the extremities of the structure. This results in a chain of consequences – reducing the mean free path of the electrons and affecting the damping parameter which in turn influences the dielectric function of the metal. That the optical properties of metals are a function of size is of central importance to this thesis, and the concept of localised resonances that occur only in nanoscale metallic structures will be introduced in Section 2.2.3.

As a result of the pioneering work of Maxwell the interaction of light with both dielectric materials and metals, the principal components of the majority of metamaterials, can be accurately modelled. However, metamaterials are composites of the two, with the inhomogeneity scale being much smaller than the wavelength of the incident light thus rendering it unable to probe the two distinct components. Applying Maxwell's equations to large scale arrays of metallic inclusions in dielectric host media would be practically impossible due to the complicated boundary conditions. As such, a

means of modelling the response of, and assigning material parameters to, such composite materials is required. This means can be found in the overarching field of effective medium theory which incorporates a variety of schemes which are able, with differing levels of accuracy depending on variables such as filling fractions, to predict parameters such as the relative permittivity. The majority of these schemes can be traced back, at least to some extent, to the Clausius-Mossotti relation which first appeared in 1850.[53]

The Maxwell-Garnett theory, introduced in 1904, describes the bulk permittivity of a solid in terms of the permittivity of the inclusions in a host of a given dielectric constant and the volume ratio of these two components.[14] It was formulated by James Clerk Maxwell Garnett who, being the son of Maxwell's scientific demonstrator at Cambridge, was named after the great physicist.[54] However, Maxwell-Garnett theory can only be applied in the case where the volume of the inclusions is significantly lower than the overall volume of the system.

Bruggeman was able to improve the Maxwell-Garnett theory by overcoming this limitation and developing the theory to allow two-phase composites of any ratio to be considered.[55] Indeed, since the theory treats each component equally it is also possible to extend it to include any number of components. The effective medium theory developed by Bruggeman in 1935, and shown in Equation 3, is arguably still the most widely used model today and is commonly known as the effective medium theory.

$$f_1 \frac{\varepsilon_1 - \varepsilon}{\varepsilon_1 + 2\varepsilon} + f_2 \frac{\varepsilon_2 - \varepsilon}{\varepsilon_2 + 2\varepsilon} = 0 \qquad [3]$$

where f_1 = filling fraction of inclusion 1

ε_1 = relative permittivity of inclusion 1

ε = relative permittivity of composite material

f_2 = filling fraction of inclusion 2

ε_2 = relative permittivity of inclusion 2

Additionally, Bruggeman's effective medium theory also predicts a critical filling fraction for metallic particles, referred to as the percolation threshold, above which a continuous conducting pathway will be formed. This insulator to metal phase transition is not predicted by the Maxwell-Garnett theory which describes the effective permittivity of a composite as a linear function of the filling fraction. It is also possible to use the effective medium theory to calculate the relative permittivity of

nanoparticles rather than the composite. This technique is commonly carried out in nanocrystal research whereby measuring the permittivity of the composite material makes it possible to work backwards and determine the particle permittivity.[56]

The effective medium theory depicted in Equation 3 is only valid for spherical inclusions in a three dimensional material however both this, and the Maxwell-Garnett theory can be modified to accommodate for non-spherical particles and lower dimensional metamaterials such as thin films of metallic nanoparticles embedded in dielectric hosts.

The manner in which electromagnetic radiation interacts with matter, in particular metals, dielectrics and composites of the two, underpins the whole field of metamaterials. However, in order to fully understand what gives metamaterials their particular properties it is necessary to delve slightly deeper and consider the nanoscale metallic inclusions in these materials in more detail.

2.2.Nanoparticles

2.2.1. Nanoparticle properties

Despite metallic nanoparticles possessing a range of very specific properties they also share a range of attributes that, in a very general manner, can be applied to small particles of any composition. The properties of a material, when reduced in dimension from the bulk through to the atomic or molecular scale, become drastically different. Nanoparticles form a bridge between these two extremes. Unlike bulk materials, whose properties should be constant regardless of size, nanomaterials can have vastly varying, and often unique, optical,[57] electrical[58] and mechanical[59] traits when their size is changed by even small amounts. The changes in properties that are observed at the nanoscale can, in broad terms at least, be ascribed to a number of differing factors. The massive increase of surface area that is observed upon reduction of scale results in unrecognisable properties when a nanomaterial is compared to its bulk counterpart. A simple calculation can show that decreasing the radius of a sphere from 1 mm to 1 nm will result in a 10^{12} fold increase of surface area if the overall mass of the sample is kept constant. This can have significant effects on reaction rates and is of particular importance for catalytic applications.[60] Another root of the differences between bulk and nanoscale materials is quantum confinement. The restriction of motion of sub-atomic particles such as electrons can result in vastly differing properties, one notable example being the increasing size of the band-gap as semiconductor particles become smaller.[61] At the nanoscale, which can be loosely defined as the intermediate size scale between molecular and bulk

matter, the individual energy states of molecules and continuous energy bands of solids become discrete – their energy separations displaying a strong dependence on the dimensions of the material.[62] Another of the major distinctions that can be made between the macro and the nanoscale is the effect that gravity has on matter. Gravity essentially becomes negligible at this scale and other forces begin to dominate. The formation of stable colloids, with each particle undergoing Brownian motion rather than sedimenting at the bottom of a liquid, for example, is evidence of this. At this scale attractive interactions between particles in solution, governed by van der Waals forces, and repulsive interactions, governed by electrostatic forces, compete with one another. This forms the basis of DLVO theory which was named after Derjaguin and Landau, who first proposed the theory in 1941,[63] and Verwey and Overbeek, who independently arrived at the same conclusion seven years later.[64] It describes the stability of colloidal solutions as a function of the two competing forces as is shown in Figure 5.

Van der Waals forces are concerned with the interaction of dipoles, permanent or otherwise, on differing particles in solution. This is generally measured as a function of the distance between the two particles with the strength of the attractive forces, shown as the red trace in Figure 5, becoming extremely large at shorter distances. At larger separations repulsive interactions set up between the electrostatic double layers (EDLs) which surround each of the particles have more of an influence. These repulsive interactions are represented by the blue trace in Figure 5. Of course each situation should be studied on individual basis but in general, when the two forces are combined, an energy barrier, seen as the peak of the green trace in Figure 5, can be ascertained. When particles maintain a separation further apart than the position of the energy barrier the colloid remains stable. If the particles approach to within distances closer than that found at the energy maximum, however, the attractive forces overshadow the repulsive ones and irreversible aggregation of the particles tends to result. Modifications to this theory, for example based on specific information such as salt concentration, can be made and result in changes in the profile of the net energy trace. The introduction of secondary minima in such traces shows the particle separation range where reversible aggregation can occur.

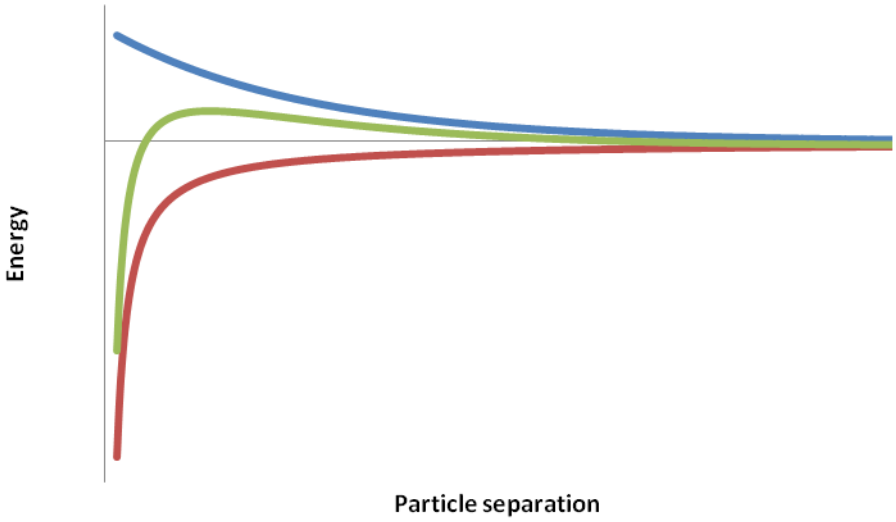

Figure 5 – Graphical representation of DLVO theory showing free energy as a function of particle separation. At low particle separation the Van der Waals forces (red trace) dominate over the electrostatic repulsion (blue trace) causing the net energy (green trace) to be lower than zero. In this regime the particles are attracted to one another and tend to aggregate.

The EDL, which exists at the surface of all charged particles in solution, serves to stabilise the particles and inhibits their aggregation. Depicted in Figure 6, the EDL is composed of solvent molecules and ions that are attracted to the charged surface of a nanoparticle in order to maintain charge neutrality. It can be defined as the volume of solvent at the surface of an object that contains an excess of counterions and a corresponding depletion of coions when compared with the bulk and this thickness defines the extent to which, and over what range, particles can interact through electrostatic forces. The characteristic length of the EDL, known as the Debye length, is shown in Figure 6, along with the Stern layer, which refers to the layer of oppositely charged ions physisorbed at the surface.

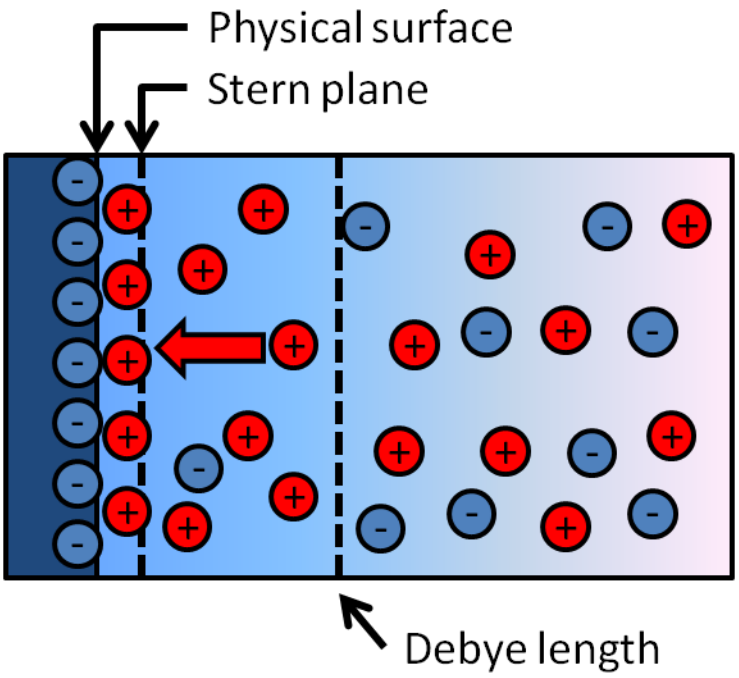

Figure 6 – Diagrammatical representation of the electrostatic double layer showing the excess of ions of opposite charge to that of the surface in this zone.

Clearly the extent to which the EDL extends into the bulk of the solution is extremely dependent on the concentration of ions in solution. As the concentration of ions is increased, through the addition of salt for example, the EDL 'collapses' and particles have to approach to within much shorter distances in order to interact electrostatically. Conversely, the removal of ions from solution, through purification techniques such as centrifugation or dialysis, causes the EDL to expand into the bulk of the solution and particles interact at greater separations. Many theoretical models, principally describing the interaction between colloidal particles, have been developed and modified over the last 150 years and are now able to describe interactions between particles of various sizes, shapes and compositions.[65] In general, however, the EDL can be thought of as consisting of two distinct regions; the Stern layer which refers to the layer of counterions adsorbed at the solvent interface and the diffuse layer which is so-called because the excess of ions found in this region are not anchored to the particle but are free to diffuse in and out of the bulk, electrostatic attraction being to some extent balanced by the somewhat random forces of thermal motion. The Debye length, κ^{-1}, is inversely proportional to the square root of the ion concentration as in Equation 4:

$$K^{-1} = \left(\frac{\varepsilon RT}{2F^2q^2C}\right)^{1/2} \quad [4]$$

where K^{-1} = Debye length

ε = dielectric constant

R = ideal gas constant

T = temperature

F = Faraday constant

q = charge number

C = ion concentration

In addition to being able to tune the Debye length by controlling the concentration of ions in solution it is also possible to influence the electrostatic properties of the system by altering the pH. Surface charge density is strongly dependent on pH. The point of zero charge, the pH at which the surface charge density is zero, is of fundamental importance to the electrostatic nature of colloidal systems where H^+/OH^- are the potential determining ions. As the pH is increased from this point the particles exhibit an increasingly negative charge, the converse being true when the pH is decreased.

Despite being an extremely useful tool that can be used to model and explain a host of different situations the standard EDL model described above does deviate slightly from the actual situation resulting in certain limitations. For example, ions in solution, which can be within an order of magnitude of the charged object itself, are effectively modelled as point charges with interactions being of a purely Coulombic nature.[65] In addition the dielectric constant is assumed to be constant throughout the solution which is virtually never the case with large variations normally existing between the particles and solvent.[65] These factors can combine to give inaccurate values for the ion distribution around a charged nanoparticle.

While electrostatic repulsion, as described by the EDL model, can be used to stabilise particles this can also be achieved through coating the particles with physical barriers such as polymers or SiO_2 layers which prevent aggregation.

2.2.2. Synthesis of metallic nanoparticles

As previously described metallic nanoparticle assemblies fabricated using bottom-up methods possess several advantages over their top-down counterparts. As well as offering design benefits such as smaller feature sizes and more ready access to 3D materials, two of the major challenges currently facing the metamaterials community, these techniques are, in general, cheaper and quicker, this being of prime importance for the eventual application of this technology. As such, over the last decades a significant amount of research effort has gone into the fabrication of metallic nanoparticles using colloidal nanochemistry. This field, despite being relatively mature, is constantly being updated and particles of a wide variety of shapes, sizes and composition can now be readily produced.[66] This large catalogue of materials, exhibiting an LSPR at optical frequencies,[67] is becoming of increasing importance to the burgeoning field of optical metamaterials. When using such particles to prepare structures with advantageous optical properties it is typically necessary to induce their organisation, normally through the exploitation of particle-substrate and interparticle interactions, into specific architectures that have been proposed by theoreticians. The development of novel and innovative methods combined with the manipulation of pre-existing ones allows this to be done. While the field is too large to give a comprehensive review of all of the bottom-up methods used to both prepare metallic nanoparticles and assemble them into structures that could be useful to the field of metamaterials, an attempt will be made in this section to introduce some of the primary techniques that have been used in this newly developing domain.

Due to their superior optical properties and their ease of handling the majority of metamaterial structures use either silver or gold, respectively. Where bottom-up techniques are concerned, these nanoparticles are generally fabricated by reducing a salt of the metal in solution. One of the most common methods used to produce metallic nanospheres is known as the Turkevich method which was first developed in 1951[68] and essentially involves the reduction of chloroauric acid by sodium citrate.[69] The citrate molecules play two roles in the synthesis; first reducing the metal ions to form the nanoparticles and secondly forming a capping layer at their surface which imparts a characteristic negative charge on them and stabilises them in solution, preventing them from aggregation. The ratio of gold to citrate in solution defines the size of the particles and allows their diameters to be accurately controlled.[69] The Lee-Meisel method, in essence analogous to that described above, can be used to produce charged silver nanospheres.[70] Another technique used to prepare metallic nanospheres is the Brust-Schiffrin technique, a two-phase method which yields metallic nanoparticles in an organic solvent.[71] In addition to spheres, metallic nanorods can readily be synthesised using a seed-mediated method that involves the addition of small ‘seed’ particles to a

growth solution containing a surfactant which stimulates preferential growth along certain crystal facets, resulting in elongated particles. Here, through the careful control of the growth conditions it is possible to tune the aspect ratio, and therefore the plasmonic properties, of the particles. Whilst being used less often in the assembly of bottom-up metamaterials, more exotic metallic nanoparticle geometries such as nanoshells,[72] nanostars and cubes,[73] nanoprisms[74] and many other forms[66, 72] can readily be prepared using colloidal nanochemistry techniques.

2.2.3. The localised surface plasmon resonance

The wide ranging catalogue of metallic nanoparticles which can now be routinely prepared, and in many cases are now commercially available, has garnered increasing interest as their use in a broad variety of applications has become apparent. This is largely due to their particular optical properties, more specifically the fact that they support an LSPR. This property is observable only in particles which fall under a certain size and as such can be distinguished from propagating plasmon resonances which relate to larger scale systems, that have at least one dimension that approaches the excitation wavelength.[75] There are two limiting factors connected to size in relation to the LSPR. The particles should be smaller than the depth to which optical radiation penetrates the material under study, also known as the skin-depth. This is on the order of 50 nm in the visible range for the coinage metals, the principal materials used in the field of plasmonics.[76] At the other extreme the particles should be larger than the distance that an electron with Fermi velocity (approximately 2×10^6 ms^{-1}) can travel during one optical oscillation. This distance, also known as the non-locality length, equates to about 2 nm considering that the oscillation period of the electrons is on the order of 2 femtoseconds.[76]

The principal materials used in plasmonics include gold and silver, because of their ease of manipulation and superior optical properties respectively. To a lesser extent heavily doped semiconductors and other coinage metals such as copper, palladium, aluminium and tungsten can also be used. The latter two examples are notable due to the plasmon resonance being pushed into the UV and NIR regions of the electromagnetic spectrum.

The plasmon resonance, which has been widely studied and documented,[67] describes the coherent dipolar oscillation of the free electrons present in a nanoparticle when excited by electromagnetic radiation of a particular frequency. The electric field of an incident light wave induces a polarisation of the surface electrons with respect to the much heavier ionic core of a spherical nanoparticle. A net charge difference is experienced only at the surface of the nanoparticle. The charge difference then acts as a restoring force, creating a dipolar oscillation of the electrons. This process is depicted

schematically in Figure 7. Particles that support LSPRs experience a uniform electric field as their dimensions are much smaller than the wavelength of the light that excites them.[75] This manifests itself as a strong extinction of the incident radiation which, depending on the material, exists in the visible part of the electromagnetic spectrum.

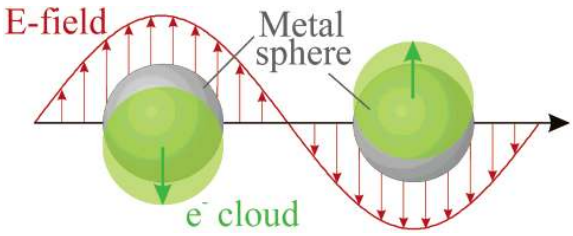

Figure 7 – Schematic of the plasmon resonance showing the displacement of the conduction band electrons relative to the ionic core of a spherical metallic nanoparticle that occurs upon incident electromagnetic radiation of a resonant frequency.[77]

The effect was first modelled by Gustav Mie in 1908 who solved Maxwell's equations for light interacting with spherical metallic nanoparticles. His equation, shown below, which includes both scattering and absorption, holds true when dipolar oscillations of the conduction electrons are considered in the limiting case where the wavelength of the incident radiation is significantly greater than the size of the metallic nanoparticles.

$$C_{ext} = \frac{24\pi^2 R^3 \varepsilon_m^{3/2}}{\lambda} \frac{\varepsilon_2}{(\varepsilon_1 + 2\varepsilon_m)^2 + \varepsilon_2^2} \qquad [5]$$

where C_{ext} = extinction cross-section

R = particle radius

ε_m = dielectric constant of the surroundings

$\varepsilon = \varepsilon_1 + i\varepsilon_2$ = complex dielectric constant of bulk metal

λ = wavelength of incident radiation

As can be seen in Equation 5, the maximum extinction occurs when $\varepsilon_1 = -2\varepsilon_m$, also known as the Fröhlich condition,[78] thus defining the position of the LSPR peak. The pioneering work which Mie executed is not limited to nanospheres and can also be modified to describe nanoparticles of other geometries such as rods.[79]

These optical properties have made the use of gold nanoparticles attractive to a number of fields interested in exploiting their potential. For example, as shown in Equation 5, the position of the LSPR peak is altered depending on the dielectric constant of the surrounding material. As such the particles can be thought of as probes that can accurately return information, observed as red or blue-shifts of the LSPR peak, on the refractive index, and therefore composition, of their surrounding medium. A host of sensing applications, where colour changes observed in the metallic nanoparticles can indicate trace changes in the concentration of analytes, can be envisaged with many already both in use and development.[80] A comprehensive review of nanostructured plasmonic sensors can be found in Reference 81.

The position of the plasmon resonance is also closely related to both the size and the shape of the nanoparticles. As can be seen in Equation 5 there is a strong size dependence between the overall extinction cross-section and the radius of the spherical particles. At smaller sizes this extinction is dominated by absorption however as the particles become larger scattering plays an increasingly important role. When non-spherical metallic nanoparticles are considered then additional plasmon resonances are induced. For example nanorods exhibit two plasmon resonances; the longitudinal plasmon resonance corresponds to the oscillation of the surface electrons along the length of the rod and occurs at longer wavelengths while the transverse plasmon resonance is related to the oscillation of the surface electrons across the breadth of the rod and can be found at higher frequencies. The exact position of these extinction peaks can be tuned by altering the aspect ratio of the rods which can be controlled through the adjustment of certain reaction conditions.[34, 82] The extent to which the position of the longitudinal LSPR peak can be tuned was described by Brioude *et al.* who modelled the relationship between peak position and aspect ratio as shown in Equation 6:[83]

$$\lambda_{max} = 96AR + 418 \qquad [6]$$

where λ_{max} = peak position of longitudinal LSPR peak

AR = aspect ratio

When this equation is considered in combination with the fact that particles with an aspect ratio of 1 (spheres) up to ~20 can now be routinely realised in a controlled manner it can clearly be seen to how great an extent it is possible to tune the optical properties of nanoparticle systems.[84]

As a result of advances made in recent years a wide range of other particle geometries are now accessible using bottom up growth methods. Each of the range of particle shapes introduced in

Section 2.2.2 possess particular plasmonic properties with peaks of differing strengths found at a variety of frequencies.

An additional approach to controlling the plasmonic properties of nanoparticle systems is by supplying, or removing, electrons to or from the nanoparticles.[78] The frequency of oscillation of the surface electrons is heavily dependent on their concentration. Taking gold nanoparticles as an example, each atom within the particle is capable of supplying one electron (from the 6s shell) that will participate in the resonant oscillation that forms the plasmon resonance. By applying a potential to a system of plasmonic nanoparticles it is possible to supply extra electrons to these systems, or conversely to deplete them, resulting in shifts of the plasmon resonance. The extent to which it is possible to use this method to control the peak position is dependent on the initial carrier concentration. Materials, such as metals, which have high carrier concentrations to begin with, will not be affected as much as, for example, semiconductor particles where the carrier concentration is initially relatively low. In these cases it is even possible to tune the position of the plasmon resonance from the infra-red into the visible. The degree to which the resonance can be manipulated, and the reasoning behind larger shifts being observed for low carrier density materials, is outlined in Equation 7:[78]

$$\lambda_f = \lambda_i \sqrt{\frac{n_i}{n_f}} \qquad [7]$$

where λ_f = final LSPR wavelength

λ_f = initial LSPR wavelength

n_i = initial electron concentration

n_f = final electron concentration

The carrier concentration in plasmonic semiconductor particles can also be tuned by altering the ratio of the constituent elements. This affords an added level of control which is not available when working with metallic particles. For example, varying the concentration of tin in indium tin oxide (ITO) nanoparticles by just a few percent can result in massive shifts of the LSPR band of several hundred nanometres.[85] The overall number of conduction electrons in a nanoparticle is known as the oscillator strength, *f*, and is typically in the range of $\sim 10^5$.[76] In comparison, the oscillator strength of an organic dye or semiconducting quantum dot is, in general, about 1. When it is considered that the absorption cross-section is directly proportional to f and the scattering cross-section is

proportional to f^2, the gains in efficiency offered through the use of plasmonic particles can clearly be seen.[76]

Some factors that affect the frequency of the plasmon resonance are maybe not as obvious and are sometimes overlooked. It is well-recognised that LSPR peaks are highly sensitive to sharp edges and protuberances however atomic scale protrusions on gold nanorods, resulting from lattice defects, stacking faults or perhaps simply from the faceting of the surface atoms that is required to form particular geometries, have been observed using high resolution transmission electron microscopy (TEM)[86] and have been shown to have a strong bearing on the position of the LSPR.[87] Acting as local 'hot-spots' increasing the surface roughness can result in red-shifts of the longitudinal LSPR peak of gold nanorods of several tens of nanometres. These additional edges and vertices can affect the electrostatic distribution of charges within the particle, resulting in differing resonant frequencies and providing another possible means of controlling the optical properties of metallic nanoparticle systems.

That different shaped nanoparticles possessing several plasmon resonances can now be readily prepared in a controlled fashion introduces the prospect of selectively exciting specific LSPR peaks. This can be achieved by either modulating the frequency or the polarisation state of the incident light. Taking a single gold nanorod as an example; when exposed to unpolarised white light both the longitudinal and transverse plasmon modes will be excited. However if the light source were to be replaced with a monochromatic source with a wavelength corresponding to that of the longitudinal (transverse) plasmon band the electrons will only be driven into oscillation along (across) the length (breadth) of the nanorod. If a linear polariser were to be placed in front of the original white light source and the orientation of the resultant polarised light is aligned with one of the two nanorod axes then it is also possible to selectively excite only one of the two resonances. This means of selecting the plasmon band becomes more complicated as more nanoparticles are considered. In addition to aligning the light source with the particle it becomes necessary to also ensure that all of the particles are, themselves, aligned. This is particularly challenging when bottom-up approaches are used as long range order is more difficult to achieve and amorphous structures tend to dominate.

In addition to the oscillator strength, which measures the number of conduction electrons available to contribute to the plasmon resonance, there are other means of expressing the relative attributes of surface plasmon resonances. The quality factor, *Q*, can be defined as the frequency of the plasmon resonance divided by the full width at half maximum of the peak and is a measure of the number of oscillations that a surface plasmon undergoes before it decays.[75] In essence a higher

quality factor denotes less damping and a stronger plasmon resonance and in general should have a value greater than ten for most plasmonic applications.[75] A formula for the quality factor based upon the real and imaginary parts of the dielectric constant of the metal in question is shown in equation 8:

$$Q = \frac{\omega(d\varepsilon_r/d\omega)}{2(\varepsilon_i)^2} \qquad [8]$$

where ω = frequency

ε_r = real part of dielectric constant

ε_i = imaginary part of dielectric constant

It also describes the increase in local field amplitude that accompanies the excitation of the plasmon resonance. The square of the quality factor, which ranges between 10 and 100 for noble metals depending on the frequency being considered, indicates the enhancement of the absorption and emission rates of molecules adsorbed at the surface of the nanoparticles.[76] The enhancements that are seen in surface enhanced Raman scattering (SERS) are proportional to Q^4 – explaining the huge enhancements that have led to single molecule sensitivity.[76, 88] Silver is the metal which displays the highest quality factor across the majority of the visible spectrum making it one of the most promising materials for plasmonic applications.[75] Another term that can be used in the description of surface plasmon resonances is the modal volume, V_m, which refers to the volume in which the conduction band electrons oscillate.[76] In a nanoparticle whose dimensions are smaller than the skin-depth the modal volume is approximately equal to the volume of the particle itself and it is partially this sub-wavelength confinement of the optical energy that results in such a wide range of applications for plasmonic nanostructures.

Electronic motion in the nanoparticles can be damped through two distinct loss mechanisms – radiative and nonradiative and, in general, plasmon relaxation times are on the order of 10 femtoseconds.[76] Radiative processes encompass both elastic and inelastic scattering of incident light and for particles smaller than ~100 nm scale as the square of the volume of the particle.[89] The scattering of light into the far field caused by nanoparticles can be measured by standard dark field microscopy and its contribution to the overall extinction is included in Mie theory. Nonradiative decay, also included in the Mie equation, refers to the decay of the plasmon oscillation through the transformation of absorbed energy into heat which is caused by collisions between the oscillating electrons and the lattice ions and can be measured by photothermal imaging.[89] The excitation of the plasmon resonance results in local heating of the particle which sets up a high temperature gradient

between the particle and its surroundings to where the energy is then transferred. The increase in temperature of the surroundings can cause local changes in the refractive index which, as discussed, can result in shifts of the LSPR peak.[89] The nonradiative properties of plasmonic particles can be of particular use in applications such as cancer therapy where nanoparticles, which have been selectively bound to cancerous cells, can be irradiated at the plasmon frequency and kill only these cells.[90] By shifting the plasmon resonance into the near infrared, a region of the electromagnetic spectrum where human tissue does not efficiently absorb, it is possible, using this technique, to avoid invasive surgery.[90]

The above discussion refers solely to the plasmonic properties of isolated particles. However one of the most interesting, and indeed useful, techniques of tuning the spectral position of the plasmon resonance is by inducing two or more of these particles, by chemical means or otherwise, to approach to within short distances of one another.

2.2.4. Plasmon coupling and hybridisation theory

Metallic nanoparticles undoubtedly have many applications, both current and future. The majority of these applications rely on the LSPR that the particles support, allowing them to, amongst other things, sense, heat, catalyse and image. The position of the LSPR peak, as discussed above and formulated in Equation 5, is dependent on a number of factors including the particle size and shape as well as the refractive index of the surrounding medium localised at the surface of the particle. However one important factor that is not considered in the equation, which analyses only a single particle, is the effect that other particles have on one another. This effect, also known as coupling, can be exploited by finding means, chemical or otherwise, to order metallic nanoparticles into specific configurations or structures. This is an additional, more flexible, method of fine-tuning the optical properties of systems and will be examined in more detail in the following discussion.

Coupling between metallic nanoparticles is very well summed up by plasmon hybridisation theory. This physically intuitive method, developed in 2003 by Peter Nordlander *et al.*,[91] uses similar constructs to those used in molecular orbital theory to describe the optical changes that occur when two metallic nanoparticles are brought together to the extent where they begin to interact. The plasmonic response of a more complex structure is constructed from the interactions that exist between its constituent elements, forming hybridised modes in much the same manner that molecular orbitals are composed from the atomic wave-functions of the individual atoms that form molecules. This interaction can be considered in its simplest form as the coupling of two nearby dipoles, although depending on the size of the nanoparticles and their distance of approach higher

order multipole moments can also be considered. Hybridisation theory predicts two distinct classes of eigenmodes for a structure of two strongly coupled metallic spheres, i.e. a dimer. The first is associated with an in phase oscillation of the electric dipole in both spheres and is therefore termed a 'bright' eigenmode since it can radiate into the far field. The second class requires a 180° out of phase oscillation of the electric dipoles of both spheres. These eigenmodes are termed 'dark' since they cannot radiate into the far field and play an important role in the field of metamaterials as the out of phase oscillation of electric dipoles can be related in some cases to a magnetic dipole moment which is the key component in many predicted applications of metamaterials.

The method of constructing hybridised plasmonic modes through the combination of two or more resonant elements is illustrated in the plasmon hybridisation diagram shown in Figure 8 and depicts the theory applied to a dimer of two metallic nanospheres.

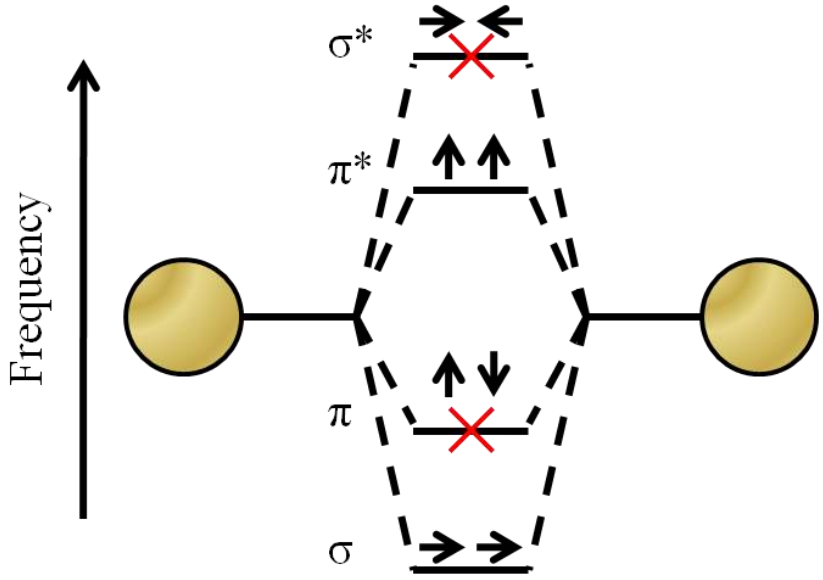

Figure 8 - Schematic showing hybridisation of plasmons of two approaching metallic nanoparticles. Red crosses indicate dark modes that only offer a weak excitation for the present configuration.

Shown are the individual nanoparticles with the dipoles that they support, the directions of which are dependent on the direction and polarisation of the incident electromagnetic fields which drives the free electrons of the metal into resonance. Similarly to molecular orbital theory these dipoles are combined in bonding and anti-bonding fashions and result in the splitting of the modes to give hybridised modes of lower and higher energy respectively. The interaction of two equal spheres results in four hybridised plasmonic modes in the coupling regime. Because of symmetry considerations, only two of these modes display a net dipole moment and will show a strong scattering of light into the far-field at relevant frequencies and angles of incidence. Conversely, both

the antibonding mode for incident light parallel to the main axis of the dimer (σ*) and the bonding mode for incident light perpendicular to the main axis of the dimer (π) have no net dipole moment and are known as dark modes (noted in Figure 8 with red crosses) that can only be observed by breaking the symmetry of the system and for large spheres with extremely small interparticle distances. These dark modes contribute predominately to the absorption of the system because the resulting quadrupole moments offer only a weak coupling to the far field.

Plasmon hybridisation theory can be used to model systems both quantitatively and qualitatively and has proven to be an invaluable tool both in explaining the optical changes observed, for example spectroscopically, and in designing new systems which should have specific optical properties. It is in no way restricted to simply describing nanospheres and has been applied to nanoparticles of a wide range of different forms such as asymmetric dimers, thin metallic films, systems of metallic nanoshells, nanorods and nanostars.[66]

2.2.5. Bottom-up organisation of metallic nanoparticles

The large potential for using bottom-up methods to organise metallic nanoparticles into assemblies that could be used as functional materials with practical applications has meant that a significant amount of research effort has been focussed in this direction in recent years. Exploiting the coupling properties that metallic nanoparticles possess and fabricating materials with tailored optical properties is one of the major motivations driving material scientists to finding novel means to induce their self-assembly. The versatility of the nanoparticles, largely resulting from the wide-ranging surface chemistry that can be used to cap them, means that a huge amount of techniques originating from disparate areas of chemistry can be used to this end. The assembly of metallic nanoparticles relies on surface chemistry and self-assembly principles using (bio-)molecules, surfactants, mesogens or polymers and makes use of intermolecular (interparticle) interactions. It is therefore logical that the bottom-up organisation of metallic nanoparticles is a research area where the border between physics and chemistry needs to be crossed.

Self-assembly is closely linked with the liquid-crystalline state of matter and it is therefore not surprising that liquid crystals have been used in order to organise gold nanoparticles. The inherent order that is present in liquid crystal systems can be used to impart organisation on the nanoparticles themselves, resulting in arrays of resonant guests in the host material.[92] This can be achieved by using one of two general strategies; either by simple mixing of the two species,[93] or modifying the surface chemistry of the particles and functionalising them with liquid crystalline ligands.[94] Whilst these techniques work to a large extent they suffer from the relatively low

solubilities of the nanoparticles in the host and the maximum size of the particles that it is possible to incorporate, although it has been reported that particles of up to 7 nm in diameter, large enough to support LSPRs, have been included in such systems.[94]

One of the most important examples of self-assembly exhibited in nature, that of the double helix structure of DNA, can also be used to organise metallic nanoparticles. The formation of ordered structures in such a way, using DNA as a molecular substrate for nanoparticle deposition, has facilitated the production of a number of different metallic nanoparticle architectures. One early example was the formation of dimers and trimers which was achieved through the functionalisation of gold nanocrystals with single stranded DNA oligonucleotides of defined length and sequence and assembling them on a complementary single stranded DNA template.[95] This work introduced the possibility of using oligonucleotides to self-organise metallic nanoparticles into well-defined and homogeneous structures. Similarly, Chen *et al.* used a chemically modified peptide to reduce a gold salt, resulting in a left-handed arrangement of gold nanoparticles along the peptide backbone.[96] The introduction of chirality to the organisation of metallic nanoparticles produces optically active materials and gives an additional means to tune the optical properties of such systems. More recently metallic nanoparticle heterodimers comprising both gold and silver nanoparticles fabricated in a similar manner were shown to be SERS active.[97] Precise nanogap engineering was achieved through the controlled growth of silver layers on top of the original gold nanoparticles and single molecule sensitivity was shown when dyes were analysed using SERS. This advance is further evidence of such work being of fundamental importance to several fields of scientific research.

Another possibility for the use of macromolecules in the ordering of metallic nanoparticles includes the creation of pseudo block copolymer systems.[50] Gold nanorods selectively functionalised at their ends with polymer chains, resulting in a 'pom-pom' structure reminiscent of an ABA tri-block copolymer, can be induced to organise the nanorods either end to end or side by side. This interchangeable organisation can be controlled by altering the molecular weight of the polymer chains or by simply altering the percentage composition of the solvent. The different affinities that the polymers at the ends of the gold nanorods and the cetyltrimethylammonium bromide (CTAB) molecules along their lengths have for different solvents provokes the redistribution of the polymer chains and stimulates the organisation of the nanorods in different manners as the concentration of water in the predominantly organic solvent is increased. A more in-depth discussion of the ramifications that such differing organisations of gold nanorods have on the optical properties, considered from the perspective of plasmon hybridisation theory, can be found in Reference 98.

Additional degrees of order compared with the systems previously discussed arise from the formation of binary nanoparticle superlattices from colloidal crystallisation methods which can result in crystals containing metallic nanoparticle inclusions.[99] Here, steric repulsion and van der Waals, electrostatic, and substrate - particle interactions, amongst others, all combine to determine the crystal structure with the type of control over particle size, shape and composition outlined previously allowing materials with tunable physical and chemical properties to be manufactured.

It would be easy to assume, on the other hand, that less ordered systems would result from the agglomeration of nanoparticles. In general this is true and such aggregation, which can occur for a variety of reasons, is normally to be avoided. However the controlled aggregation of colloidal gold nanospheres has been used to selectively produce dimers and trimers, which were subsequently used to catalyse the formation of ZnO nanowires in solution.[100] The aggregation, occurring as a result of a reduction of the EDL, is achieved through the addition of HCl and the particles are simultaneously stabilised by encapsulating polymers. An optimal pH for dimer formation was found to exist and high yields could be isolated upon enrichment by density gradient centrifugation. This control over the aggregation kinetics provides a route to the fabrication of ensembles with well-defined nanoparticle inclusions.

Several theoretical studies have shown that spherical arrangements of metallic nanoparticles are of significant interest to metamaterials research due to the possibility of introducing magnetic resonances, a necessary building block of negative refractive indices.[27, 41-42] By replacing the citrate capping shell that stabilises gold nanoparticles fabricated using the Turkevich method with 11-mercaptoundecylether it is possible to provoke the self-organisation of the particles into spherical units of around 1 μm in diameter.[101] These spheres, in turn, were also observed to assemble into larger structures, forming hierarchical arrangements of metallic nanoparticles that closely resemble structures that have been proposed as possible negative refractive index materials.[42] Other means, for example using oil-in-water emulsion technology, have also been used to produce spherical arrangements of metallic nanoparticles by bottom-up methods.[102] Due to this unambiguous association with the excitation of magnetic dipole resonances, by confining suitably functionalised particles to an oil phase that has been dispersed as small spherical globules in a non-miscible solvent such as water it is possible to create another possible building block for use in the fabrication of bulk metamaterials at optical frequencies.

By combining top-down and bottom-up techniques it is also possible to exploit the advantages of both, resulting in substrates with metallic nanoparticles that self-assemble into structures that also exhibit long range order. Two-dimensional square arrays of gold nanoparticle clusters can be

prepared, for example, by inducing their template directed self-assembly into holes prepared by laser interference lithography.[103] These hybrid techniques can be implemented when required and provide an additional layer of flexibility when it comes to preparing structures of a particular design.

This introduction has given a small snapshot of some of the principal bottom-up self-assembly routes towards nanoparticle organisation and is by no means comprehensive. As shown, the field of bottom-up assembly of metallic nanoparticles is already highly developed in terms of what is achievable and the wide range of methods that exist to accomplish design goals set. Of course, one of the principal advantages of the bottom-up approach is its flexibility and often a combination or variation of one or more of the techniques discussed above is required to achieve the desired results. Indeed, one could argue that problems of either a scientific or practical nature should be considered on a case by case basis when searching for bottom-up solutions. The continual introduction of new techniques and their combination with existing ones means that this is an extremely fast moving area of research that is continually making notable advances. This means that only the surface has been scratched in terms of what can be achieved with respect to metallic nanoparticles structures and highlights both the power and versatility of the techniques discussed.

2.2.6. Applications of metallic nanoparticles

The optical properties outlined in Section 2.2.3 have made the use of metallic nanoparticles attractive to a number of fields interested in their application. As shown in Equation 5, the position of the LSPR peak is shifted upon changes in the dielectric constant of the surrounding material. As such the particles can be thought of as probes that can accurately return information, observed as red or blue-shifts of the plasmon peak, on the refractive index, and therefore composition, of their surrounding medium. A host of sensing applications, where colour changes observed in the metallic nanoparticles can indicate trace changes in concentration of analytes, can be envisaged with many already both in use and in development.[80] A comprehensive review of nanostructured plasmonic sensors can be found in Reference 81.

One specific area of interest where sensing and metallic nanoparticles are concerned is in the field of SERS. This effect was discovered in 1974 by Fleischmann[104] and relies on the extremely strong electromagnetic fields that exist in the nanogaps between metallic nanoparticles. This facilitates massive enhancements of the Raman signal, as high as $10^{14} – 10^{15}$ times more than that observed under normal conditions,[66] which is sufficient to allow the detection of single molecule analytes. This is extremely useful as the Raman signal can return detailed information on the vibrational levels of the analyte, allowing the technique to be used for both detection and structure determination.[80]

SERS has now developed to the extent that spectra can be measured *in vivo*.[105] In principle this could facilitate faster acquisition times and was a significant breakthrough for the use of metallic nanoparticles in medical and biological applications. A more detailed discussion of the enhancement mechanism observed and specific SERS applications can be found in Refserences 106 and 107. In a similar manner the enhanced E-field that exists at the surface of, and particularly in the nanogaps between, nanoparticles is also capable of enhancing the efficiency of infrared absorption and fluorescence emission processes resulting in equivalent surface enhanced spectroscopic techniques.[108]

Biomedical studies of metallic nanoparticles began in the 1970s following the discovery of immunogold labelling.[109] Since then a wide array of biological sensing applications have been developed.[110, 111] Gold nanoparticles used for medical diagnostics have even become commercialised where they form an integral part of certain pregnancy tests which are currently on the market. However metallic nanoparticles are not limited to sensing applications. One major reason for the wide-spread use of gold nanoparticles for biomedical applications is their relatively low cytotoxicity which makes them particularly suitable for *in vivo* applications such as drug delivery,[112] bioimaging[113] and cancer therapy.[90] An innovative form of cancer therapy involves suitably modified gold nanoparticles, functionalised with antibodies that recognise antigens expressed by cancerous cells and allows them to specifically bind to these cells.[90] The excitement of the LSPR through irradiation with a suitable source results in the fast conversion of the absorbed energy to heat which, as the particles are localised at the cancerous cells, is sufficient to destroy these cells whilst leaving healthy ones undamaged. In addition to the control over the surface chemistry that is required it is also necessary to push the LSPR of the nanoparticles into the infrared region of the electromagnetic spectrum as otherwise the incident radiation used to excite the LSPR would be absorbed by the first few millimetres of skin. Infrared radiation, on the other hand, can penetrate significantly further and facilitates the excitement of the plasmon resonance of particles that are located at the cancerous cells. By using gold nanorods, the position of whose longitudinal plasmon resonance can be readily tuned in the growth process through altering the aspect ratio of the particle, this problem can be overcome.

As well as being able to use nanoparticles in diagnostics and in the treatment of medical conditions they have also found a niche application in measuring nanoscale distances, particularly in biological samples, and can be thought of as being ‘plasmonic rulers’.[114] The system is based on the strength of the coupling between a pair of metallic nanoparticles which is itself strongly dependent on the distance between them. Stronger and weaker coupling manifests itself as red and blue shifts of the

LSPR peak respectively and after adequate calibration it is possible to correlate these shifts in the optical properties to the separation of the nanoparticles. Dynamic separations of up to 70 nm can be monitored allowing information on both distance and configuration to be elucidated.[114] A number of advantages exist over other methods used to determine molecular distances such as Förster resonance energy transfer measurements. Here, low and fluctuating signal intensities along with limited observation times and upper measurement limits of approximately 10 nm mean that plasmonic solutions such as the ones described may be more appropriate in certain situations.[114] However, certain issues, including the extent to which the adsorption of nanoparticles to biomolecules affects their overall structure have not been unequivocally resolved. Despite this, the power and potential that plasmonic rulers possess with respect to structure elucidation is clear to see.

An equally important field which makes use of metallic nanoparticles is that of catalysis. Despite being historically considered as merely a chemically inert metal, supported gold nanoparticles were first found to reduce the activation energy for the oxidation of CO around two decades ago.[60] The high surface area, and therefore number of active sites, provides obvious advantages. There exists a strong dependence of catalytic activity on particle size, with a large decrease in activity for particles larger than 6 – 10 nm being observed.[60] Therefore one of the major challenges facing the field is finding a means to maintain particle stability under the reaction conditions required. A more recent study, directly using the plasmonic properties of metallic nanoparticles, researches the catalytic properties that are induced upon the localised heating produced when the particles are in resonance.[115] Here, a solvent mixture of ethanol and water was passed through a microfluidic cell constructed with an array of gold nanoparticles. When excited with a low power laser the heat produced at the surface of the particles was sufficient to catalyse the breakdown of the solvents and the formation of CO_2, CO and H_2.[115]

Plasmonic structures can also be used to increase the efficiencies of photochemical and photoelectrochemical processes.[116] A number of mechanisms resulting in the increased efficacy of these reactions have been proposed. For example it has been suggested that accelerated reaction rates occur due to the enhanced electromagnetic fields that exist at the surfaces of, and particularly in the nanogaps between, metallic nanoparticles by elevating the molecules involved in the reactions to excited electronic states. The metallic nanostructures essentially act as optical antennas that harvest photons and then concentrate the electromagnetic field produced to excite target molecules in the vicinity. It has also been proposed that other effects associated with excited plasmon resonances such as localised heating and mechanical oscillation may also play a role in

increasing the efficiency of these reactions.[116] The first experimental observation of this effect was reported in 1983[117] and in more recent studies remarkable enhancements of molecular excitement have been reported.[118] Such systems have potential applications in the development of organic solar cells and photoelectrochemical biosensing devices.[118]

An additional application of metallic nanoparticles structured by bottom-up techniques, and one that has been described at length in earlier sections, is in the field of metamaterials, where they are of fundamental importance. The potential contribution that metallic nanoparticles could make to this field is only beginning to be tapped and with the obvious benefits that the use of such methods would entail, increasing efforts are currently being made to further develop the application of metallic nanoparticles.

2.2.7. Nanoparticle safety

No chemicals are 100% safe and with the ever increasing influence that nanomaterials have on modern technology it is inevitable that concerns are raised as to the effect that these substances may have on human health and the environment. This is wholly justified as several examples exist of materials which were once considered to be safe, and indeed advantageous, but whose effects on living organisms were not fully understood and are now regarded as being highly toxic. Asbestos, thin fibrous crystals of silicate minerals, for example, were at one time considered to an excellent material due to their fire-retardant properties and were widely used in the construction industry. When broken up into smaller particles, however, they are now recognised as being highly toxic, causing numerous lung illnesses. This example of a large difference in toxicity, dependent on the size of the material, leads to serious concerns as to the safety of nanomaterials.

Nanoparticles are of such great interest principally as a result of the special properties that they display and these properties exist uniquely at the nanoscale. As such, it is reasonable to assume that they may also possess significantly differing toxicity levels from their bulk counterparts. The properties of nanomaterials are themselves often size and shape dependent and samples of nanoparticles generally display a distribution of both parameters. This can also have a knock-on effect on the toxicological profile of the sample. As a result, nanoparticles should be subject to thorough testing and stringent controls ensuring, to the greatest possible extent, that their potential harm is fully understood. Several review articles exist giving an overview of what is now a not insubstantial body of work that has been carried out in this area.[119, 120, 121, 122] While it is encouraging that such work is now being carried out more extensively it is difficult to draw specific conclusions for a variety of reasons. Not least of which is the apparent lack of standardisation of testing methods

and terminology which would allow direct comparisons to be drawn.[62] Nevertheless several general pieces of information have been abstracted from the literature by Ozin et al. in their book 'Nanochemistry – A Chemical Approach to Nanomaterials'[62] and are listed below:

i) *Nanostructures should be prevented from dissolving into the organism. Even iron oxide nanocrystals can elicit toxicity if their surface is unprotected.*

ii) *Surface coatings greatly limit the dissolution of the nanostructure.*

iii) *Organic coatings on the nanoparticles often determine the majority of the toxicity as the employed molecules can be themselves toxic.*

iv) *Surface-charged nanocrystals are more toxic than neutral nanocrystals. Cationic ones especially.*

v) *Toxicity is often bound to internalisation of the nanostructure by the cells.*

vi) *Colloidal nanostructures often aggregate leading to their accumulation in the liver and spleen. Colloidal stability and probably the hydrodynamic radius are key to the successful excretion of the nanostructures.*

The effect that nanomaterials can have on human health is of paramount importance but it is not the only issue that has to be considered. Nanoparticles can also have deleterious effects on the environment and their ubiquity in modern life, from UV blocking titania particles in sun cream to anti-bacterial silver nanoparticles in socks, means that their potential impact is of ever increasing importance. Governmental bodies throughout the world are beginning to recognise both the potential benefits and possible harm entwined with novel technologies that use nanoscale substances and several guidelines now exist detailing what exactly constitutes a nanomaterial and the special risk assessments and controls that should be carried out prior to their production and use. This can be considered as a step in the right direction but clearly much remains to be done in terms of further research and standardisation of procedures and terminology to ensure both safety and public perception of safety in this field.

2.3.Polyelectrolyte multilayers

The use of electrostatic forces to assemble metallic nanoparticles, and indeed other nanoscale materials such as polymers,[123] semiconductors[57] and oxides[124] to name but a few, has proven to be one of the most versatile techniques available to materials scientists endeavouring to prepare superstructures from these smaller units. Electrostatic interactions between two charged species can be either attractive or repulsive and both the strength and range can be controlled by regulating the density of the charges on the species, altering the concentration of ions in solution or adjusting

the dielectric constant of the surrounding solvent.[65] In nanoparticulate systems the origin of the charge derives predominantly from one of two sources; charged or dipolar functionalities contained within the molecular capping layer which coats the particles or the EDL which is set up in the volume surrounding the particles and which was discussed in greater detail in Section 2.2.1. As a result of this charge the nanoparticles lend themselves to self-assembly methods governed by electrostatic forces. Self-assembly techniques using these forces were first reported in 1966 by Iler, who assembled oppositely charged silica particles,[125] however it was not until the 1990s that these methods rose to prominence with the advent of PE multilayers.[123]

The layer-by-layer assembly of PEs – polymers with high densities of charged units built into the structure – allows the construction of thin films of dielectric materials and is one of the most flexible and widely used techniques for self-assembly.[123] While studies of the layered adsorption of molecular species have existed for several decades, perhaps most notably using Langmuir-Blodgett or chemisorption techniques,[126] several advantages exist when using charged polymers to build up structures fabricated from defined numbers of distinct layers. No special equipment is required and the method is quick, cheap and applicable to a host of different situations. For example, unlike other coating systems, it is possible to implement the technique on an industrial scale – coating macroscopic samples while at the same time maintaining control over the composition of the coatings at a molecular level. The assembly of PE multilayers is an exceptionally environmentally friendly process, being predominantly aqueous based, and can be applied to substrates of almost any shape or form – from planar surfaces through to colloidal nanoparticles and porous solids. The process essentially involves the deposition, on a charged substrate, of a polymer of opposite charge using nothing more than electrostatic interactions. After a washing step another polymer layer, again of opposite charge, can be deposited. The second polymer not only compensates the charge on the layer below but overcompensates it – allowing the repetition of the deposition process in a cyclic manner as many times as is required for the purpose at hand. While a periodic structure results there is still an appreciable degree of interpenetration between subsequent layers.[127] With the majority of polymer systems that are suitable for this technique, including the two 'classic' PEs poly(4-sodium styrene sulfonate) (PSS) and poly(allylamine hydrochloride) (PAH), the structures of which are shown in Figure 9, film thicknesses increase linearly as a function of the number of layer pairs deposited.[128] However, in certain systems supralinear film growth has been observed.[129] The exponential growth of film thickness as a function of the number of depositions allows thicker films to be assembled in significantly less time. Materials such as silicon, glass and poly(dimethylsiloxane) (PDMS), selected for their electronic, optical and mechanical properties respectively, can be

functionalised in a facile manner in order to induce the electrostatic interactions that are required for the use of this method.[130]

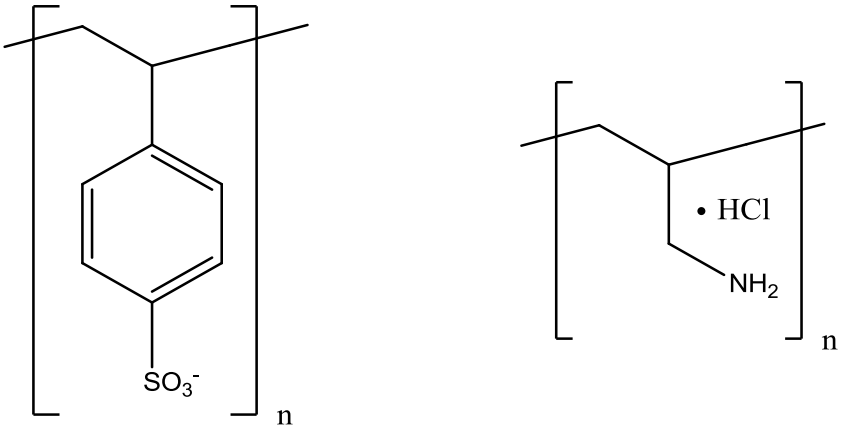

Figure 9 – Chemical structures of the 'classic' polyelectrolytes. On the left is the negatively charged poly(4-sodium styrene sulfonate) and on the right is the positively charged poly(allylamine hydrochloride).

It is generally accepted that certain properties of PE multilayer films are wholly dependent on the last deposited layer or species. The surface potential, wettability, as well as certain biological properties (the film could act as a pro or anticoagulant)[131] all depend entirely on the polymer layer at the film interface. Despite the importance of the surface layer to the properties of the film there are also a number of factors that can affect the final form and bulk properties of the PE multilayer film. It has been shown that drying the film between subsequent depositions can increase the surface roughness and therefore the overall thickness of the film.[132] However it must be noted that the extent to which this plays a role is dependent on the choice of PE and the effect is not always observed. The polydispersity of polymer chains also plays a significant role for the stability of PE multilayer films. It has been reported that such films, when exposed to an NaCl salt solution, will etch to a greater extent when they are constructed from polymers possessing a higher polydispersity index.[133]

Film stability can also be improved by crosslinking separate PE layers, forming covalent bonds between them and thus increasing the overall mechanical strength of the film and reducing its sensitivity to external stimuli. This can, of course, only be carried out when suitable polymers are used, with polymers containing carboxyilic acid and amino groups particularly lending themselves to this process due to the relatively facile formation of amide bonds.[127] This can be carried out, for example, by simply heating the film to 130 °C[134] or by incubating the film in a solution of carbodiimide.[135] In the heat assisted method the extent of crosslinking, which can be measured using infra-red techniques, can be increased by further raising the temperature used to cure the

sample. The formation of the covalent network throughout the bulk of the film completely changes its properties – a notable example being the reduction of the permeability of films to $FeCN_6^{3-}$ complexes by several orders of magnitude.[134]

Another means of tuning PE multilayer film properties is through the construction of films that are not based on only two components. With each polymer having its own specific properties derived from its chemical structure it is possible to create a system that incorporates several of these in a multilayer system. There is also the potential to create blends of two or more polyanions or polycations within a single layer which would allow for the continuous change of properties throughout a film by gradually altering the molar fractions of each component within the blend.[127] In the majority of cases where such blended films have been produced it has been found that there is a strong preferential deposition of one component over another meaning that the molar fraction of each in solution is not necessarily the same as that in the eventual film.[127] This however can be tuned to a large extent allowing the desired composition in the film to be achieved.

Additionally, the assembly of PE multilayers can be carried out by a variety of different means – each one having attributes that make it suitable for particular situations. By far the most common method is simple dip-coating, allowing the layers to self-assemble on the substrate in solution. Both the adsorption and washing process can be carried out in around two minutes and can be relatively easily automated using a simple dip-coater. However these polymers can also be spin-coated[136] and even sprayed[137] onto substrates, resulting in even faster depositions. This can even be considered as another means of tuning the properties of PE multilayers. Studies have shown that films prepared by spin or spray-coating tend to be thicker, more stratified and less rough than their dip-coated counterparts.[138, 139]

A wide variety of analytical techniques can be used to measure the growth of PE multilayers. The adsorption of distinct layers can be directly measured using techniques such as UV-vis[140] and infrared spectroscopy, as well as quartz crystal microbalances.[132] X-ray[45] and neutron scattering[141] techniques have also been used to determine the thickness and interpenetration of individual polymer layers. Non-direct techniques such as ellipsometry can also be employed to model parameters such as layer thicknesses and refractive indices of the thin films.[128]

PE multilayer films have found uses in a diverse range of applications, predominantly in four principal domains; biomaterials coatings, electronic devices, membrane technology and ultrastrong coatings.[127] In the biological domain there is much promise that they could be used in drug delivery systems[142] while conductive polymers have been used to create light emitting diodes[143] and more

recently dye sensitised solar cells.[144] The fact that PE multilayer films can incorporate ions gives rise to possible applications as ion selective membranes[145] and the possibility of incorporating materials such as clays or carbon nanotubes into PE multilayer films has opened up the possibility of preparing structures that mimic that of high strength biocomposites like bone.[146]

Several theoretical studies describing a variety of aspects such as; hypothesised growth models;[147] the interpenetration of consecutive PE layers[148] and the threshold level for short-range attraction strength required for multilayer formation[149] have also aided the development of a fuller understanding of thin film fabrication using PE multilayer techniques.

The combination of the optical properties given to the material by the nanoparticle inclusions with the stimuli responsivity of certain polymers that can be incorporated into PE multilayers leads to a wide range of potential 'smart' materials. For example, selected polymers are capable of swelling or contracting upon changing ionic or pH conditions, interacting with incident light or electromagnetic fields, undergoing conformational changes upon increases or decreases of temperature and can be sensitive to mechanical or electrochemical stimuli.[127] Active materials such as these, already in existence, represent the future of PE multilayer research – moving the field from a novel means of preparing thin films to their incorporation in functional devices in an extremely rapid timeframe.

2.4.Characterisation of metamaterials and metallic nanoparticles

The versatility in fabrication that is offered by bottom-up techniques requires that an equally diverse array of characterisation techniques should be used in order to accurately describe both the structural parameters of assemblies and any properties that they may possess. Of course researchers, working from a design predicted to have advantageous properties, will already have a good idea of what the structure of any prepared assembly *should* look like. However it is important to be able to verify this and structural organisation can be studied through a variety of direct and indirect techniques. When preparing structures at the nanoscale the characterisation of the structure can be particularly challenging and often highly advanced techniques must be applied to obtain topological information.

One such technique is electron microscopy which can be broadly sub-divided into scanning electron microscopy (SEM) and TEM. SEM allows images of a sample surface to be produced by scanning it with a high energy beam of electrons in a raster pattern. Commonly either back-scattered or secondary electrons are collected by detectors placed above the sample surface. High quality images of sample surfaces are achievable, with magnifications of up to 5 x 10^5 times allowing features in the

order of 1 – 5 nm to be resolved. In addition, the technique can also return accurate information on the chemical composition of samples due to the dependence of the intensity of back-scattered electron signal on the atomic number of the point of the sample being scanned. TEM, on the other hand, works on a different principle and forms an image from electrons that are transmitted through a sample. TEM gives access to higher resolution images than SEM, in some cases allowing individual atomic layers and columns to be resolved. However as only transmitted electrons are detected sample thickness is limited to around 100 nm. Whilst this is useful to obtain detailed images of individual metaatoms and, in certain cases, ultrathin slices that have been prepared from larger samples, the use of this method is restricted by these limitations.

Atomic force microscopy (AFM) offers the possibility of imaging surfaces with demonstrated resolution of fractions of a nanometre. Rather than scanning a fine beam of electrons across a sample, as in SEM, a fine tip attached to a cantilever is used. When the tip is brought into close proximity of the sample and scanned across its surface forces between the two cause the tip to move up and down with the form of the surface. Laser light is focussed on the cantilever and reflected onto a detector. It is possible to use the deflection of the beam on the detector to return information on the profile of the sample. As well as providing a two-dimensional image of a sample surface, variations in height are also determined allowing a detailed impression of the three-dimensional profile of a sample to be constructed. In addition to AFM other scanning probe microscopy techniques, such as scanning near-field optical microscopy (SNOM), are also used in the characterisation of nanostructured surfaces.

Other means, such as X-ray diffraction, can be used to reveal in detail the structure of metamaterials. One particular example of such techniques includes grazing incidence small angle X-ray scattering (GISAXS) which is particularly useful when characterising self-assembly in thin films. In essence, a thin film sample, ranging in thickness from a few to several hundreds of nanometres, is struck with a beam of X-rays, incident at a small angle – close to that of total external X-ray reflection. The diffuse scattering from the sample is detected and the diffraction pattern used to reconstruct an accurate impression of the organisation of the units within the sample that scatter the radiation. The technique combines the accessible length scales of small-angle scattering with the surface sensitivity of grazing incidence diffraction.

Although structural information can also be extrapolated from other less direct techniques, for example a red-shift of the surface plasmon resonance indicating two plasmonic nanoparticles moving closer together, these methods are primarily used to return information on the electromagnetic properties of the assemblies under study.

As electromagnetic characteristic parameters cannot be measured directly alternative means must be found to acquire this information. Fortuitously it is possible to retrieve such parameters, normally ε and μ which were introduced in Section 2.1.1, through the post-processing of measured data. The extraction of these parameters from the reflection and transmission coefficients of a sample can be carried out using the classical procedure known as the Nicolson-Ross-Weir method.[150] This is now the most common method of electromagnetic characterisation of composite media and was first applied to metamaterial layers in 2002.[151] However in optics the technique requires difficult precision measurements of the phase of optical signals and other methods, namely spectroscopic and ellipsometric, can be employed in its place to measure the electromagnetic properties of structures.

As has been previously discussed metamaterials are increasingly being fabricated from nanoscale metallic inclusions. Due to their exhibition of a plasmon resonance in the visible region of the electromagnetic spectrum UV-vis spectroscopy, in both reflectance and transmission, is a vital tool in their characterisation. Despite being a relatively simple and cheap technique a surprisingly large amount of structural information, as well as the optical properties mentioned above, can be inferred from such measurements. For example, it is possible to determine both the size and composition of metallic nanoparticles from the position of the plasmon resonance and the full width at half maximum will give an idea of the size dispersity. By analysing the form of a UV-vis spectrum the geometry of the particles under study can be determined, with rod-like particles exhibiting two plasmon peaks compared with only one for spherical particles. In addition, when coupled nanoparticle systems are being studied UV-vis spectra can be interpreted to reveal information on the organisation of assemblies and even interparticle separation. Moreover, when the technique can be combined with an integrating sphere the extinction spectra can be resolved into their absorption and scattering components which is of particular importance for some cloaking applications.[27]

In addition to the experimental techniques described above it must also be noted that theory, and the computing power that supports it, has advanced to the extent that it is now possible to predict the optical properties of structures before they have been fabricated and characterised by measurements. Consequently, this now not only forms an integral part of the design process but also gives a means of verifying results obtained by experimental measurements.

Rather than returning any structural information on metamaterials under study, SERS is a characterisation technique that is *enabled* by metallic structures with features on the nanoscale. SERS, which was discussed in greater detail in Section 2.2.6, essentially involves the enhancement of the Raman scattering from molecules adsorbed on nanoscale metallic surfaces. Raman scattering

refers to the inelastic scattering of photons incident on a material and is an inherently weak process. Only one in ten million photons loses energy to, or gains energy from, the material under study, resulting in Stokes and anti-Stokes Raman scattering respectively. The presence of the nanoscale metallic surfaces enhances this process to the extent where single molecules can be detected and allowing practical applications to be found for the technique.

Whilst being by no means comprehensive this section provides a brief overview of some of the key characterisation techniques, all of which were used during the research carried out as part of this thesis, that are employed to analyse metamaterials prepared and enabled by the bottom-up organisation of metallic nanoparticles. A host of other techniques, many being combinations of several or subtle variations on one another, exist in order to give as full a picture as possible of both the structural detail and electromagnetic properties of such assemblies.

3. Experimental

Unless stated otherwise all chemicals were purchased from Sigma-Aldrich and all solutions were prepared using Milli-Q water (18.2 MΩ-cm).

3.1. Preparation of metallic nanoparticles

3.1.1. Preparation of gold nanospheres

Gold nanospheres with a diameter of approximately 20 nm were prepared according to the well-known Turkevich method.[69] Briefly, 500 mL of an aqueous solution of $HAuCl_4$ (0.25 mM), under constant magnetic stirring, was heated to 100 °C in an oil bath. The gold was then reduced through the addition of 12.5 mL of an aqueous solution of sodium citrate (0.03 M). A series of colour changes was observed before a deep-red solution was produced and after 15 min the reaction vessel was removed from the oil bath and allowed to cool to room temperature.

By altering the ratio of gold salt to sodium citrate it is possible to tune the size of the gold nanospheres.[69] As such, larger gold nanospheres were prepared in much the same manner as described above – simply adding 4 mL of an aqueous solution of sodium citrate (0.039 M) in place of the volume and concentration mentioned above. These larger particles, however, come at the expense of both shape and monodispersity.

3.1.2. Preparation of silver nanospheres

Silver nanospheres can be prepared in an analogous fashion to that described above for gold nanospheres, simply replacing the gold salt for a silver based one, in what is known as the Lee-Meisel method.[70] 1 mL of sodium citrate (0.039 M) in water was added to 25 mL of an aqueous solution of $AgNO_3$ (1 mM) which had been heated to boiling. The solution was left under magnetic stirring for one hour before cooling to room temperature. This resulted in predominantly spherical particles with an average diameter of approximately 40 nm.[152]

Smaller silver nanospheres (~ 6 nm diameter), still stabilised by citrate molecules but using a different reducing agent were prepared by first cooling 196 mL of water in an ice-bath. 2 mL of aqueous solutions of $AgNO_3$ (25 mM) and sodium citrate (25 mM) were added under vigorous magnetic stirring before the reducing agent, 600 µL of an aqueous solution of $NaBH_4$ (0.1 M) was introduced in a dropwise fashion. The solution was left stirring in the ice-bath for a period of two

hours to allow the reaction to achieve completion before the silver nanospheres were stored in a fridge.

3.1.3. Preparation of gold nanorods

Gold nanorods were prepared according to the well-documented seed-mediated growth method.[153, 154] which involves the addition of small seed particles to a growth solution which induces anisotropic growth.

For the growth solution; 250 mL of an aqueous solution of CTAB (0.2 M) was added to a round-bottomed flask kept at 27 °C in an oil bath to ensure that the CTAB does not precipitate out of solution. 12.5 mL of $AgNO_3$ (4 mM) in water and 250 mL of an aqueous solution of $HAuCl_4$ were added to the flask. Three minutes after the addition of the gold salt solution 3.5 mL of an aqueous solution of ascorbic acid (79 mM) was measured into the flask.

The seed solution, again due to the presence of CTAB, was prepared at 27 °C in an oil bath. 5 mL of an aqueous solution of $HAuCl_4$ (0.5 mM) and 5 mL of an aqueous solution of CTAB (0.2 M) were mixed before adding 0.6 mL of freshly prepared, ice-cold $NaBH_4$ (1 mM). The solution was stirred for a further two minutes and left to stand for a duration of five minutes before 0.8 mL of the seed solution was introduced into the growth solution. The reaction was left for a period of around 12 hours upon which the growth of the nanorods was complete.

After the growth of the nanorods is complete it is then necessary to remove excess CTAB in solution. This is achieved through two rounds of centrifugation at a rate of 14000 relative centrifugal force (RCF) for 30 minutes using a Kühner Sigma3-18K centrifuge. After each stage the supernatants, containing the excess CTAB, were removed and the nanorods were redispersed in the same volume of water – ensuring that their concentration remained constant throughout.

3.2.Functionalisation of substrates

3.2.1. Glass and silicon

3.2.1.1. Planar substrates

Glass and silicon substrates, used for spectral measurements and electron microscopy, respectively, were prepared according to the same method. They were first rinsed with water and ethanol before being dried under a stream of compressed air. The surfaces were then cleaned and hydroxylated through immersion in a piranha solution (3:1 mixture of concentrated sulphuric acid to 30%

hydrogen peroxide) for 30 minutes. Piranha solution is strongly acidic and highly oxidising and should be handled with caution. The substrates were next rinsed with copious amounts of water and again dried under a stream of compressed air. Subsequently, the surface chemistry was altered through the functionalisation with an organosilane.[130] Here, the substrates were immersed in a 5% (v/v) solution of N-[3-(trimethoxysilyl)propyl]ethylenediamine in ethanol for 30 minutes before being rinsed with water, dried, and set in an oven at 120 °C for a further 30 minutes.

3.2.1.2. Spherical substrates

Uniform silica microspheres with a mean diameter of 260 nm were purchased from Bangs Laboratories, Incorporated. 0.5 mL of the as-bought microspheres was added to 2 mL of a 5% (v/v) solution of N-[3-(trimethoxysilyl)propyl]ethylenediamine in ethanol and mixed under magnetic stirring for 30 minutes. Excess organosilane was removed by centrifuging the solution at 2000 RCF for 10 minutes before removing the supernatant and redispersing the now functionalised silica microspheres in 2 mL of ethanol.

The same microspheres, when already deposited on planar substrates (as described in Section 3.3.1), could be functionalised by exposing to a 5% (v/v) solution of N-[3-(trimethoxysilyl)propyl]ethylenediamine in ethanol for 30 minutes before rinsing with water and drying under a stream of compressed air.

3.2.2. Polydimethylsiloxane

The surface chemistry of PDMS, prepared and supplied by colleagues, can also be functionalised using similar reactions to those described above for silica and silicon. The substrate was first exposed to a low power air plasma for 90 seconds before being immersed in a 1% (v/v) aqueous solution of (3-aminopropyl)triethoxysilane for 30 minutes. It was then washed in copious amounts of water before being dried under a stream of compressed air.

3.3.Deposition

3.3.1. Nanoparticles

3.3.1.1. Silver and gold nanosphere arrays

Both silver and gold nanospheres were deposited on planar substrates (silicon, silica, PDMS or silica microspheres adsorbed on a planar substrate) either functionalised with amino groups or a positively charged PE layers by immersing them in a solution of the nanoparticles for a period of two

and a half hours. The substrates were then washed with water and dried under a stream of compressed air.

3.3.1.2. Core-shell nanoclusters

Core-shell nanoclusters were prepared by adding 10 µL of functionalised SiO_2 microparticles (260 nm diameter) to 40 mL of as prepared gold nanospheres under vigorous magnetic stirring.

3.3.1.3. Gold nanorod arrays

A functionalised substrate coated in a single layer of PSS (see Section 3.3.2) was immersed in a solution of gold nanorods which had been adjusted to have a concentration of 200 mM of NaCl. The substrate was left in the solution overnight to maximise surface coverage before being removed, washed in water and dried under a stream of compressed air.

3.3.1.4. Silica microparticle arrays

Large area arrays of SiO_2 microspheres (150 nm diameter) were deposited on functionalised glass or silicon substrates by immersing the substrates in a solution of the particles which had been adjusted to pH 5 through the addition of a dilute solution of HCl. The substrate was then removed, washed with water and dried in a stream of compressed air.

3.3.2. Polyelectrolytes

PE layers were deposited from 5 mg/mL solutions of PAH and PSS in a solution of sodium chloride in water (0.1 M). The structure of both of these polymers can be seen in Figure 9. PE layers were deposited for 1 minute before being rinsed with water and dried under a stream of compressed air. The electrostatic nature of the fabrication process allows for the cyclic build-up of multiple gold nanoparticle and PE layers. Where a large number of polymer layers were to be assembled a purpose built dip-coater was used.

Rather than using electrostatic interactions to build up a series of polymer layers, hydrogen bonding can also be exploited in layer-by-layer deposition techniques.[127, 155] Poly(acrylic acid) (PAA) and poly(ethylene glycol) (PEG) layers were deposited on functionalised glass substrates by immersing them in 2 mg / mL aqueous solutions of the polymers which had been adjusted to pH 2 through the addition of dilute HCl. The construction of these polymer layers was carried out using a purpose built dip-coater and all washing steps were conducted using water which had also been adjusted to pH 2.

3.4.Nanoparticle density

The citrate capping molecules at the surface of metallic particles organised into arrays can be replaced by exposing the array to a solution of thiol molecules which have a particularly high affinity for gold. This results in the mobilisation and reorganisation of the particles at the substrate surface. Arrays of gold nanoparticles were exposed to an ethanolic solution of dodecane-1-thiol overnight before being gently rinsed with ethanol and dried in a stream of compressed air. With further gold nanoparticle deposition in-between the process can be repeated in a cyclic manner allowing several reorganisation steps to be carried out.

3.5.Characterisation

3.5.1. UV-vis spectroscopy

UV-vis spectra were primarily measured on a Cary Varian 50 Bio UV-Visible spectrophotometer.

3.5.2. Scanning electron microscopy

Scanning electron micrographs were primarily acquired on a JEOL JSM-7600F scanning electron microscope.

3.6.Miscellaneous

3.6.1. Optical lithography

The positive photoresist AZ® 1518 was diluted in a 1 : 1 ratio with AZ® 1500 Thinner (both chemicals supplied by Microchemicals) and spin-coated at speeds of 1000 – 3000 r.p.m. in order to achieve a film thickness of 500 nm onto pre-functionalised (see Section 3.2.1.1) silicon substrates. The substrate was then baked at 40 °C for 30 minutes before increasing the temperature to 50 °C for a further 30 minutes. The pattern of choice was then set into the resist by exposing it through a chromium mask for 1 to 5 seconds on a MABA 8 machine from Süss Microtech. Development of the photoresist was then carried out through exposure to AZ® 351B which had been diluted in the ratio 1 : 8 with water.

3.6.2. Surface enhanced Raman scattering

1 µL of an aqueous solution of Nile blue (0.1 mM) was dropcast on the samples and allowed to dry at under standard conditions.

The SERS spectra were recorded with a WiTEC GMbH Raman microscope using 633 nm laser light as the excitation source. The laser was focussed on the sample using a 100x microscope objective, giving a resultant power of 0.5 mW incident on the samples. A CCD camera operating at -65 °C was used to detect the scattered Raman radiation.

4. Results and discussion[3]

4.1. Planar arrays of metallic nanoparticles

4.1.1. Introduction

For the reasons expounded in Section 1.3, not least of which being their potential application in sub-wavelength imaging,[28] stratified arrays of metallic nanoparticles are of significant interest to metamaterials researchers. While top down methods can be used to prepare metallic nanostructures on planar substrates it is not trivial to extend these structures into the third dimension meaning that, in general, only in-plane interactions between the structures can be studied. Geometry can often be tailored to unprecedented precision using techniques such as EBL however resolution, in terms of structure separation for example, remains limited by resist materials, proximity effects and electron beam width. In addition, the perfect order that is normally observed in samples prepared by top down procedures can, in certain cases, introduce strong spatial dispersion which hampers the unambiguous designation of effective material parameters.[156]

Bottom up techniques, on the other hand, offer solutions to many, if not all, of the above problems. Metallic nanoparticles can be grown with a large degree of control over a variety of material parameters such as particle shape, size, composition and surface chemistry. Polymer materials present the perfect foil to metallic nanoparticles when looking to make such layered arrays by bottom up techniques. As dielectric spacers they allow metallic nanoparticles to be separated by exceptionally low distances that could not be achieved using top down methods. Samples are no longer restricted to two-dimensions and, in general, bottom up methods result in amorphous arrays of particles which do not result in spatial dispersion.

As a result, combinations of nanoparticles and polymers were chosen as ideal systems with which to study a wide range of material properties. The flexibility of fabrication allows factors such as interparticle separation, particle size effects and coupling properties between particles, amongst others, to be characterised with high precision. Such systems also have the additional advantage that samples can be readily fabricated at comparatively large scales (cm^2). This allows them to be characterised using standard spectroscopic techniques and in the long-term raises the chances of applications being developed and their incorporation into functional devices.

[3] Some passages in this section will be published in the chapter entitled 'Bottom-up organisation of metallic nanoparticles' written by Alastair Cunningham and Thomas Bürgi contained in the book 'Amorphous Nanophotonics'. Edited by Carsten Rockstuhl and Toralf Scharf, the book will be published in 2013 by Springer-Verlag Berlin and Heidelberg GmbH & Co. KG.

A variety of methods that facilitate the preparation of such samples exist, each having their own beneficial and detrimental attributes. For example, the interactions between different polymer blocks and the ligands capping the nanoparticles control the selective spatial distribution of the nanoparticles in particular block copolymer microdomains or, alternatively, the interface between two blocks. This difference in affinity has been shown to induce their organisation into, depending on the relative ratio of each polymer component, lamellar arrays or hexagonally packed cylinders.[157] The fabrication process, involving spin-coating of solutions onto substrates, allows for the facile application of this technology. Macroscopic samples can readily be produced using infrastructure that is already well developed. However it can be difficult to achieve thin films where only a single layer of nanoparticles are found in each array. Additionally, the area over which organisation of the block copolymers, and therefore nanoparticles, exists is generally limited to smaller ordered domains.

The use of PE multilayers, introduced in Section 2.3, offers an alternative route to stratified metallic nanoparticle arrays. Like the block copolymer technique described above, spin-coating can be applied to create large scale substrates.[158, 159] As previously, due to its widespread use in a variety of industries, for example the manufacture of compact discs, this technique lends itself to the mass production of samples. It was also found that the density of nanoparticles adsorbed is strongly dependent on the deposition time allowing high density films to be prepared.[158] However it is difficult to judge what deposition time is required for full surface coverage with longer times possibly resulting in defects and inhomogeneities at the film surface.

One, perhaps more elegant, solution which results in almost absolute control over the geometrical parameters and the optical properties of such structures would be to allow the components to self-assemble at the surface of the substrate resulting in the true bottom-up assembly of metallic nanoparticle and polymer composites.[45, 160] While possibly more time consuming than spray or spin-coating techniques this method retains the ability to be translated to large scale systems and as such is not limited to laboratory scale applications. Structures prepared by these methods will be discussed in more detail in this section (4.1).

4.1.2. Single array

The construction of metallic nanoparticle and charged PE multilayers occurs purely as a result of electrostatic interactions between the relevant components. To deposit an array of gold nanoparticles, which are inherently negatively charged at pHs above their point of zero charge, on a substrate it is first necessary to functionalise that substrate in order to render it positively charged.

This process was fully described in Section 3.2.1. Once functionalised it suffices simply to immerse the substrate in a solution of the particles and allow them to self-assemble at the surface as a result of the attractive electrostatic forces that exist between the two. The time taken for complete surface coverage is dependent on a number of factors such as the concentration of the nanoparticle solution and whether or not the solution is mechanically agitated. The overall density of the final film is determined largely by the extent of the electrostatic repulsion between individual nanoparticles which prevents a second particle from closely approaching one that is already adsorbed at the surface.

The adsorption of gold nanoparticles on planar functionalised substrates can be modelled using the random sequential adsorption (RSA) model.[161] This model, as the name suggests, describes the adsorption of a species at a random location on a substrate surface in a sequence of 'events' that proceed linearly with time. In the model, a species will adsorb if no prior adsorption event has already taken place within a radius that would overlap with the successful adsorption of the incoming body. In this manner the percentage coverage of the surface of the substrate, also known as the filling fraction, increases, at first rapidly before decreasing in rate as the number of potential adsorption sites diminishes. The maximum filling fraction predicted by the standard RSA model, also known as the jamming limit, is 0.55 assuming that there is no interaction between the spheres and that they are allowed to contact each other. This is considerably lower than what would be observed if perfect hexagonal close-packing of equally sized spheres were to be achieved (0.91) and highlights one of the effects that disorder can have on a system.[162] Several variations of this model, each with differing levels of complexity and describing differing situations, exist. While the standard model describes irreversible adsorption, modifications, including the possibility of reversible desorption based on kinetics and sticking coefficients, allow equilibrium states to be more accurately modelled.[163] Other similar models include the ballistic deposition (BD) model which allows the incoming particle to 'roll over' a pre-adsorbed species, if the deposition event involves overlap between the two, and follow the path of steepest descent to the surface.[164] This has a dramatic effect on the probability that a specific event will result in the successful adsorption of an additional species and is perhaps again a means of more accurately modelling the true situation as more than one preadsorbed particle is required to block the adsorption of another. Another outcome found when using the BD model is that the density of particles at saturation coverage increases to 0.61 when compared to the standard RSA model.[164] This is as a result of the rolling mechanism that allows, at least to some extent, a degree of surface rearrangement. Other, more advanced, developments have allowed the deposition of liquid particles, complete with incorporation and coalescence events, to be modelled.[162] While perhaps not quantitatively reflecting the final density

achieved, this model at least reasonably accurately describes the process of gold nanoparticle adsorption at the surface of a planar substrate.

An example of a glass microscope slide that has been suitably functionalised and coated in a complete array of well dispersed and approximately equally spaced gold nanoparticles can be seen in Figure 10a. It displays a characteristic pink colour which originates from the strong extinction peak that exists at around 520 nm – the LSPR wavelength. The colour is surprisingly strong, given that only a single layer of nanoparticles, with a diameter of around 20 nm, has been adsorbed at a relatively low density or filling fraction. The particles, which are, at least to some extent, mobile at the surface, are capable of rearranging to find an organisation representing a low energy state. This is why, post-deposition, we observe the particles at reasonably well defined distances from one another, as can be observed in the SEM micrograph shown in Figure 10b. No long range order, however, is perceived which, as can be expected, is due to the random adsorption processes described above. The only limitations in terms of overall substrate size that can feasibly be coated are of a practical nature. The arrays are virtually defect free and as such this technique quite easily lends itself to applications on relatively large scales.

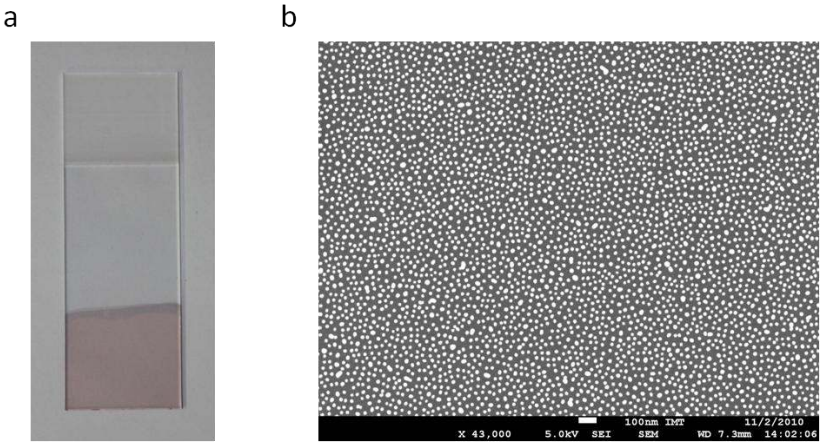

Figure 10 - a) Photograph of single array of gold nanoparticles deposited on a functionalised glass microscope slide. b) Corresponding SEM micrograph showing organisation of a single array of gold nanoparticles (~20 nm diameter) on a Si substrate which had been previously functionalised.

Detailed analysis of the SEM micrograph shown in Figure 10b using image processing programs such as *ImageJ*[165] enable such arrays to be more fully characterised. It is possible to count thousands of particles over relatively large areas to achieve accurate average values for important material parameters such as particle density and size. Such an analysis reveals that the particles deposit at the surface with an average density of around 850 particles / μm^2 which equates to a filling fraction of 27%.[160] That this is significantly lower than the jamming limit predicted by the RSA model is no

surprise as the particles are not able to approach to within contact distance due to the citrate capping molecules that induce electrostatic repulsion. Taking this into account, it is reasonable to assume that a modified RSA model could accurately predict the filling fraction experimentally observed.

Figure 11 shows the extinction spectra of an array of gold nanoparticles immobilised on a functionalised glass microscope slide (blue trace, left-hand axis) and the solution of gold nanoparticles from which they were deposited (red trace, right-hand axis).

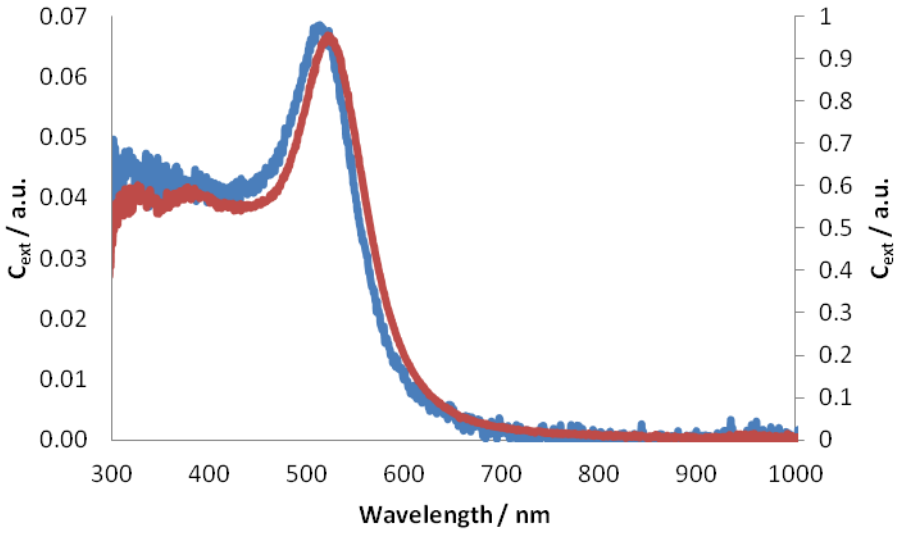

Figure 11 – Extinction spectra of an array of gold nanoparticles with a diameter of approximately 20 nm adsorbed at the surface of a functionalised substrate (blue trace, left-hand axis) and a solution of gold nanoparticles with the same diameter (red trace, right-hand axis).

Comparing the optical properties in such a manner reveals that there is only a slight shift in the plasmon resonance, which occurs at 513 nm for the array deposited on the substrate and at 521 nm for the gold nanoparticles in solution. The slight discrepancy in the precise position of the surface plasmon resonance can be explained by the differences in environment in which they were measured. While the gold nanoparticles in the array are also in contact with the substrate they are predominantly exposed to air which has a refractive index close to that of vacuum (n = 1). In solution the gold nanoparticles are completely surrounded by water which, due to its higher refractive index (n = 1.33), is sufficient to cause the shift in surface plasmon resonance observed, as was discussed in Section 2.2.3. Metallic nanoparticles must approach to within the order of the diameter of a single particle in order to interact with each other to an appreciable extent.[37] That only a slight shift in plasmon resonance is perceived demonstrates that the array of nanoparticles is not of a high enough density to induce strong coupling between the nanoparticles within the plane. When considered

alongside the SEM image shown in Figure 10b, it becomes even more evident that the nanoparticles are not close enough to couple with one another. This, for certain situations, has significant advantages. In the case where a second array of metallic nanoparticles were to be deposited on top of the first, with a dielectric spacer in-between, any changes in the optical properties can be solely attributed to the interaction of gold nanoparticles from separate arrays. Such interactions will be discussed in more detail in Section 4.1.4.

While the fabrication of such large scale amorphous arrays of metallic nanoparticles is certainly extremely useful, not least in terms of the lack of spatial dispersion and ease of which the technology could be developed into potential applications, in some cases a degree of order is required when preparing such structures. This can be readily achieved when the above functionalisation and deposition techniques are combined with photolithography. By coating a functionalised substrate, glass or silicon, with a photoresist and exposing this to light through a suitably designed mask it is possible to recreate the form of the mask in the resist. Either positive or negative photoresists, which after exposure to light become soluble or insoluble to developing solutions respectively, can be used to create patterned surfaces. After this process, only certain areas of the functionalised substrate, when immersed in a solution of metallic nanoparticles, will be exposed to the solution and will form nanoparticle arrays. Examples of this work, which was carried out in collaboration with Toralf Scharf and Irène Philipoussis Fernandez of the École Polytechnique Fédérale de Lausanne, can be seen in Figure 12.

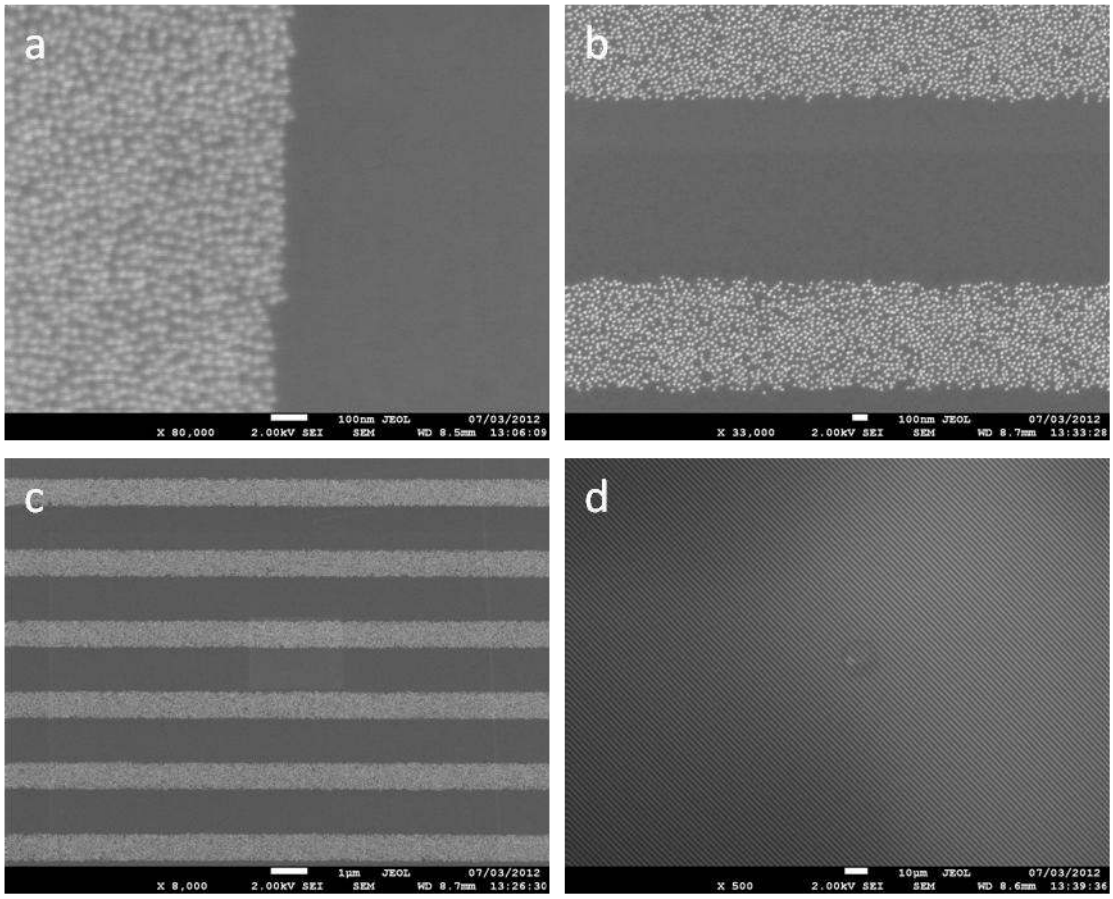

Figure 12 – SEM images of a striped array of gold nanoparticles (~20 nm diameter) deposited on functionalised Si substrates pre-patterned using optical lithography techniques. Images at four different magnifications are shown: a) 80000×, b) 33000×, c) 8000× and d) 500×.

As can be seen, the samples exhibit extremely good line sharpness and very few defects over large areas. The extent to which large areas can be easily coated with patterned arrays of metallic nanoparticles can be seen in Figure 13, where nanoparticles have been deposited in certain areas that show up as white in the SEM image, which shows a total area of approximately 5 mm^2. Figure 13 also shows that arrays prepared by combining lithographic and bottom-up self assembly techniques are not limited to regular patterns and that arrays of any form, dependent solely on the mask in use, can be fabricated.

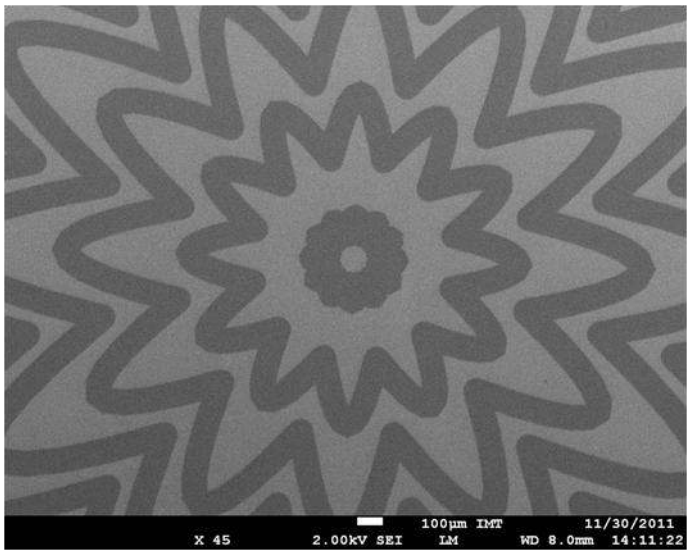

Figure 13 – SEM image showing patterned array of gold nanoparticles (~20 nm diameter) deposited on functionalised Si substrates pre-patterned using optical lithography techniques.

The resolution of structures prepared by photolithography, despite massive advances in the technology, remains significantly lower than that achievable by other means, one notable example being EBL. In principal the same procedure described above could be applied using this more powerful technique to write even smaller structures into resists which have been coated on functionalised substrates. This could allow individual nanoparticles, which in Figure 12 and Figure 13 are larger than the achievable resolution of the writing technique, to be placed in essentially any order and pattern desired.[166] This has obvious benefits in the preparation of metamaterials at optical frequencies. Whereas some of the architectures introduced in Section 1.3, such as SRRs and fishnet structures, are inaccessible using pure bottom-up techniques this hybrid approach could lead to their fabrication while all of the benefits resulting from bottom-up techniques are maintained. In addition to the potential advancements in the field of metamaterials using the more sophisticated lithographic techniques, other applications, such as plasmonic waveguides and diffraction gratings, could also be envisaged from structures, such as the ones shown above, prepared by optical lithography.

The planar arrays of gold nanoparticles discussed above, patterned or not, all have a filling fraction of approximately 27%. While such a relatively low surface coverage can result in a strong colouration of substrate, and in many respects results in several advantages, there may be instances whereby it could be desirable to have surfaces that were coated to either a greater or lesser extent. For example some simulations[102] suggest that for a sufficiently high dispersion in the effective permittivity to be achieved the filling fraction of arrays of metallic nanoparticles, such as the ones

under discussion here, should be higher than 30%. For smaller filling fractions the large magnitude of the permittivity, necessary to observe Mie-resonance for sufficiently small spheres, is not achieved. Consequently a reliable means must be found to control the density of nanoparticles deposited in such arrays of metallic nanospheres.

4.1.3. Controlling nanoparticle density

4.1.3.1. Deposition time and concentration

The most obvious way to control nanoparticle density on a planar substrate is to alter either the deposition time or the concentration of the solution from which the nanoparticles are deposited. Decreasing the deposition time from the point at which complete surface coverage is achieved will result in lower density arrays of nanoparticles. When considered in terms of the RSA model set out in Section 4.1.2. it can be seen that this can be equated with decreasing the number of deposition events that are allowed to occur. Similarly, decreasing the concentration of the nanoparticle solution will result in lower density arrays when compared to substrates immersed in more concentrated solutions for the same length of time. Again, considering the RSA model, this can be likened with simply decreasing the rate of the deposition events. It is clear, however, that either of these techniques can only be used in order to tune the density of the particles up to the point at which surface coverage is complete and will not aid in preparing the higher density arrays that are required for some applications.

4.1.3.2. Controlling the electrostatic double layer

Given that the prime limiting factor governing the final density of metallic nanoparticles in an array is the charge that exists on the particle surface, it is clear that in order to prepare higher density arrays this charge must be, at least to some extent, mitigated. As introduced in Section 2.2.1, the repulsion between two nanoparticles in solution is a consequence of the EDL. The Debye length, being inversely proportional to the square root of ion concentration, can be decreased through the addition of salt to the solution, thus allowing the closer approach of particles in both solution and on surfaces.

Figure 14 shows SEM images of arrays of gold nanoparticles, approximately 20 nm in diameter, that have been deposited from solutions containing different concentrations of NaCl. The solution of gold nanoparticles used to fabricate the arrays shown in Figure 14a had been dialysed to remove any excess sodium citrate. The solutions from which the samples shown in Figure 14b and Figure 14c had been deposited had NaCl added to a final concentration of 1 mM and 10 mM respectively. The

increase in nanoparticle density as the concentration of salt is increased, measured using *ImageJ* and tabulated in Table 1, can also clearly be seen in the SEM images in Figure 14. In the sample that underwent a dialysis process the EDL is extended and the close approach of individual nanoparticles, either in solution or at the surface of the substrate, is inhibited. On the other hand, when NaCl is added to the solution the Debye length diminishes and the nanoparticles are free to approach one another to a greater extent. However, if too much salt is added the electrostatic repulsion between particles is no longer great enough to ensure particle stability and they can be seen to aggregate, as is the case in Figure 14c.

Sample	Filling fraction	Nanoparticles / μm^2
Dialysed	0.13	420
1 mM NaCl	0.37	1180
10 mM NaCl	0.47	1450

Table 1 – Table showing filling fraction and nanoparticle density for gold nanoparticle arrays deposited from solutions containing different concentrations of NaCl.

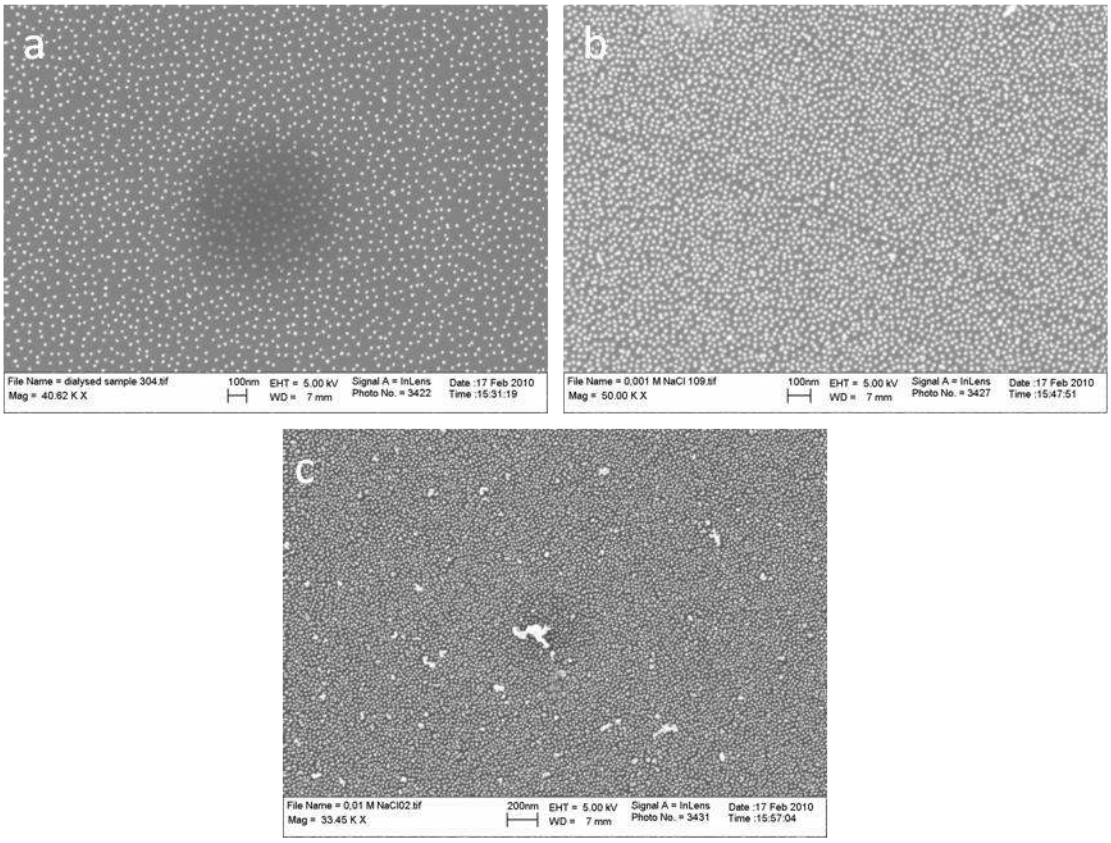

Figure 14 – SEM images showing gold nanoparticle (~20 nm diameter) arrays deposited from solutions with varying NaCl concentrations. a) – Dialysed sample, b) – solution containing 1 mM NaCl, c) – solution containing 10 mM NaCl (corresponding to data in Table 1).

4.1.3.3. Thiol wash process

Rather than reducing the mutual repulsion between nanoparticles by regulating the distance that the EDL extends from their surface an additional approach is the removal, at least to some extent, of the citrate molecules that cause this repulsion in the first instance. One means of realising this is through making use of the strong sulphur – gold bond and the high affinity that thiol molecules have for gold.[167] When an array of gold nanoparticles is exposed to a solution of thiol molecules a proportion of the citrate capping molecules, largely dependent on the relative concentrations of the two ligands, will be replaced in an exchange reaction. As such, the pre-existing negative charge on the particles is, at least partially, removed along with the barrier to closer approach and reorganisation at the surface.[168] This part replacement of the citrate molecules which previously formed a protective shell at the surface of the nanoparticles results in a number of changes in terms of the organisation and morphology of the gold nanoparticle array. Disadvantageously, a number of gold nanoparticles are solubilised and desorb from the surface as their electrostatic attraction to the

substrate is diminished. This, due to the high affinity that the thiol molecules have for gold, is unavoidable.

However, the same removal of charge which causes this desorption of a small proportion of the nanoparticles also induces a reorganisation of the ones that remain at the surface. This has a number of consequences in terms of changing the optical and morphological characteristics of the sample as well as opening up a number of possibilities with respect to flexibility of structure fabrication and meeting design goals. Where previously, as shown in Figure 10b, an array of well-separated gold nanoparticles is formed, when the barrier to reorganisation has been removed the particles increase in mobility and tend to aggregate into small chains and clusters of around 5 – 10 particles. This process is thought to be driven by the energetically favourable formation of bilayers of the relatively long alkyl chains that form the second functionality of the thiol molecules employed in this work, namely 1-dodecanethiol. Crucially, any coalescence of the particles is prevented by the bilayers of the thiol molecules that are formed as they are drawn together which is essential in terms of maintaining the plasmon resonance that they exhibit. The thiol molecules, or more importantly the length of the alkyl chain, also determine the closest distance to which the gold nanoparticles can approach one another which in this case is on the order of 1 – 2 nm. A by-product of forming these clusters, along with the desorption of a limited number of particles, is the appearance of large areas of void space at the surface of the substrate. Previously the particles were well-dispersed and equally spaced indicating that a steady state had been reached and a maximum surface coverage, under these particular conditions, had been reached. After exposure to the thiol solution this is now clearly not the case. It is possible, as the void areas at the surface remain functionalised with the silane compound, to subject the substrate to a second deposition process. This second round of adsorption will fill in these gaps with arrays of well-spaced particles similar in form to that of the original. The new array will in turn, if exposed to the same thiol solution, undergo an identical mobilisation and reorganisation process, forming larger clusters of closely packed gold nanoparticles. This process can be easily followed using SEM, as shown in Figure 15, and if repeated several times results in a much higher density array of gold nanoparticles which, in small domains at least, are organised in a close-packed manner. This is clearly a significant step towards achieving higher density arrays of metallic nanoparticles which are required, in some cases, to give specific optical properties.

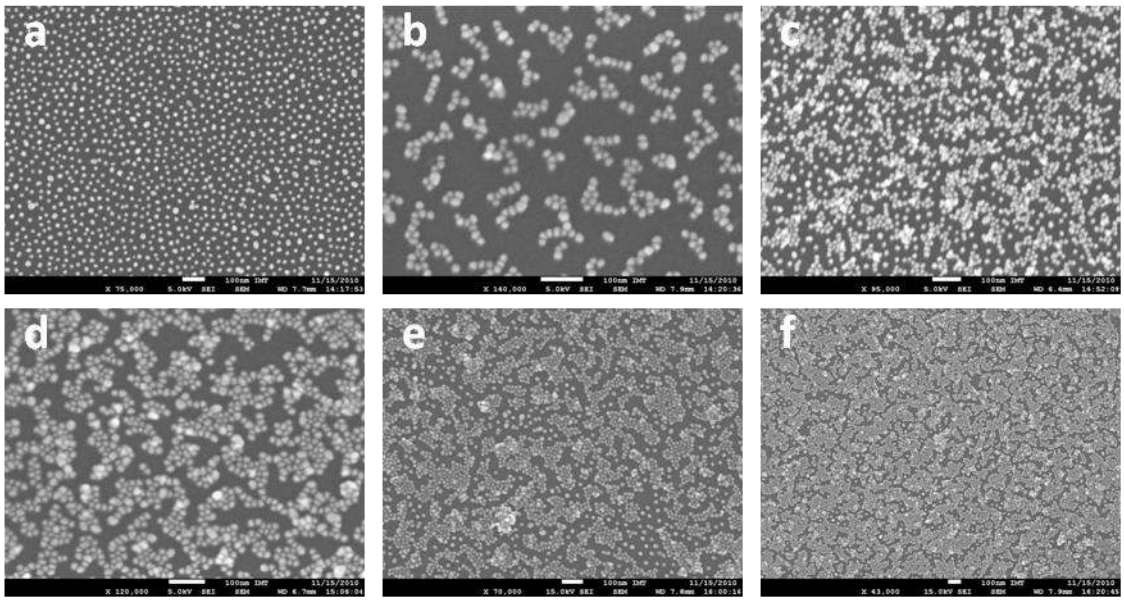

Figure 15 - SEM micrographs depicting various stages of the deposition and reorganisation process as described in the main body of the text. Shown are the morphology that could be expected after a) the first deposition, b) the first reorganisation, c) the second deposition, d) the second reorganisation, e) the third deposition and f) the fourth deposition. An increase in particle density as well as the introduction of a degree of order can clearly be observed. All scale bars 100 nm.

The increase in filling fraction and order after this process is carried out is clear to the eye when SEM images are compared and contrasted. However, it is also possible to quantify these changes by analysing the micrographs using *ImageJ*.[165] Figure 16a shows the radial distribution function for a low density array of gold nanoparticles before it has undergone the reorganisation and deposition process while Figure 16b shows the radial distribution function after 5 cycles of reorganisation and refilling have been completed. In both cases the corresponding SEM image is shown in the inset. The radial distribution function is a means of measuring the correlation between particles within a system or, more specifically, a measure of the probability of finding a particle at a distance *r* away from a given reference particle. A peak indicates an increased prospect of finding particles at that given distance from a central reference particle while an intensity of 1 corresponds to the average particle density. An intensity of less than one reveals that there is a diminished probability of finding a particle at this distance.

Focussing on the low-density situation shown in Figure 16a, and considering moving radially away from a central reference particle, several important features can be noted. Firstly, the trough at short distances indicates that, as expected, there is a low probability of finding particles, due to the strong electrostatic repulsion involved, close to others. One prominent peak, at a distance which

corresponds to the average separation between any given particle and its nearest neighbours, is then observed before another trough corresponding to a second region of reduced probability is seen. Outwith this radius the distribution function tends to 1, showing that no additional order can be discerned. Two important differences can be noted, however, in Figure 16b. Again moving radially away from a central reference particle it can be seen that the first peak occurs at a much smaller distance. This is a mark of closer packing and a good indicator of overall filling fraction. Secondly, several, perhaps as many as 5, peaks can now be discerned, showing that there is a considerable increase in the order observed in this sample.

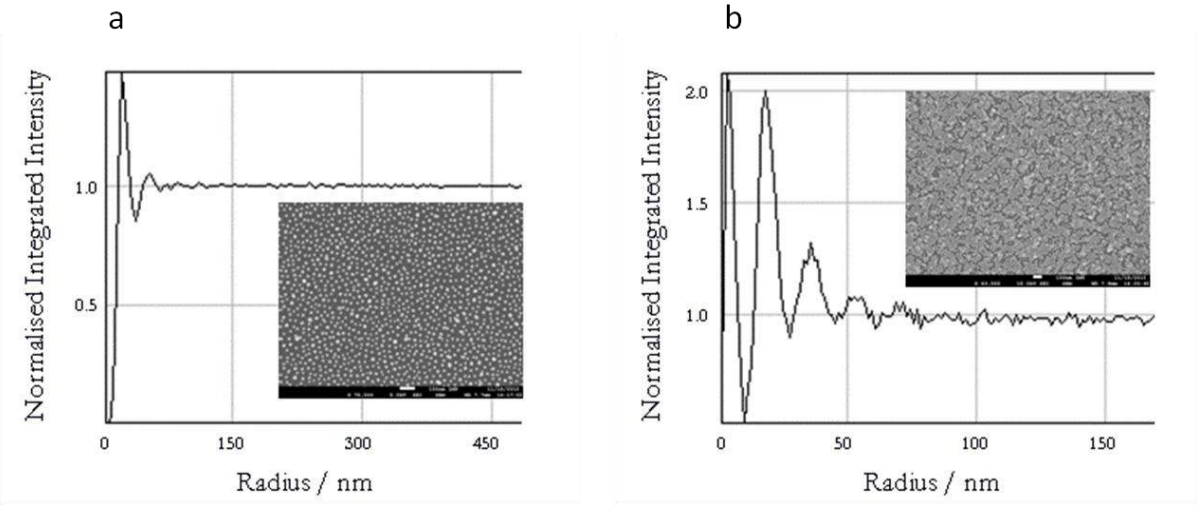

Figure 16 - Radial distribution functions a) before and b) after reorganisation and deposition processes. The corresponding SEM micrographs are shown in the insets.

The morphological changes described, at each stage of the process, result in significantly differing optical properties that can be tracked by UV-vis spectroscopy. A typical example is shown in Figure 17. The initial array of gold nanoparticles, with a diameter of approximately 20 nm, can be seen in the lower blue trace. Here, as described in Section 4.1.2, the individual particles are suitably well-separated and have no significant influence over one another. The strength of coupling decreases exponentially as two resonant particles are moved away from one another and an appreciable interaction is only observed when they are brought to within a distance of approximately one particle diameter. As such, in the low density case the optical properties of the array are not substantially different from that of an individual particle. Upon exposure to the thiol solution a large red-shift of the surface plasmon resonance is induced, as can be seen in the lower red trace. This corresponds to a reorganisation of the particles at the substrate surface with nanoparticles being brought to within the coupling limit - therefore altering the optical properties. Successive deposition (blue traces) and reorganisation (red traces) steps are shown in Figure 17, steadily progressing to

higher extinction coefficients. Overall the process results in a substantial red-shift of the LSPR of approximately 100 nm over five reorganisation steps as well as the concomitant increase in extinction that would be expected from the deposition of a higher volume of material.

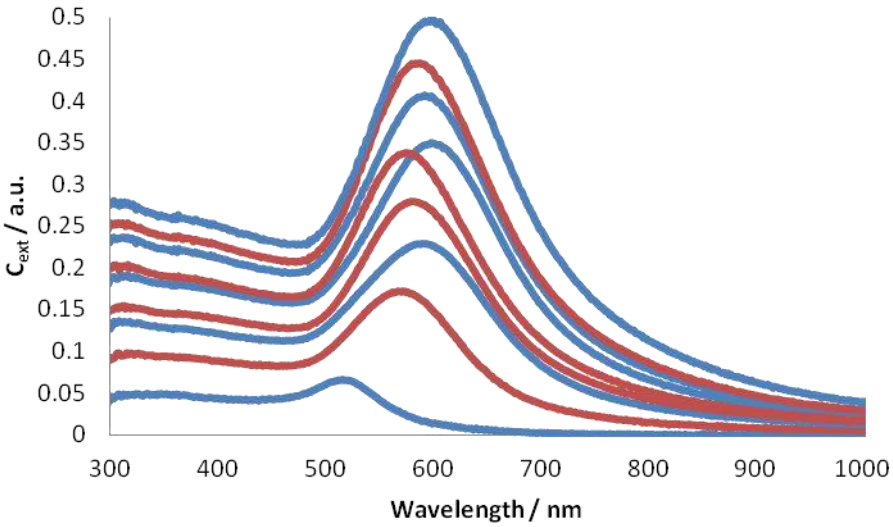

Figure 17 – Extinction spectra of gold nanoparticle arrays that have undergone several reorganisation and additional deposition steps. Deposition steps are shown as blue traces, progressing from low extinction coefficients to higher extinction coefficients while reorganisation steps are shown as red traces, again progressing from low coefficients to higher extinction coefficients.

4.1.4. Extending into 3rd dimension – the bulk-assembly of polyelectrolyte layers and multiple gold nanoparticle arrays[4]

As has been shown, a significant amount of control is afforded over the organisation of gold nanoparticles within a single planar array. However, for a variety of applications it is also extremely desirable to extend these gold nanoparticle arrays into the third dimension. Using the same electrostatic interactions that were exploited to create the single gold nanoparticle arrays discussed in Section 4.1.2 it is possible to build upon this base and deposit layers of PEs and additional gold nanoparticle arrays resulting in structures such as the one shown in Figure 18. Here, it can be seen that two gold nanoparticle arrays are separated by several PE layers. The only requirement placed on the number of polymer layers being that an odd integer number should be used in order to maintain an electrostatic attraction between the constitutive elements.

[4] Much of the work presented in this section appeared in: Cunningham A.; Mühlig S.; Rockstuhl, C.; Bürgi, T.: Coupling of Plasmon Resonances in Tunable Layered Arrays of Gold Nanoparticles. *J. Phys. Chem. C* **2012**, *115* (18), 8955-8960.

Further advantages offered by this method include that unlike the Langmuir-Blodgett technique,[126] for example, the deposition of PEs can be applied to surfaces of virtually any topology and that the deposition occurs extremely quickly, over a period of seconds. In addition, similarly to the size of the initial substrate functionalised, only practical limitations exist both in terms of how many gold nanoparticle arrays are deposited and their relative separations. Other than that the system is extremely flexible and a variety of differing sample architectures, with as many nanoparticle arrays as desired separated by tunable distances, can be easily and inexpensively fabricated on a large scale.

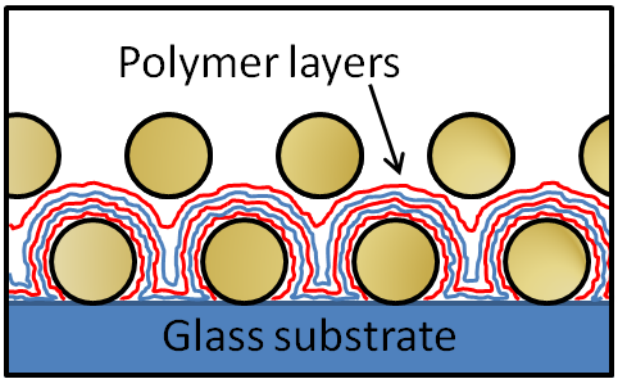

Figure 18 – Diagrammatical representation of two gold nanoparticle arrays separated by five polyelectrolyte layers.

To determine the distance between gold nanoparticle arrays, and therefore the thickness of an individual PE layer, GISAXS were carried out on samples with varying degrees of array separation by Xiangbing Zeng and Feng Lui of the University of Sheffield. Measurements were conducted with the incident angle just above the critical angle in order to exclude total reflection at the interface between the sample and the substrate. Very similar diffraction patterns, shown in Figure 19, were observed for each of the four samples investigated. Each sample, comprising two gold nanoparticle arrays separated by 5, 11, 15 and 21 PE layers (Figure 19a-d respectively), displayed a ring-like feature which is determined by the size and shape of the nanoparticles. Assuming that the nanoparticles are spherical with a uniform density throughout, the diameter was found to be 13.0 $\pm$ 0.5 nm. Additionally, the two streaks observed at either side of the meridian indicate that the average distance between two particles within a single array is approximately 31 nm. While the data retrieved for the average diameter of the nanoparticles is slightly lower than that shown in SEM images (~17 nm, Figure 10) it is still in the correct range. The separation determined is also comparable with that shown in Figure 16a and, importantly, provides further supporting evidence that the particles within a single array are separated to the extent that there is no appreciable interaction between them. This shows that any shifts in the optical properties observed upon the

deposition of a second gold nanoparticle array must, necessarily, be as a result of coupling between the two distinct arrays.

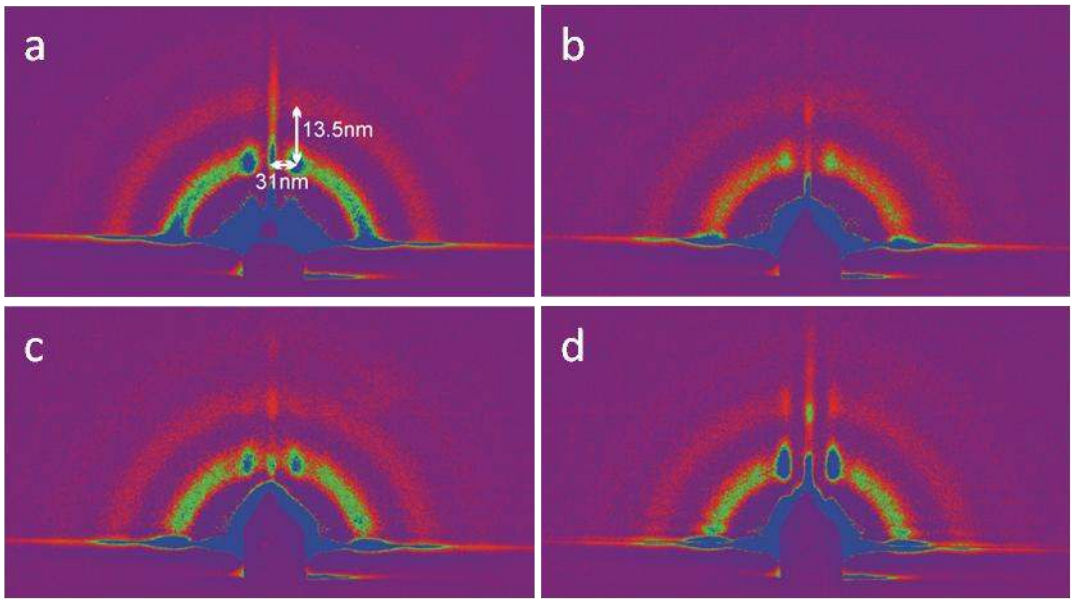

Figure 19 - GISAXS patterns made at low angle of incidence for samples with (a) 5, (b) 11, (c) 15 and (d) 21 polymer layers in-between two gold nanoparticle arrays.

Information concerning the separation between the two nanoparticle arrays is better elucidated when using higher angles of incidence. This results in the splitting of the two streaks found at either side of the meridian as can be seen in Figure 20. Again, Figure 20a-d refer to the samples separated by 5, 11, 15 and 21 PE layers respectively. The splitting was barely discernible in Figure 20a, indicating that the two gold nanoparticle arrays, while still separated from each other, cannot be thought of as existing in two discrete planes. Here a significant amount of overlap between the two arrays exists. On the other hand, separations of 40, 49 and 65 nm can be resolved in the other three samples, assuming the nanoparticle diameter of 13 nm determined in Figure 19. This corresponds to an average thickness of 2.5 nm for an individual PE layer which ties in extremely well with figures quoted in related literature.[45, 128] The best correlation is found in the samples with more PE layers deposited in-between the nanoparticles. One possible explanation is that additional PE layers gradually smooth out the unevenness that originates from the form of the nanoparticles. This can be seen clearly in the sketch of the system shown in Figure 18. While it remains a basic diagrammatical representation of the true situation it is, nevertheless, rather informative and shows how the polymer layers can be thought of as depositing on top of and in-between the gold nanoparticles.

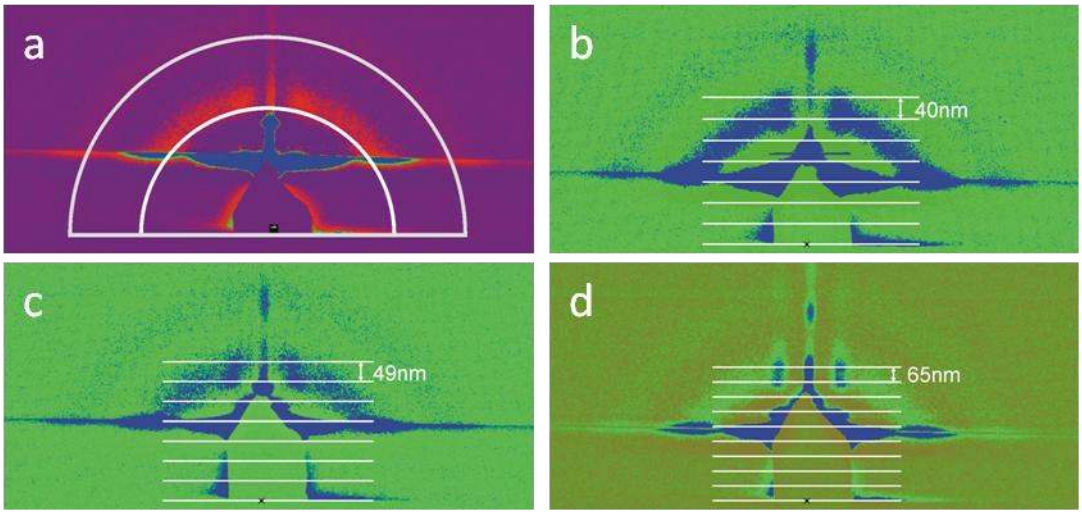

Figure 20 – GISAXS patterns made at higher angles of incidence for samples with (a) 5, (b) 11, (c) 15 and (d) 21 polymer layers in-between two gold nanoparticle arrays. Array separation, where discernible, is highlighted in the Figures.

Interestingly, it is also possible to investigate both the geometrical form of gold nanoparticle arrays and the extent to which they are separated in samples with varying number of PE layers by SEM. Four SEM micrographs of two gold nanoparticle arrays that have 1, 5, 11 and 31 separating PE layers in-between can be seen in Figure 21a-d respectively. While the technique cannot be used to return accurate information on the separation between two gold nanoparticle arrays it is particularly instructive in revealing the differing forms of samples as additional PE layers are deposited between the arrays. This information can then be used to determine the point at which the system can actually be considered as being constructed from distinct arrays. Appreciable differences can be seen in the SEM images shown below.

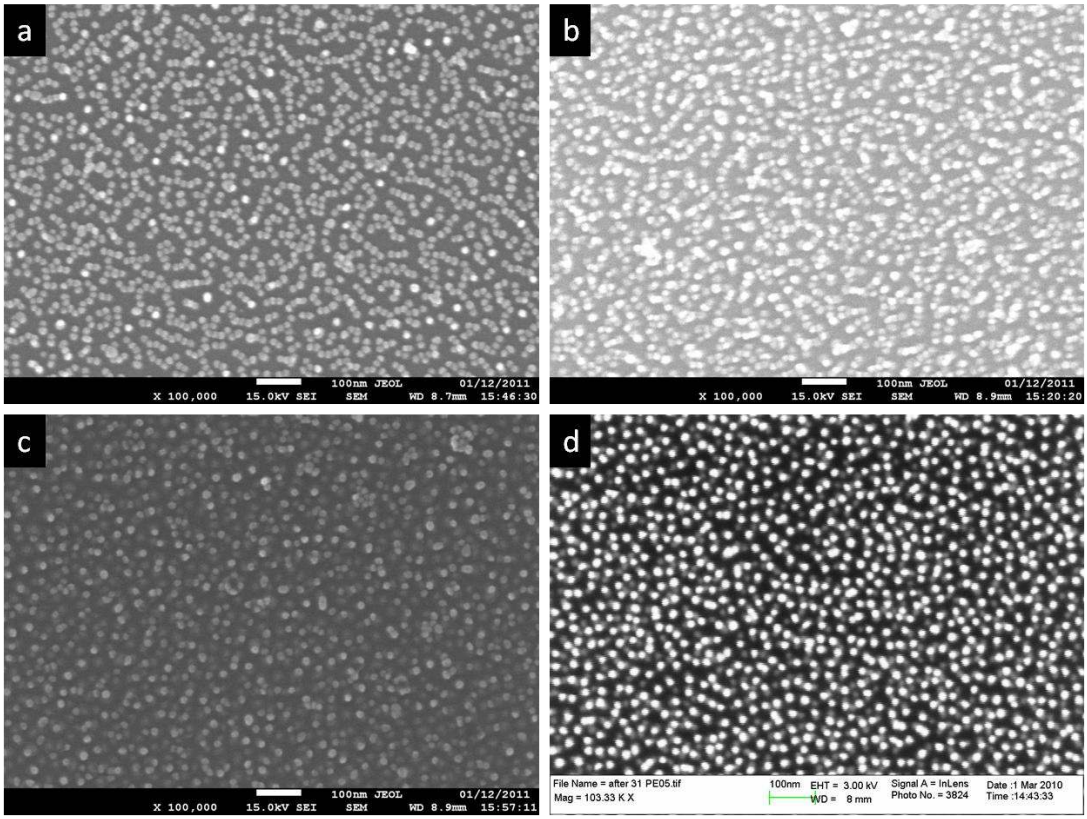

Figure 21 – SEM images showing two gold nanoparticle arrays (~20 nm diameter) with (a) 1, (b) 5, (c) 11, (d) 31 polyelectrolyte layers higher in-between.

While it is clear that gold nanoparticles will remain separate and will not be able to physically contact one another when even a single PE layer has been deposited it can be seen in Figure 21a that in no way could such a structure be considered as consisting of two distinct gold nanoparticle arrays as depicted in Figure 18. Neither is it possible to ascertain which particles originate from which nanoparticle deposition; the first or the second. Instead a rather amorphous structure results whereby small aggregates, predominantly in the form of chains containing approximately 5 – 10 particles take shape. For the most part these chains of nanoparticles are adsorbed directly at the surface of the substrate with only isolated particles, identifiable in Figure 21a as brighter, whiter dots, being present out of this plane. That this is the case is not surprising given that the first PE layer is only capable of coating the nanoparticles themselves. When the second gold nanoparticle deposition takes place the incoming particles are attracted to both this PE layer at the surface of the nanoparticles and also to the uncovered gaps at the surface of the functionalised substrate. As such, the most energetically favourable position for an incoming particle to take, maximising its interactions with oppositely charged surfaces, would be in contact with one or more nanoparticles and the substrate surface. The mobility of the particles, which has already been shown in Section 4.1.3.3, allows reconstruction of the surface structures and the formation of chains and other more

irregular aggregates which maximise the interactions between oppositely charged species. Such structures lead to interesting optical characteristics which will be discussed at length later in this section.

In Figure 21b, in line with the conclusions drawn from the GISAXS experiments summarised in Figure 20a, it can be seen that increasing the number of separating PE layers from 1 to 5 does not result in distinct stratified arrays of gold nanoparticles. While a larger proportion of particles than in Figure 21a can be seen out of the plane of the substrate surface it is clear that a significant number from the second deposition continue to find energetically more favourable positions closer to the substrate surface. The continuing presence of chain-like aggregates also indicates that 5 PE layers are not sufficient to adequately separate the gold nanoparticles into two distinct arrays.

When the number of PE layers separating two gold nanoparticle arrays is increased to 11, as can be seen in Figure 21c, it can be seen that two irregular arrays of particles, each similar to that which is present after a single nanoparticle deposition (Figure 10b), can be discerned. The absence of the chain-like aggregates, along with the differences in brightness of the particles – indicating their position in the upper or lower arrays – show that 11 PE layers are sufficient to separate two arrays. Increasing the degree of separation to 31 polymer layers, as shown in Figure 21d, only serves to enhance the extent to which the two separate arrays can be distinguished. Each particle in this image can be unambiguously attributed to either the upper or lower array and no aggregates of any description can be perceived.

The evolution of the SEM images shown in Figure 21a-d demonstrate that as an increasing number of PE layers are used to separate two gold nanoparticle arrays a transition from amorphous chain-like aggregates to distinct stratified arrays occurs. After this transition, which can be thought of as taking place when around 7 PE layers are deposited, the separation of the arrays becomes increasingly apparent. This is as a result of the surface roughness of the exposed surface gradually decreasing. As the polymer layers built up on the comparatively rough gold nanoparticle array fill in the gaps more planar surfaces result. Of course the number of PE layers required to fill in these gaps is a function of the surface roughness which is itself dependent on a variety of factors. For instance, the use of larger gold nanoparticles than those under study in this work would result in a greater surface roughness and presumably more polymer layers would be required to prepare a near-planar surface on which to deposit a second nanoparticle array. On the other hand, surface roughness can also be seen to be a function of nanoparticle density. Comparing a high density array, such as one of the ones discussed in Section 4.1.3.3, with the standard array seen in Figure 10b, it can be seen that there are far less gaps in-between the nanoparticles in the array of higher density. It would be

expected that this comparatively low surface roughness would require fewer polymer layers to fill in these gaps and present a relatively planar surface upon which a second, wholly distinguishable nanoparticle array could be deposited.

While it is principally the changes in optical properties that arise from the coupling between the nanoparticles in two distinct arrays that are of interest it should be noted that the deposition of PE layers also causes relatively large shifts in the plasmon resonance. This, as outlined in Equation 5, is due to the change in local refractive index surrounding the particles as air is gradually replaced with polymeric material. The extent to which the deposition of PE layers can affect the optical properties of a gold nanoparticle array are shown in Figure 22. The wavelength of the LSPR as a function of the number of PE layers deposited on top is illustrated with both experimental (blue diamonds) and simulated (red squares) data shown. All simulations related to this work, the details of which can be found in Reference 160, were carried out by Stefan Mühlig and Carsten Rockstuhl of the Friedrich-Schiller-Universität Jena.

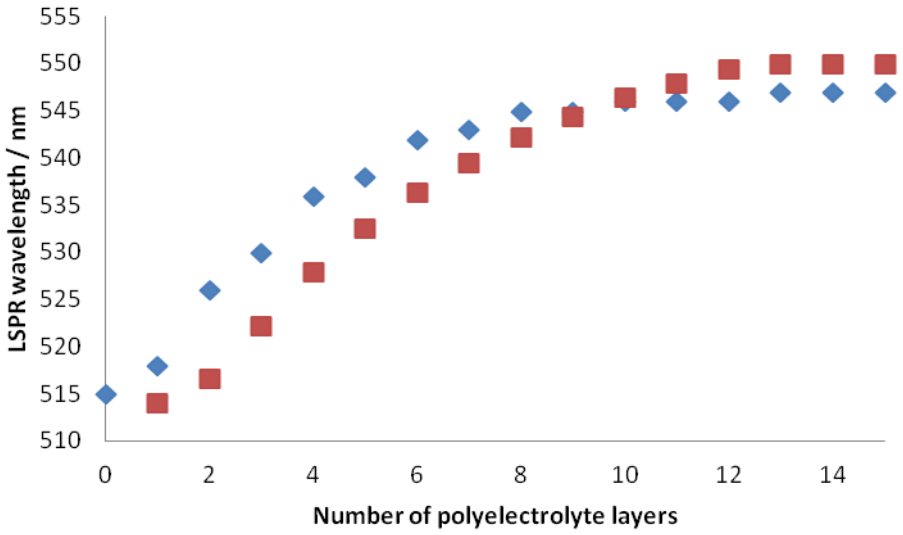

Figure 22 - LSPR wavelength of a single array of gold nanoparticles (~20 nm diameter) on a glass substrate as a function of the number of covering PE layers deposited. Both experimental (blue diamonds) and simulated (red squares) data are shown.

It can be seen that, as expected, replacing the air surrounding the gold nanoparticles within the array results in a red-shift of the plasmon resonance. As is clear from Figure 22 this shift is comparatively greater for the layers that are closer to the surface of the nanoparticles. This is a result of the exponential decrease in influence that changing the refractive index of the surroundings of a metallic nanoparticle has on its optical properties as the distance from its surface is increased.[37] It can also be seen that above a certain number of deposited layers the effect saturates and the

addition of more polymer layers does not further influence the optical properties of the gold nanoparticle array. This is again due to the exponentially diminishing effect that changing the refractive index of the surrounding material has on the peak position of the plasmon resonance. While technically this effect extends to infinity, in practice only changes 1 – 1.5 nanoparticle diameters distant from the surface will make a measurable difference.[37] As a result the number of polymer layers required to fill the volume which can have a bearing on the position of the plasmon resonance, shown in Figure 22 to be approximately 13 for particles with a diameter of ~20 nm, is also dependent on the nanoparticle diameter itself. The optical properties of an array of larger gold nanoparticles will continue to be affected by the adsorption of polymer layers after the 13th layer has been deposited, while the shift induced in arrays composed of smaller gold nanoparticles will saturate before this point.

Another interesting feature of Figure 22 is that larger red-shifts of the plasmon resonance can be discerned when the negative PE layers (even numbers), rather than the positive ones (odd numbers), are deposited. As the refractive indices of the two polymers, PAH and PSS shown in Figure 9, are very similar (1.38 and 1.395 respectively)[169, 170] it is reasonable to assume that the larger shifts caused by the deposition of the negative polymers are as a result of thicker layers. The thicknesses of PE layers depend on a number of factors, including the molecular weight of the polymer and the structure of the repeating unit, and thicker layers, taking up a proportionally larger volume around the nanoparticle, will have a greater influence on the optical properties.

The extent to which the shifts shown in Figure 22 actually change the optical properties of an array of gold nanoparticles can be seen in Figure 23 which shows a series of functionalised glass microscope slides upon which a single array of gold nanoparticles (~20 nm diameter) and differing numbers of PE layers have been deposited. Moving from left to right the samples have had 0, 1, 3, 5, 7, 11, 21, 31 and 41 PE layers deposited and, according to Figure 22, the change in colour perceived corresponds to a red-shift of approximately 30 nm. That such an impressively strong colour originates from a single, low-density array of nanoparticles and that the precise position of the plasmon peak can be accurately tuned depending on the number of PE layers deposited on top serves to highlight the potential that such systems have. The possibilities for use in sensing applications are particularly well illustrated by this example.

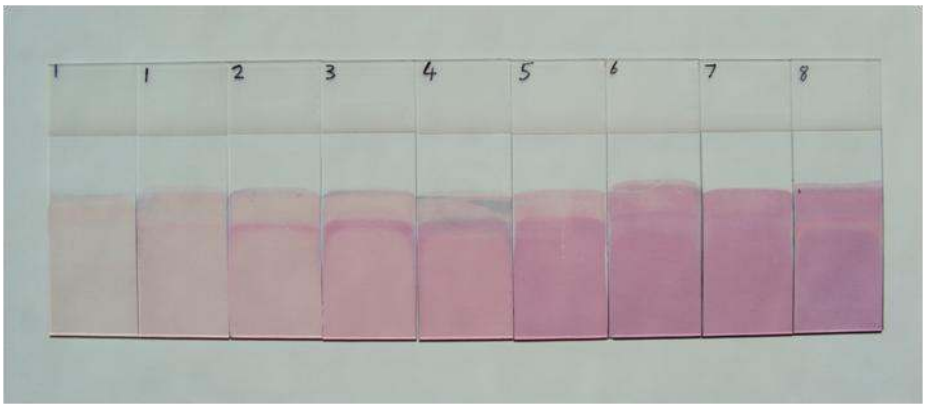

Figure 23 – Photograph of functionalised glass microscope slides coated in a single array of gold nanoparticles (~20 nm diameter) and, left to right; 0, 1, 3, 5, 7, 11, 21, 31 and 41 polyelectrolyte layers.

The colour changes perceived as PE layers are progressively deposited on an array of gold nanoparticles only takes into account one facet of their local surroundings. The other aspect which should not be forgotten is, of course, the substrate. Different substrates have different refractive indices and this can also have a bearing on the position of the plasmon resonance. Certain substrates, such as ITO-coated glass for example, may also provide a route to actively controlling the optical properties of an array of metallic nanoparticles through the application of a potential which would see the withdrawal or donation of electrons from the nanoparticles and a red or blue shift in the position of the plasmon resonance respectively.

As well as red-shift of the plasmon resonance that is observed resulting in a significant change in colour it is also evident from Figure 23 that the overall intensity of the extinction increases. This is quantified in Figure 24 where in addition to the overall red-shift that is seen as polymeric material gradually replaces air as the medium surrounding the nanoparticles an extremely large increase in extinction is also observed. This increase in extinction, in a similar manner to that seen for the shift in plasmon position in Figure 22, is seen to saturate after approximately 15 polymer layers have been added.

One explanation for this could be that the imaginary part of the permittivity of gold, which controls the absorption, is dispersive and as the resonance position is shifted across the spectral domain the particles will incur different losses. Increases in extinction as dielectric materials of increasing thickness are placed around metallic nanoparticles are not unprecedented. Similar observations were made by Okamoto who showed that coating gold particles in silica shells caused both a red-shift in the plasmon resonance as well as an increase in the absorption cross-section.[171] An additional explanation could be an increase in scattering which could result from an increase in size

of the entities at the substrate surface or that the polymer layers themselves are not completely transparent at the frequencies under consideration. While it is difficult to determine the dominating factor any of these explanations could, to varying extents, contribute to the effect observed.

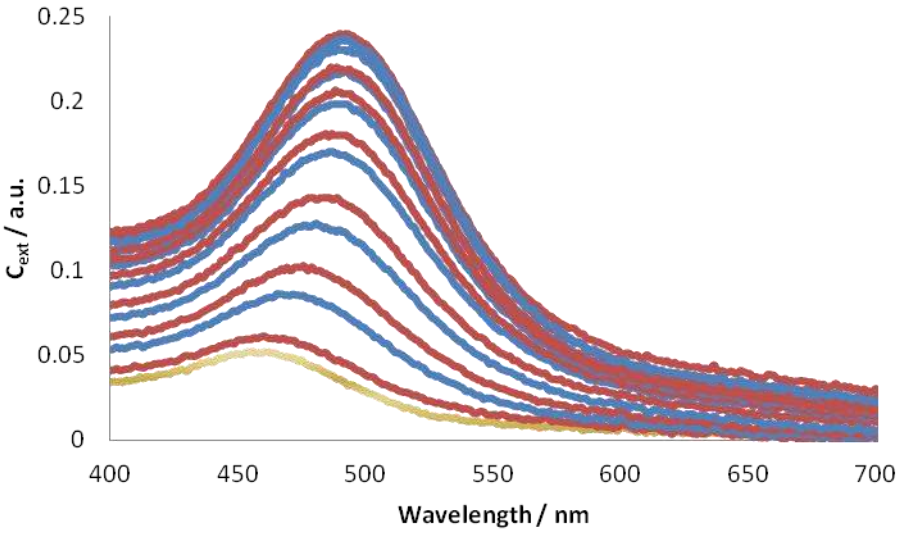

Figure 24 – Extinction spectra of an array of gold nanoparticles (gold trace) upon which positive (red traces) and negative (blue traces) polyelectrolyte layers have been deposited. Nanoparticles have a diameter of ~20 nm.

When two metallic nanoparticles approach they can interact and shift the frequency of the LSPR. The extent to which they interact is strongly related to the distance between them. Outwith the coupling limit, this interaction is negligible however the strength increases exponentially as the particles approach within this range. Due to the flexibility of the fabrication process this effect can be measured by separating two gold nanoparticle arrays by a series of PE layers. That the thickness of a single PE layer is on the nanometre scale allows accurate and reproducible measurements to be carried out using dimensions that would be inaccessible using top-down techniques.

The results of this study are summarised in Figure 25 which shows the red-shift of the LSPR peak as a function of the number of PE layers separating two gold nanoparticle arrays. Experimental (solid points) and simulated data (dashed lines) are shown for arrays of ~20 nm (blue plots) and ~40 nm in diameter (red plots). In order to accommodate the additional red-shift, originating from the deposition of the PE layers and highlighted in Figure 22, Figure 23 and Figure 24, the shift in resonance due to coupling was extracted by subtracting the plasmon resonance wavelength of the first gold nanoparticle array after the deposition of a finite number of PE layers from that of the second gold nanoparticle array after the deposition of the same number of polymer layers.

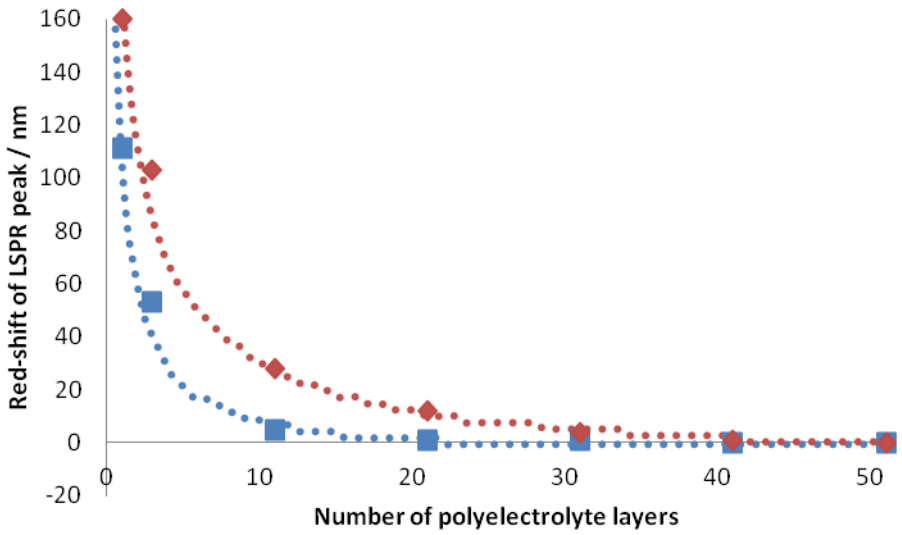

Figure 25 – Red-shift of localised surface plasmon peak of two gold nanoparticle arrays as a function of the number of polyelectrolyte layers separating them. Experimental (solid points) and simulated data (dashed lines) are shown for arrays of ~20 nm (blue plots) and ~40 nm in diameter (red plots).

Focussing on the smaller nanoparticle arrays, it can be seen that the exponential trend expected is observed with much higher red-shifts observed for gold nanoparticle arrays separated by lower numbers of PE layers. From Figure 25 it is also possible to discern the point at which the two gold nanoparticle arrays are removed to the extent whereupon they no longer couple with one another. In the case of the nanoparticles with a diameter of ~20 nm this point occurs when approximately 15 PE layers have been deposited in-between the arrays, tying closely matching the value provided in Figure 22.

Figure 25 also shows the effect that particle size has on systems such as these with larger particles, ~40 nm in diameter, being used to fabricate the same structure. It can be seen that the interaction between particles, as would be expected from theoretical studies,[37] is even stronger and extends further for larger particles. This is a result of coupling limits essentially being a function of particle size. A more pronounced red-shift is observed for comparable separations when larger particles are used and further distances are required, in the order of 35 PE layers, to remove the particles to the point at which they no longer couple.

In each case the experimental results were seen to agree excellently with simulations, which were provided by Stefan Mühlig and Carsten Rockstuhl of the Friedrich-Schiller-Universität Jena. The simulations, the full details of which can be found in Reference 160, do not consider the coupling between two large scale gold nanoparticle arrays but rather two single nanoparticles, more commonly known as a dimer. As has been shown by UV-vis spectroscopy (Figure 11), the

characterisation of SEM images (Figure 16 and Figure 21d) and GISAXS measurements (Figure 19) the distance between nanoparticles within a single gold nanoparticle array is too great for the particles to appreciably interact with one another. On the other hand the thickness of PE layers, in the order of the nanoscale, allows the extremely close approach, with a high degree of control, of two nanoparticles. As such it is clear that the optical response of two stacked gold nanoparticle arrays separated by PE layers should be dominated by the interaction of particles from different arrays. As a consequence, the structure considered in the simulations was reduced to an isolated dimer. Strong agreement between the experimental results and the simulations confirm the validity of this approach.

While a good indication of the degree of control afforded over the optical properties, simply through the coupling of gold nanoparticles in two separate arrays, is given by Figure 25 it is perhaps more instructive to consider the actual spectra to gain an overall impression of the extent to which it is possible to induce shifts in the spectral position of the plasmon resonance. This information is shown in Figure 26 which allows the comparison of a single array of gold nanoparticles (black trace, left-hand axis) with two gold nanoparticle arrays separated by 11, 21 and 41 PE layers (blue, red and green traces respectively, right-hand axis). The nanoparticles in the arrays depicted in Figure 26 have a diameter of ~40 nm. The addition of PE layers and a second gold nanoparticle array results in a large increase in extinction as well as the shift in spectral properties. That the precise position of the plasmon resonance can be tuned over such a wide range and with such high precision is one of the principal advantages offered by this system.

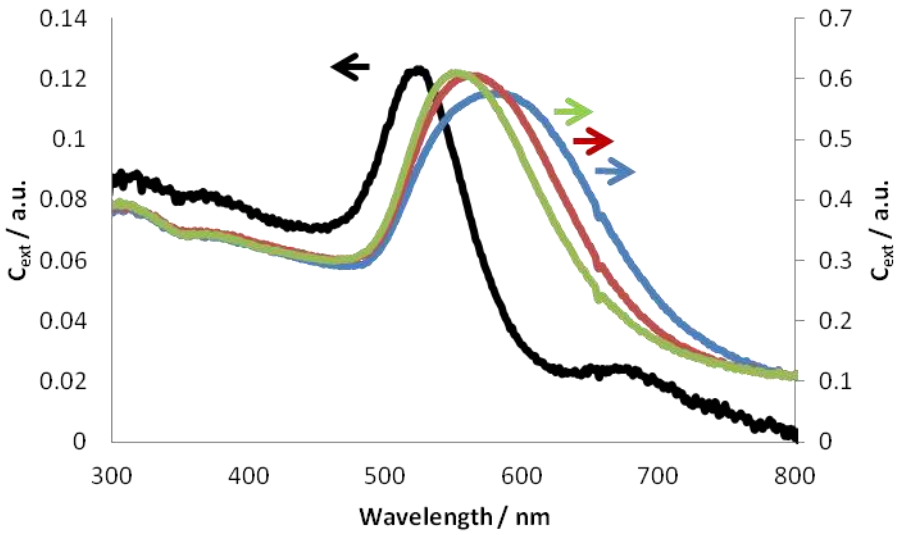

Figure 26 – Extinction spectra of a single gold nanoparticle array (black trace, left-hand axis) and two gold nanoparticle arrays separated by 11, 21 and 41 polyelectrolyte layers (blue, red and green traces respectively, right-hand axis). Nanoparticles have a diameter of ~40 nm.

As outlined in Section 2.2.4, the coupling of two spheres can be described with the principles of plasmon hybridisation theory, shown schematically in Figure 8. The addition of a second array of gold nanoparticles results in a splitting of the single resonance into two, where the dominant one is strongly red-shifted. As the optical response within a single gold nanoparticle layer was dominated by the LSPR of a single sphere, this red-shifted resonance is governed by the mutual coupling of spheres from distinct gold nanoparticle arrays.

When gold nanoparticle array separation is extremely small, for example by depositing only a single PE layer between two arrays, the rather amorphous structure, shown in Figure 21a, containing a variety of dimer orientations relative to the incident wave vector results. In such a configuration, all of the bonding and antibonding eigenmodes can be excited.[172] Importantly, only the eigenmodes with a resulting dipole moment dominate the extinction spectra. As a consequence, both such modes should be simultaneously excited and the plasmon peak should split into two individual and resolvable resonances. This has been both observed experimentally and predicted by simulation as can be seen in Figure 27.[160] Both eigenmodes with a resulting dipole moment, π* and σ in Figure 8, can be observed with the π* (σ) coupled plasmon being observed at shorter (longer) wavelengths.

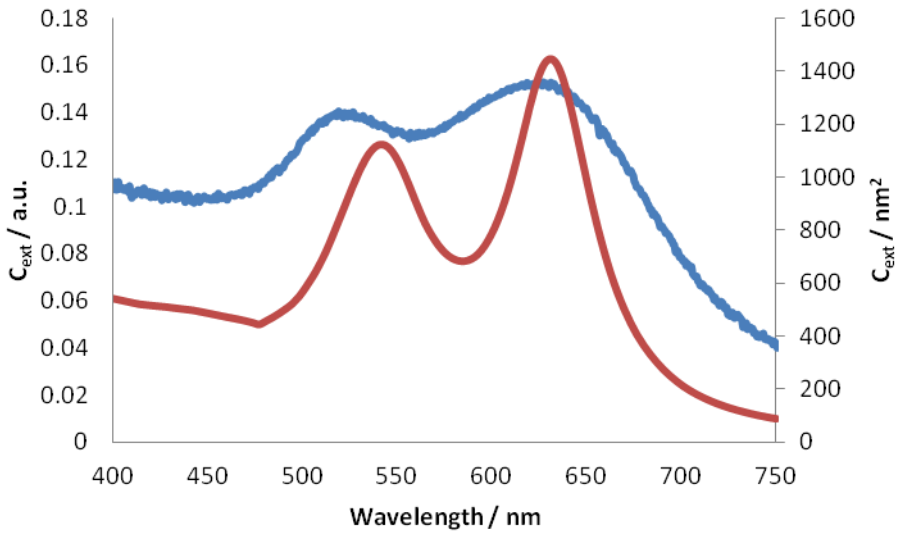

Figure 27 - Experimental (blue trace) and simulated (red trace) extinction spectra of two gold nanoparticle arrays separated by 1 polyelectrolyte layer. Nanoparticles have a diameter of ~20 nm.

As outlined in the Introduction the stated aim of the Nanogold project was the fabrication of *bulk* electromagnetic metamaterials. While it is difficult to classify what exactly is meant by this term one definition which is generally thought of as being reasonable is that the smallest length scale should be on the same order as, or larger than, the wavelength of light of interest. When working with structures assembled from gold nanoparticles then the smallest dimension of a material should be on the order of 500 nm, the position of the plasmon resonance. The structures discussed thus far, despite covering several square centimetres, do not approach anything like these sizes in the third dimension. For example, two gold nanoparticle arrays, using nanoparticles with a diameter of ~20 nm, separated by 11 PE layers will form a film with a maximum thickness of around 65 nm. However this value is likely to be, on average, significantly lower as it would require two nanoparticles to deposit directly in line with one another and for there to be no interpenetration or compression of the PE layers in-between.

One solution that could be employed in order to overcome this problem would be the construction of multiple layers of gold nanoparticles. The only requirement of the extremely flexible fabrication process is that a depositing species should exhibit the opposite charge to that which is exposed at the surface of the structure under assembly. This allows for virtually any conceivable architecture of layered arrays of metallic nanoparticles. There are few practical limitations to the number of either metallic nanoparticle arrays or PE layers used to separate them which can be deposited and after the assembly of a sufficiently high number of strata the thickness of the film will be great enough in order to meet the condition outlined for bulk materials. It must be noted that one possible limitation

to using this technique would be that, upon the deposition of too many metallic nanoparticle arrays, the overall extinction of a sample could become too great and the sample would appear black – essentially not letting any light pass. However, where larger numbers of PE separating layers are used this should not pose a problem before bulk dimensions are reached. An alternative to simply using larger numbers of PE layers to separate individual gold nanoparticle arrays would be to use these larger numbers of polymer layers to separate coupled arrays. By moving several strongly coupled arrays outwith the coupling limit of each other it would be possible to build up bulk metamaterials which possess the desired functionality without overly increasing the overall absorption of the system. It should be noted that when discussing the assembly of high numbers of metallic nanoparticle arrays that the size of the nanoparticles used should also be considered – larger particles providing thicker layers but at the same time scattering incident light to a much greater extent.

The extinction spectra of assemblies of gold nanoparticles (~20 nm diameter) can be seen in Figure 28. This work, carried out by Brittany Cindric of the University of Geneva within the framework of an internship and under the supervision of Alastair Cunningham, represents the first steps towards developing the structures discussed previously in this section into what could be considered as bulk metamaterials. Many of the features observed in the simpler systems containing only two gold nanoparticle arrays can also be seen here. The splitting of the plasmon resonance into two separate eigenmodes, as was shown previously in Figure 27, is still seen when additional arrays are added. However, interestingly, the longer wavelength resonance becomes increasingly prominent in relation to the shorter wavelength resonance (Figure 28a). Figure 28b and Figure 28c also display an interesting, and somewhat unexpected, trend. The plasmon resonance initially shifts to longer wavelengths upon the deposition of additional gold nanoparticle arrays as would be expected and as was observed in all of the samples with only two arrays. However at a certain point this resonance begins to shift back to higher frequencies. This behaviour is more pronounced in the sample where the nanoparticle arrays were separated by 5 PE layers and the reasons behind this remain, as yet, unexplained. It should not be confused with the blue-shifts that are seen throughout Figure 28 between a sample coated in PE layers and the subsequent gold nanoparticle array. These two spectra cannot be legitimately compared as in one the uppermost gold nanoparticle array is coated in several layers of polymer while in the other the uppermost gold nanoparticle array is exposed to air. This difference in refractive index between the two materials causes the position of the resonance to shift back and forth. The degree of separation between the gold nanoparticle arrays represented by the extinction spectra shown in Figure 28d is large enough to preclude any

substantial coupling between separate arrays and as such no significant shift in plasmon resonance, other than that caused by the deposition of the PE layers, is observed.

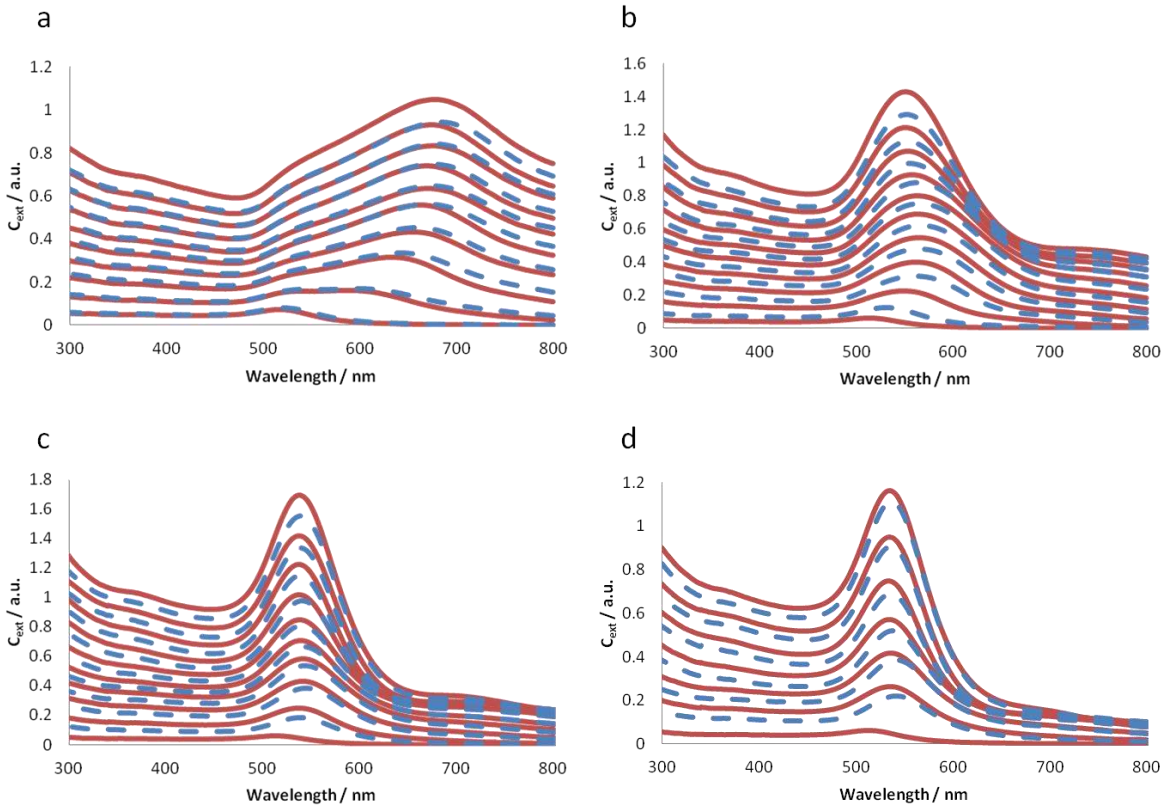

Figure 28 – Extinction spectra of assemblies constructed from multiple gold nanoparticle (~20 nm diameter) arrays and polyelectrolyte layers. Gold nanoparticle arrays are separated by a) 1 polyelectrolyte layer, b) 5 polyelectrolyte layers, c) 11 polyelectrolyte layers, d) 25 polyelectrolyte layers. In each case the spectra taken directly after the deposition of the gold nanoparticle arrays (red solid traces) and the requisite number of polyelectrolyte layers (blue dashed traces) are shown.

4.1.5. Compositionally asymmetric arrays of metallic nanoparticles[5]

The concept of bright and dark eigenmodes considered within the bounds of plasmon hybridisation theory, introduced in Section 2.2.4., plays an important role in the field of metamaterials since the out of phase oscillation of electric dipoles can be related in some cases to a magnetic dipole moment - a key component in many predicted applications. One way to excite dark eigenmodes is to use structures that exhibit a considerable amount of asymmetry. Until now the study of metallic nanoparticle structures which show asymmetry in either size, shape, or composition has been limited to discussions, both theoretical[173, 174, 175] and experimental,[176] relating to interactions

[5] Much of the work presented in this section appeared in: Cunningham A.; Mühlig S.; Rockstuhl, C.; Bürgi, T.: Exciting Bright and Dark Eigenmodes in Strongly Coupled Asymmetric Metallic Nanoparticle Arrays. *J. Phys. Chem. C* **2012**, *116* (33), 17746-17752.

between low numbers of isolated particles. For example, using asymmetric structures Brown *et al.* demonstrated Fano resonances and optical nanodiode effects[176] while the observation of both bright and dark eigenmodes along with coupling between plasmonic modes and interband absorption transitions was seen by Sheikholeslami *et al.*.[177] Lithographically produced dimers of gold and silver nanodisks have also recently been shown to act as nanoantennas for directional colour routing, which opens the door to a variety of different applications.[178] Other work concerning heterodimers has shown the possibility of using such structures as nanolenses.[179]

While this relatively small scale research is capable of providing interesting insights into the properties of asymmetric systems the development and application of the fabrication techniques that have been introduced in Sections 4.1.2 and 4.1.4 would allow these properties to be probed on a scale that could be incorporated into functional devices. The flexibility of these fabrication techniques, requiring only that the incorporated species are charged, easily allow arrays of metallic nanoparticles, incorporating a degree of asymmetry, to be developed. Initially it was thought that this asymmetry could be achieved through the construction of arrays of gold nanoparticles of differing size.[177] However it was found that, while in theory this should have resulted in asymmetric coupling, the shift in resonance between the nanoparticles of different size was not sufficient to make any effect observable. As a result, structures composed of large scale arrays of strongly coupled gold and silver nanoparticles, separated by layers of PEs, were investigated. A diagrammatical representation of this structure can be seen in Figure 29.

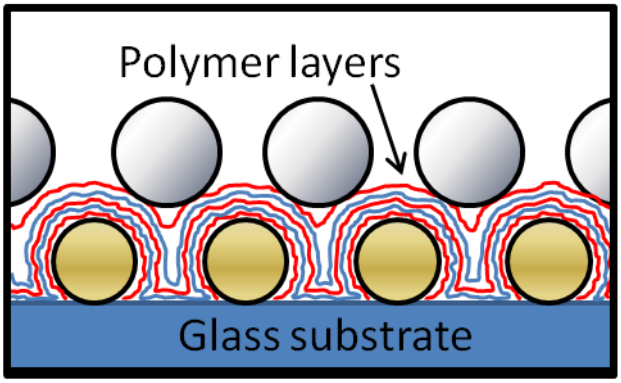

Figure 29 - Diagrammatical representation of silver and gold nanoparticle arrays separated by five polyelectrolyte layers.

The required asymmetry of the system is induced due to the vastly different plasmon resonance frequencies of silver nanoparticles and gold nanoparticles which is highlighted in the plasmon hybridisation diagram shown in Figure 30. Unlike the plasmon hybridisation diagram of the homodimer shown in Figure 8, where the dipole moments of the individual particles completely

cancel in two of the four hybridised modes, the asymmetry introduced means that this is no longer the case. Heterodimers, such as that represented in Figure 30, display a net dipole moment in each of the four hybridised eigenmodes and it is due to this broken symmetry that all modes can be excited at normal incidence, unlike in the previous case.

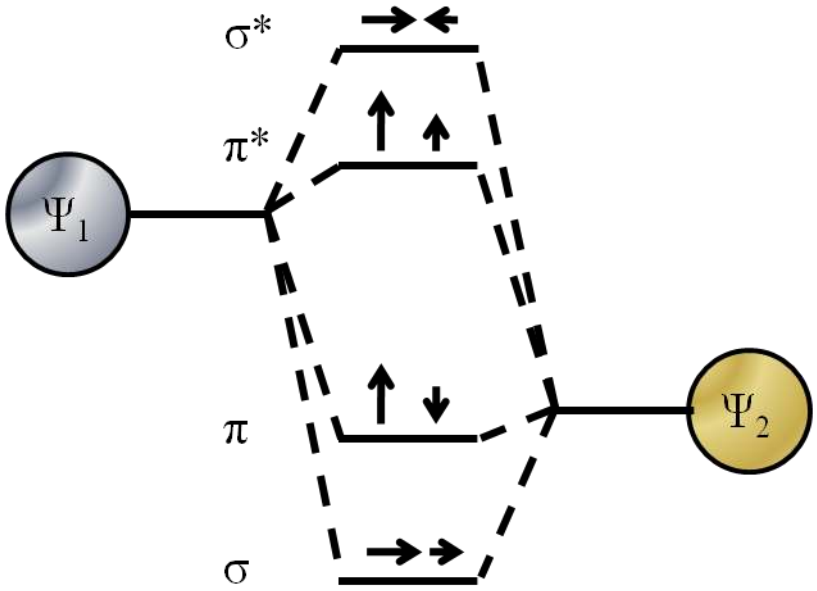

Figure 30 - Plasmon hybridisation diagrams showing the coupling between, and the dipole moments on silver and gold nanospheres set up in a dimer configuration.

Due to the success achieved in modelling the gold nanoparticle arrays separated by dielectrics by considering them as a dimer[160] a similar approach was adopted by Stefan Mühlig and Carsten Rockstuhl of the Friedrich-Schiller-Universität Jena and applied to this system. Full details of the simulations performed can be found in Reference 152.

There were, however, several challenges that made both the fabrication of the samples and the interpretation of the results more demanding than in the previous work. As before, the separation between the gold nanoparticles within the lower array was shown to be considerably larger than that between distinct arrays, thus precluding any lateral interactions and meaning that all coupling observed is between arrays that are separated by a distinct number of PE layers. This can be seen in Figure 31 where the smaller gold nanoparticles form a standard array. However, the silver nanoparticles, also seen in Figure 31, tended to coat the substrate in a less homogenous fashion, with both isolated particles and small aggregates being observed. In addition, as can also be readily observed in Figure 31, silver nanoparticles produced by the Lee-Meisel method exhibit a wider range of particle sizes and shapes when compared to the Turkevich method used for gold nanoparticles,

thus making the spectral interpretation of the ensembles more challenging. Nevertheless, the dominating resonances of the system can be fully described by considering a dimer consisting of one gold nanoparticle and one silver nanoparticle from each array. In other words, the structure under investigation can be thought of as an amorphous arrangement of heterodimers that consists of one gold and one silver nanoparticle.

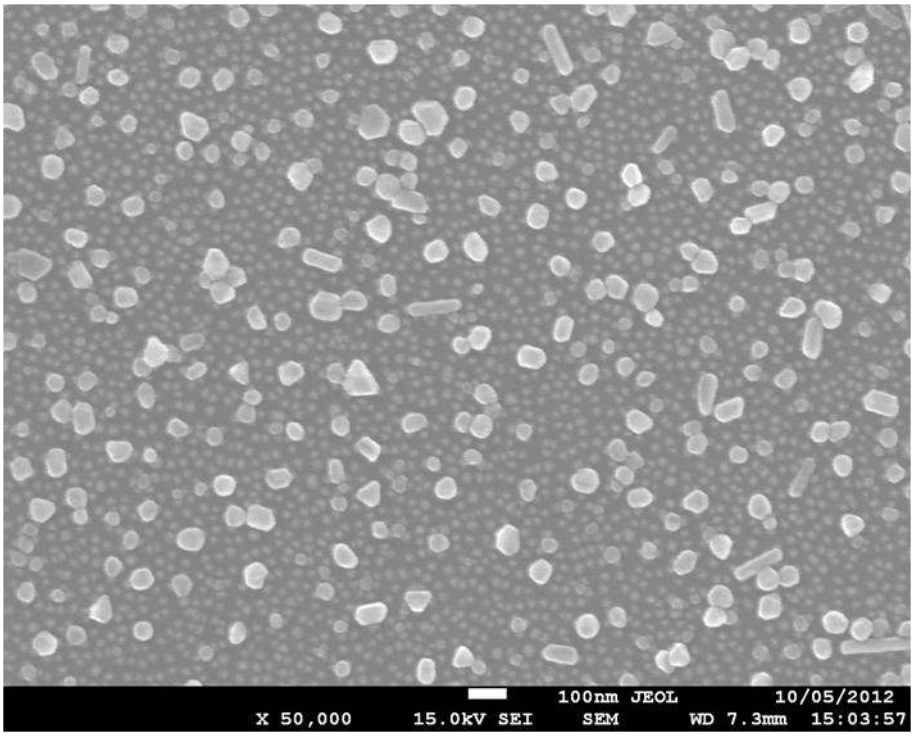

Figure 31 - SEM image showing an array of gold nanoparticles (~18 nm diameter) and an array of silver nanoparticles (~43 nm diameter) separated by seven polyelectrolyte layers. Because of the difference in height, the gold nanoparticles, which are underneath, appear slightly out of focus.

The spectra corresponding to single arrays of gold nanoparticles and silver nanoparticles shown in Figure 31 along with the simulated spectra of single nanospheres of each metal can be seen in Figure 32. In the simulations isolated spheres were considered whereas the measurements were performed on single layers of gold and silver nanoparticles with a filling fraction of 27 and 23 % respectively. The morphological differences between the two arrays have a large effect on their optical properties. A single peak, at the same frequency as an individual particle, is observed for the well separated gold nanoparticles while two peaks, that of the isolated particles and that of the aggregates, are discernible in the case of the silver nanoparticles. The small aggregates, on average comprising 3 – 4 particles, result in a significantly red-shifted peak that, in addition, is somewhat broadened owing to the variety of both the number of the particles in the aggregates and the size of the particles that form them. With the exception of the aggregates in the silver nanoparticle array

discussed above, the principal source of coupling in the final structure results from inter-array interactions. The coupling of spheres in one layer can either be neglected (in the case of the gold nanoparticle array) or only weakly contributes to the optical response of the entire structure (in the case of the silver nanoparticle array) meaning that any observable phenomena are dominated by the mutual coupling of the particles from separate arrays.

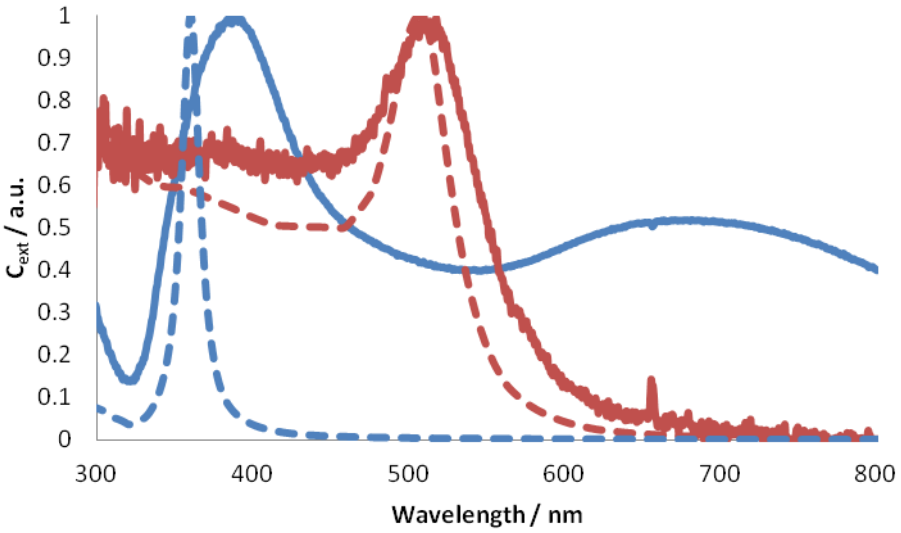

Figure 32 - Extinction spectra of single arrays of gold (red traces) and silver (blue traces) nanoparticles. Both experimental (solid lines) and simulated (dashed lines) are shown.

It was shown in Section 4.1.4 that the adsorption of a second gold nanoparticle array on top of another induces a red-shift of the LSPR peak. This shift is dependent on the degree of separation, defined by the number of PE layers, between the two arrays. When compositionally asymmetric structures are fabricated the dominant resonances observed are the bonding modes. However, as can be seen in the extinction spectra shown in Figure 33 other peaks are also perceived. For reasons of clarity only two samples are shown in the figure, corresponding to gold and silver nanoparticle arrays that are separated by 1 (blue trace) and 21 (red trace) PE layers. Two peaks can clearly be distinguished at approximately 380 and 395 nm, which correspond to the σ* and π* modes outlined in Figure 30, for the samples with greater degrees of separation. In this case it is difficult to conclusively identify which peak corresponds to which mode due to their relatively low separation and the potential influence of coupling between the plasmonic modes and interband absorption processes which has been noted in literature[177] as being capable of disrupting the order of the hybridised modes shown in Figure 30. For the trace relating to the two arrays that are separated by only one PE layer, two longer wavelength peaks can also be observed at approximately 510 and 600 nm, corresponding to the π and σ bands shown in Figure 30. This represents, to the best of our

knowledge, the largest scale observation of all four bonding and anti-bonding modes that presently exist in coupled systems of asymmetric metallic nanoparticles.

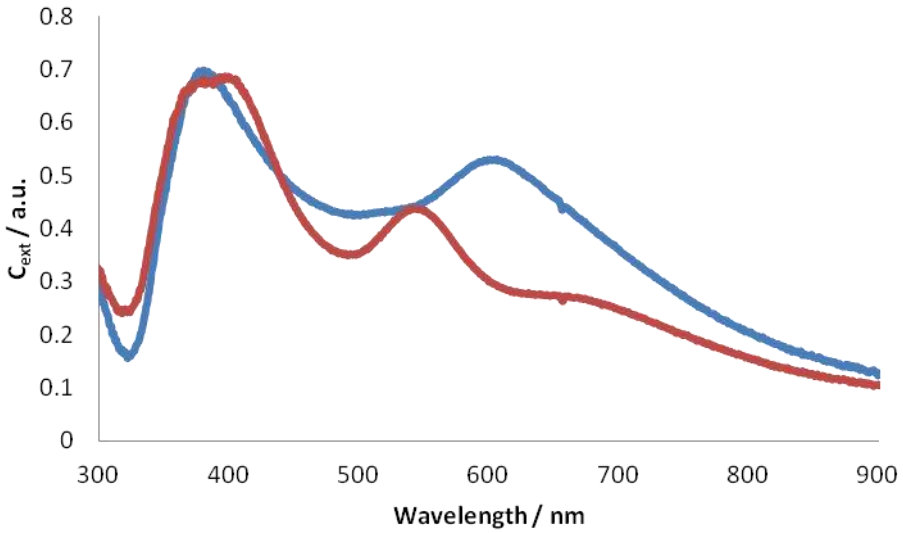

Figure 33 - Extinction spectra of arrays of gold and silver nanoparticles separated by 1 (blue trace) and 21 (red trace) polyelectrolyte layers.

Following the observance of all four hybridised plasmon resonances an in-depth study was conducted into their behaviour as a function of metallic nanoparticle array separation. Several samples were fabricated with a variety of differing array separations, achieved by altering the number of PE layers in-between. Taking the stronger of the two long wavelength peaks as an example it can clearly be seen that as the number of PE layers separating the two nanoparticle arrays is decreased it undergoes a significant red-shift. As can be seen in Figure 34, the observed red-shift follows the expected exponential trend, falling to zero at the point at which the two arrays are no longer able to interact due to the distance between them being too great. This shows that the near-field coupling between compositionally asymmetric metallic nanoparticle arrays is strongly dependent on, and can be tuned simply by controlling, the inter-array distance.

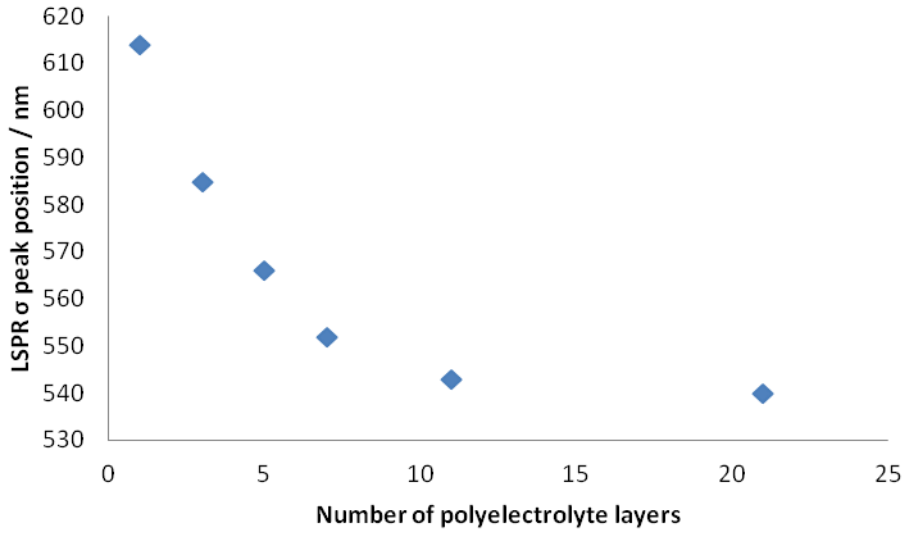

Figure 34 - LSPR peak positions of σ mode of two separated arrays of gold and silver nanoparticles as a function of array separation.

In addition to being able to control the frequency of the individual resonances it is also possible to control their relative extinctions. This can be achieved through exciting the sample at oblique angles of incidence. By rotating the sample the geometrical configuration of the two arrays relative to the incident beam is altered with the two transverse modes, corresponding to light polarised perpendicularly to the main dimer axis becoming increasingly important. As the sample is rotated and the transverse modes become more dominant in the spectral analysis the longitudinal modes, those corresponding to light polarised along the main dimer axis, become correspondingly less prevalent. What essentially results is an angular dependent extinction of light whereby certain modes can be preferentially excited over others depending solely on the angle of incidence of the impinging radiation. This is outlined in Figure 35 which shows the extinction spectra of the samples with both 1 (a) and 21 (b) separating PE layers with incident light at both 0 ° (blue trace) and 70 ° (red trace) to the plane of the sample. It can be seen from these two figures that there is a significant change in the relative extinction intensity between the resonances that are excited by transverse and longitudinal polarisation. This ratio is plotted in Figure 35c and Figure 35d (for the samples separated by 1 and 21 PE layers respectively) as a function of the angle of incidence of the impinging light beam. Here, it can be seen that in both cases there is a smooth transition as the transverse modes are, in each case, increasingly excited.

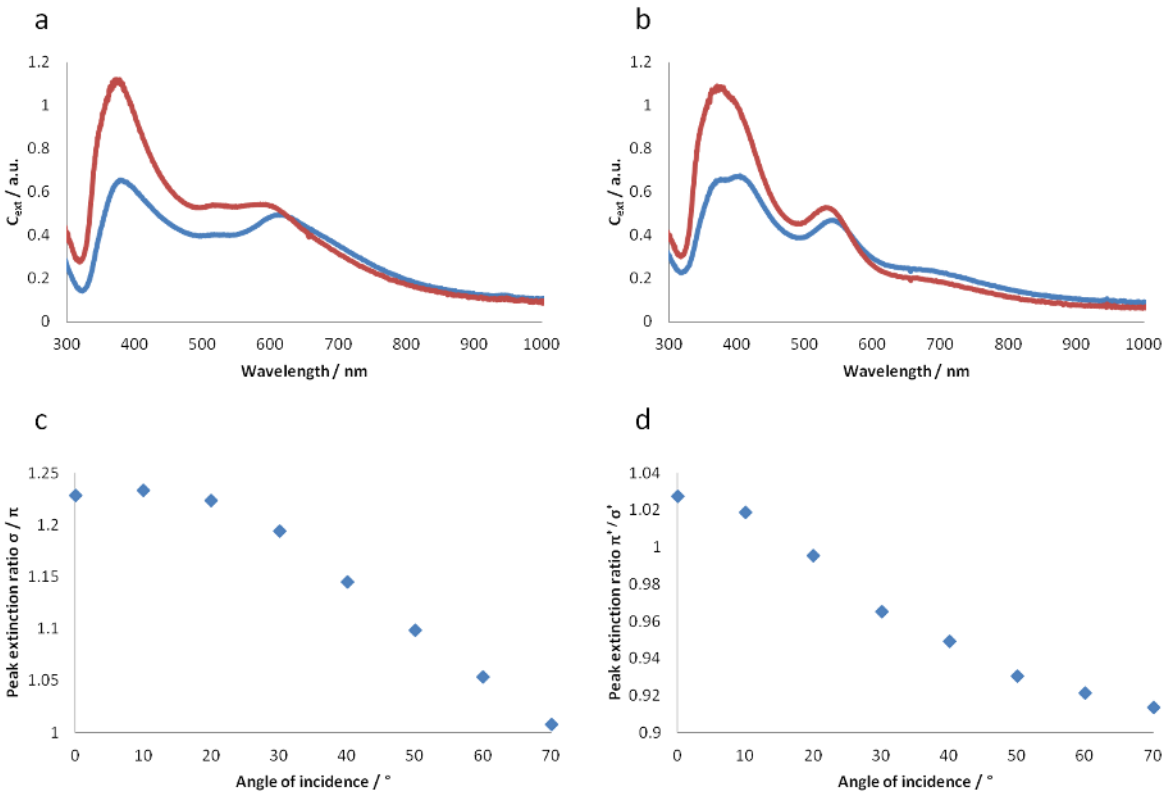

Figure 35 - a) Extinction spectra of gold and silver nanoparticle arrays separated by 1 polyelectrolyte layer at 0 ° (blue trace) and 70 ° red trace. b) Extinction spectra of gold and silver nanoparticle arrays separated by 21 polyelectrolyte layers at 0 ° (blue trace) and 70 ° red trace. c) Ratio of σ mode peak intensity to π mode peak intensity for gold and silver nanoparticle arrays separated by 1 polyelectrolyte layer. d) Ratio of π* mode peak intensity to σ* mode peak intensity for gold and silver nanoparticle arrays separated by 21 polyelectrolyte layers.

Rotating the polarisation state of the incident light will similarly induce the preferential excitation of either the transverse or longitudinal modes and is another means of observing this effect. In contrast to work by other groups pertaining to symmetry breaking in heterodimers which concentrates solely on single dimers,[177] rather than the more complex ensembles studied here, it is not possible to 'switch off' specific modes depending on the angle of incidence or polarisation state of the incident radiation. This is as a result of a number of different nanoparticle dimer orientations existing over a large surface area which partially averages out the observed polarisation and orientation dependence.

4.1.6. Surface enhanced Raman scattering applications

As outlined in Section 2.2.6, one of the principal applications of metallic nanoparticles is currently in the field of SERS. The large increase in electric field observed between metallic nanoparticles results in massive enhancements of the Raman signal and opens up the technique of Raman spectroscopy

for a variety of uses. Recent investigations have highlighted the importance of arrays of both silver and gold nanostructures to the advancement of these techniques.[180] As such, it was considered that the stratified arrays developed in the previous sections would form an ideal prototypical structure from which to study enhancements measured as a function of several material parameters. For instance, the magnitude of the hotspots, and in principal therefore the enhancement, decreases with particle separation. This, along with other factors such as particle size and composition can easily be examined with the layered arrays of metallic nanoparticles.

Samples were prepared and sent to Dana Cialla and Karina Weber of the Institute of Photonic Technology, Jena, who carried out all measurements to determine potential enhancements of the Raman signal. A standard fluorescent dye used in SERS experiments, Nile blue, was used as the analyte and samples were excited using a laser with a wavelength of 633 nm. Measurements were conducted on two series of samples. Each series was constructed from two arrays of nanoparticles, of either 20 nm in diameter and 40 nm in diameter, and separated by a range of PE layers.

Shown in Figure 36a are the trends in SERS enhancements that would be expected from two gold nanoparticle arrays with a diameter of 20 nm separated by a number of differing PE layers. It can clearly be seen that the greatest enhancement would be expected for two gold nanoparticle arrays separated by a single PE layer. At greater separations there is a large drop off in terms of the enhancements anticipated upon which there appears to be a quasi-exponential decline in the enhancements (shown in greater detail in the inset of Figure 36a). These simulations, along with the ones presented in Figure 37 and Figure 38, were supplied by Stefan Mühlig and Carsten Rockstuhl of the Friedrich-Schiller-Universität Jena. As can be seen from Figure 36b there are two major discrepancies between the predicted results and the actual measured enhancements. Firstly, the absolute values of the simulated enhancements are significantly lower than those of the measured enhancements. This is due to the units in the experimental measurements being completely arbitrary. As such only the general trends seen in the simulations and experiments can be compared. The second difference, which is perhaps more interesting in terms of understanding the enhancement and self-assembly processes involved, is that the measured enhancement for two gold nanoparticles arrays separated by only a single PE layer is lower than that of the samples with greater separation. The simulations, on the other hand, forecast that the sample with the lowest separation should exhibit by far the greatest enhancement. A number of potential reasons for this exist. One hypothesis could be that the intense electric fields that exist between two resonant nanoparticles separated by only one PE layer are sufficiently high to cause the degradation of the analyte molecules. While this is plausible it would suggest that the PE between the nanoparticles

would also be susceptible to such breakdown and throughout the course of this research no indications pointed towards this. A more likely explanation can be constructed through electrostatic arguments. Given that only a singular positively charged PE layer is present between the two gold nanoparticle arrays, and that the analyte molecule, Nile blue, is itself slightly positively charged, it is conceivable that electrostatic repulsion between the polymer and the dye result in the exclusion of the dye from the nanogaps between the metallic particles. As the volumes where the highest enhancements would be expected are directly between the nanoparticles this could result in the lower than expected enhancements observed.

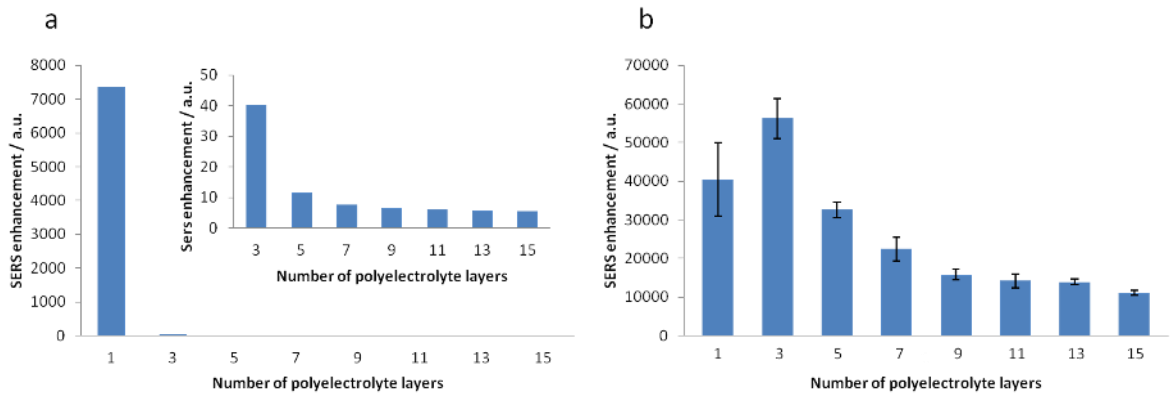

Figure 36 – a) Simulated enhancement of Raman signal of Nile blue as a function of the number of polyelectrolyte layers between two gold nanoparticle arrays (20 nm diameter). b) Experimental enhancement of Raman signal of Nile blue as a function of number of the number of polyelectrolyte layers between two gold nanoparticle arrays (~20 nm diameter).

Disregarding this anomaly, the magnitude of the Raman enhancement can be seen to decline exponentially as a function of nanoparticle array separation. A contributing factor to this decrease in enhancement is likely to be the diminishing magnitude of the electric field between the nanoparticles as they are moved to greater separations. An additional explanation for the magnitude of the enhancement decaying in such a manner, other than the strength of the 'hot-spot' decreasing at greater degrees of separation is the overlap of the laser radiation used to excite the analyte, which has a wavelength of 633 nm, with the plasmon band of the gold nanoparticle structures. This can be seen in Figure 37a where the simulated extinction spectra of two gold nanoparticle (~20 nm diameter) arrays with differing numbers of PE layers in-between are shown. The extinction at 633 nm for each of these spectra is plotted as a function of the number of PE layers in-between the arrays in Figure 37b. While the effect is not as dramatic as that shown in Figure 36a it can clearly be seen that for each of the samples there is a difference in the overlap between the extinction spectra and the wavelength of light used to excite the analyte molecule. This means, therefore, that in each

sample the plasmonic resonance, which is essentially the mechanism that bestows the enhancement effect seen, is present to differing extents. While this does not help to explain the discrepancy between the anticipated and observed results in the sample where only a single PE layer is employed it does aid in the explanation of the overall decrease in enhancements seen in all of the other samples.

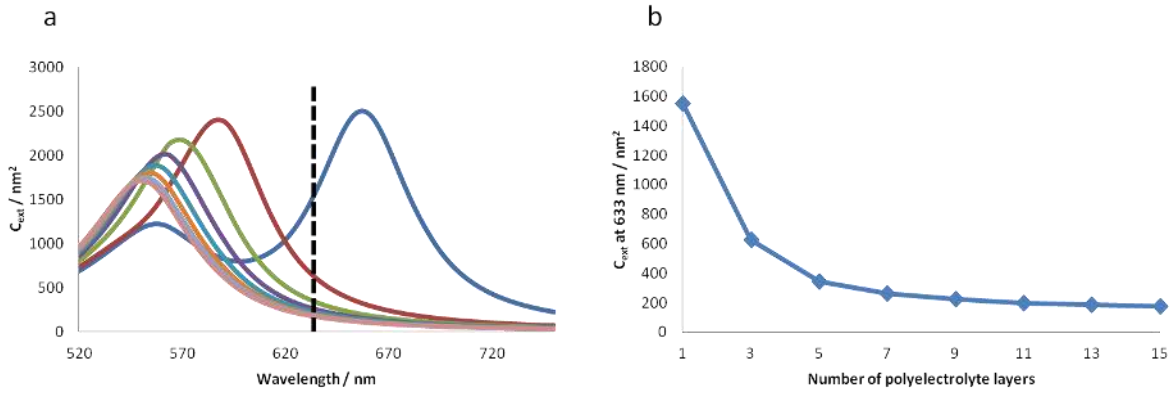

Figure 37 - a) Simulated extinction spectra of two gold nanoparticle (~20 nm diameter) arrays separated by (from right to left) 1, 3, 5, 7, 9, 11, 13 and 15 polyelectrolyte layers. The dashed vertical line is drawn at 633 nm. b) The extinction coefficient of each of the simulated spectra in a) at 633 nm.

Similar trends can be observed in the samples where larger nanoparticles were used. Shown in Figure 38a are the simulated enhancements that would be expected from two arrays of gold nanoparticles (~40 nm diameter) when the overlap between the extinction spectra of the samples and the excitation wavelength (633 nm) is taken into account. This overlap between the excitation wavelength and the extinction spectra for each of the samples is shown both qualitatively and quantitatively in Figure 38c and Figure 38d respectively. In this case, the plasmon resonance of the sample separated by only a single PE layer is red-shifted to such an extent that the cross-section of extinction at 633 nm is relatively low. Consequently, the surface electrons of the metallic nanoparticles are not driven into resonance at this frequency and very little enhancement is expected. This is mirrored in the experimental results shown in Figure 38b where, as with the samples constructed from the smaller nanoparticles, there is considerably less enhancement measured in the sample with the lowest separation between the arrays. Of course, as could be seen in the samples fabricated with smaller nanoparticles, the overlap between the plasmon resonance and the wavelength of the incident laser radiation does not tell the full story and it is expected that the other factors discussed above, for example the exclusion of the analyte molecules due to electrostatic repulsion will also play a role in this case. In addition, while it can be seen that an overall trend of decreasing enhancements at greater nanoparticle array separations is observed it is

also clear that this is not as smooth as in the series with the smaller nanoparticles. In general, throughout the course of this research, it was found that the most homogeneous arrays were achieved with nanoparticles of around 20 nm in diameter. This is one possible reason for this small incongruity between the two series of samples.

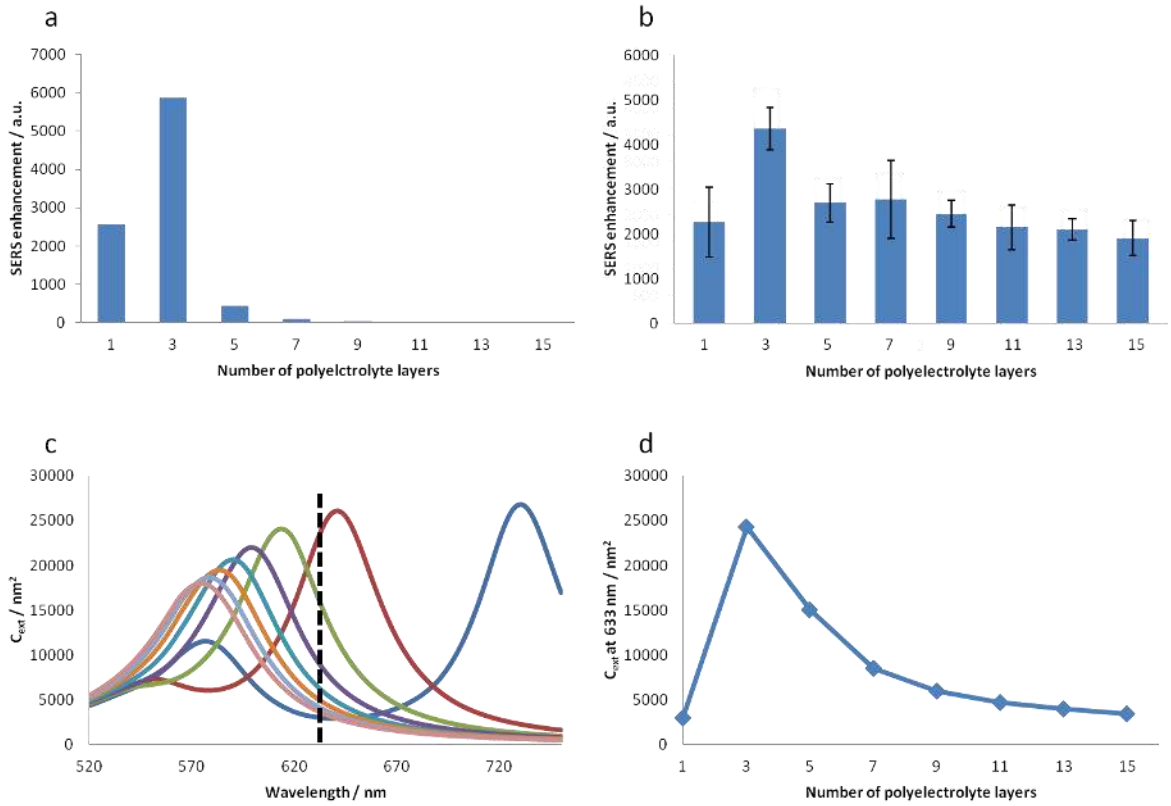

Figure 38 - a) Simulated enhancement of Raman signal of Nile blue as a function of the number of polyelectrolyte layers between two gold nanoparticle arrays (~40 nm diameter). b) Experimental enhancement of Raman signal of Nile blue as a function of number of the number of polyelectrolyte layers between two gold nanoparticle arrays (~40 nm diameter). c) Simulated extinction spectra of two gold nanoparticle arrays (~40 nm diameter) separated by (from right to left) 1, 3, 5, 7, 9, 11, 13 and 15 polyelectrolyte layers. The dashed vertical line is drawn at 633 nm. d) The extinction cross-section measured at 633 nm as a function of the number of polyelectrolyte layers between two (~40 nm diameter) gold nanoparticle arrays.

It must also be taken into account that while the simulations refer to a single dimer, and as such represent and idealised situation, the experimental measurements were conducted on samples fabricated from two large scale arrays of amorphously arranged nanoparticles covering several square centimetres. There is no direct correlation between the positioning of the particles from different arrays, resulting in a number of different configurations being measured and enhancements being averaged out. Additionally, as was shown in the GISAXS and SEM data presented in Section 4.1.4, gold nanoparticle arrays separated by only a few PE layers cannot be

considered as existing in two separate planes and rather form chains and small aggregates at the surface of the substrate. This could also be a contributing factor to any discrepancies seen between simulations and experimental data.

The work described above involved the drop casting of the Raman active dye on top of the nanoparticle structure, allowing it to penetrate into the volume between the particles. The imprecise nature of this process, with no means of controlling or discerning the exact location of the dye molecules at the time of measurement could also lead to inconsistencies between simulated and measured data.

This potential source of error motivated the conception and fabrication of alternative structures. The block copolymer poly(fluorescein isothiocyanate allylamine hydrochloride) is composed of both positively charged and fluorescent units in the ratio of 50:1 respectively. It was initially thought that the ability to precisely and reproducibly adsorb this polymer layer at specified distances between the two nanoparticle arrays would allow the enhancement effects discussed above to be more accurately measured. This was, unfortunately, found not to be the case as an adequately strong Raman signal could not be detected from the chromophore incorporated into the polymer. However the only requirement for a more in-depth investigation of this system is a Raman active compound, not necessarily polymeric, which, in addition, exhibits the multiple charges essential for the assembly process.

The systems investigated did not exhibit the astonishing enhancements reported by some groups. However, through the optimisation of certain parameters such as particle composition and size it is believed that significant improvements could be made. Additionally, one of the major challenges facing researchers working on SERS is the reproducibility of results. It is thought that using large scale arrays of amorphously placed nanoparticles could be one means of achieving this through the averaging out of the uncertainties which cause these problems.

Despite the discrepancies highlighted above the general trends shown above in the simulations and experimental results are certainly consistent with one another. That certain limitations in agreement between the two occur only serves to demonstrate that a number of factors, some of which are yet to be fully understood, can be probed using these systems and that a great deal of research opportunities remain unexplored in this branch of science.

4.1.7. Polymeric substrates

Due to their transparency at visible wavelengths glass substrates are adequate for the vast majority applications involving metallic nanoparticles. However the rigidity that they possess imposes limitations and restricts several potential functionalities that could otherwise be achieved. PDMS substrates on the other hand are extremely flexible and exhibit a high degree of elasticity – the result of an extremely low glass transition temperature. In addition they display a number of other qualities, such as their low cost, ease of fabrication, optical transparency and their high levels of thermal and oxidative stability.[181] As a result of these impressive physical properties it would be of significant interest to prepare gold nanoparticle arrays on PDMS substrates with a wide array of potential applications envisaged. PDMS is already extensively used in the construction of microfluidic devices however the combination with metallic nanoparticles opens up routes to optical strain detectors,[182] SERS substrates[183] or microchip electrophoresis,[184] for example.

Metallic nanoparticles could either be deposited on the surface of the PDMS substrates, as in the work outlined in previous sections, or alternatively incorporated into the bulk of the material itself.[185] Several means, ranging from metal layer coatings to surfactant treatments, exist to modify PDMS surfaces[181] however one of the most practical involves the functionalisation of the surface with a tri-functional organosilane in much the same manner to that used for glass and silicon substrates. Prior to this it is first necessary to modify the surface of the PDMS by a plasma treatment which creates the Si-OH bonds at the surface required for the functionalisation step.[181] One challenge faced when using this technique, however, is that of hydrophobic recovery which is caused by the migration of uncured PDMS oligomers towards the surface and the replacement of the Si-OH functional groups created by the plasma procedure. This can result in instability of the modified layer but does not pose significant problems if direct functionalisation is carried out.

An example of functionalised PDMS substrates that have been decorated with arrays of gold nanoparticles is seen in Figure 39. Similarly to that which was seen previously with the glass and silicon substrates the gold nanoparticles completely cover the surface of the substrate and, by eye at least, appear to form relatively homogeneous arrays. After a single array has been adsorbed at the surface it is again possible to assemble PE layers and additional nanoparticle arrays. Samples 1-3 are constructed from two gold nanoparticle (~20 nm diameter) arrays separated by 21, 11 and 5 PE layers respectively while sample 4 represents a single gold nanoparticle array. These samples were prepared with a view to investigating any potential changes in optical properties that may be observed upon stretching of the substrates. As has been extensively shown in Section 4.1.4 the position of the surface plasmon resonance of a metallic nanoparticle array is strongly dependent on

the strength of coupling between the individual nanoparticles which is, in turn, a function of the distance between the particles. It was thought that by stretching the substrates the positions of the nanoparticles would alter sufficiently for a shift in plasmon resonance to be observed. One particular structure that was of interest was that containing two gold nanoparticle arrays separated by PE layers. It was anticipated that stretching of this structure in the plane of the arrays could result in the two arrays approaching each other and would result in a red-shift of the plasmon resonance. Unfortunately this was not found to be the case and no reproducible trend could be discerned.

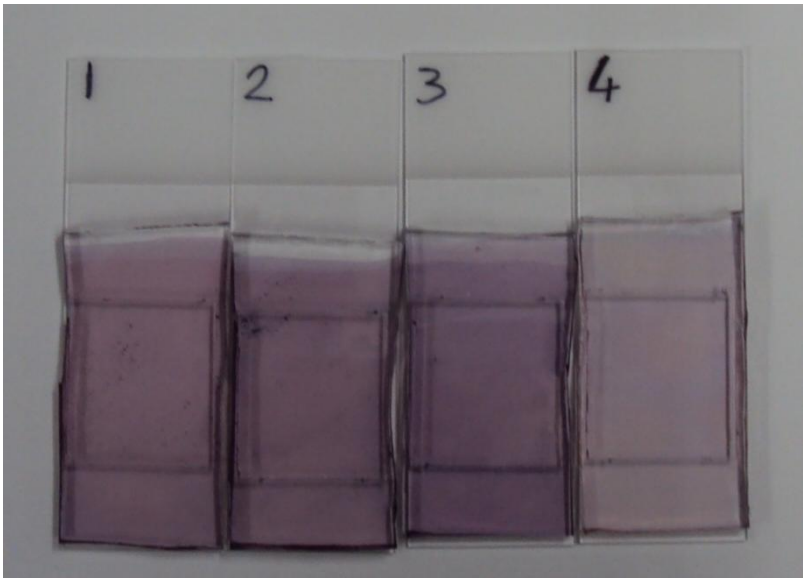

Figure 39 – Gold nanoparticle (~20 nm diameter) arrays on PDMS. Samples 1-3 are constructed from two gold nanoparticle arrays separated by 21, 11 and 5 polyelectrolyte layers respectively. Sample 4 is a single gold nanoparticle array.

Shown in Figure 40 are the extinction spectra corresponding to the samples shown in Figure 39. The blue trace represents a single gold nanoparticle array while the red, green and purple traces show two gold nanoparticle arrays separated by 21, 11 and 5 PE layers respectively. As would be expected the optical properties follow very similar trends to those observed for similar structures prepared on glass. There is a significant increase in extinction from the sample with a single gold nanoparticle array to those with two. In addition, the position of the plasmon resonance follows a similar trend to that seen previously with less separating PE layers resulting in further red-shifts. An additional peak can be observed in all of the samples at around 700 nm. This is assumed to be caused by small scale aggregation of gold nanoparticles. While this is not significant and the optical properties are dominated by the principal resonance at approximately 520 – 550 nm these small areas of aggregation can, nevertheless, be seen in the photograph of the samples in Figure 39.

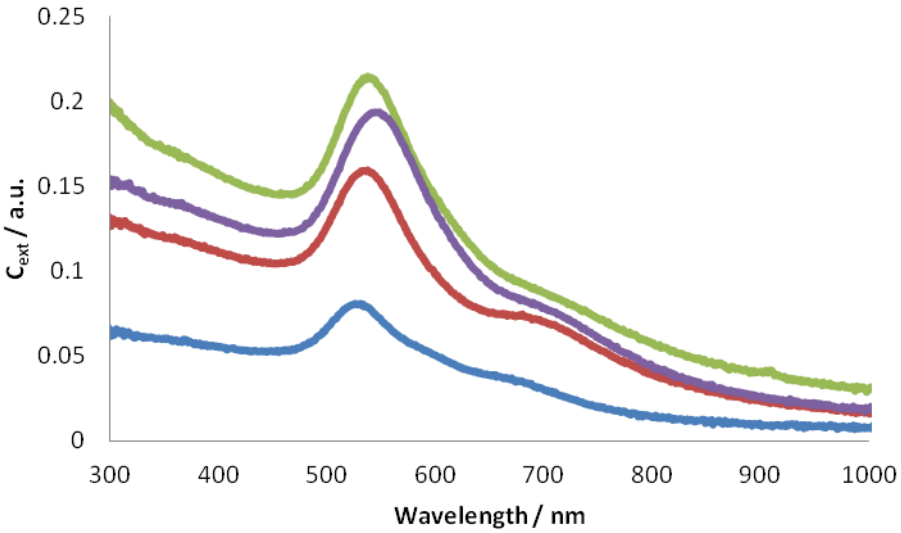

Figure 40 – Extinction spectra of gold nanoparticle (~20 nm diameter) arrays on PDMS substrates. The blue trace represents a single gold nanoparticle array while the red, green and purple traces show two gold nanoparticle arrays separated by 21, 11 and 5 polyelectrolyte layers respectively.

4.1.8. Layer-by-layer film lift-off technique

For certain specific applications the use of substrates such as glass, silicon or PDMS as a base on which to fabricate layered arrays of metallic nanoparticles is sufficient. However, if this technology were to be developed to the extent that it could be incorporated into some form of functional device then it is easy to imagine that it would be necessary to make it applicable to a wider range of situations. A clear example of this is in the display industry where device weight and thickness are of crucial importance. The need for a bulky glass substrate, several orders of magnitude thicker than the nanoparticle arrays that it supports, becomes disadvantageous in such circumstances. As such, a means of fabricating stand alone polymer films with metallic nanoparticle inclusions would be desirable. This can be achieved, again, through the application of the layer by layer assembly of polymeric species.

In addition to the methods based upon electrostatic interactions used to assemble polymer layers introduced in Section 2.3 and applied in Section 4.1.4 it is also possible to utilise other principles to prepare multilayers of polymers. One example is the exploitation of hydrogen bonding between two different polymer species in order to create the multilayers in an analogous process to that described for the electrostatic systems. Of course, by their very nature, hydrogen bonds are intrinsically pH sensitive and as such changes in pH can lead to film decomposition once a critical

value is reached. This critical value is extremely dependent on the system of polymers used to fabricate the multilayers. While films that decompose may not at first glance appear to be extremely useful, many applications, particularly in the field of controlled drug delivery, can be conceived.[186]

Some polymers possess the ability to form multilayers through either hydrogen bonding or the more conventional electrostatic processes. As a result it is possible to combine these two techniques and fabricate hybrid structures. By first depositing the pH sensitive layers and then the layers assembled by electrostatic techniques it is possible to alter the pH to break the hydrogen bonds and release a stable stand alone composite polymer film.[155] It has been shown that self-supporting PE multilayer membranes with thicknesses of 55 to several hundred nanometres and areas of a few square centimetres could be prepared.[155]

The polymers chosen to achieve this were PAA and PEG which, in combination, have a critical pH of 3.6.[127] On top of this were deposited PAH and PSS layers, the standard PEs used throughout this work. Of course, the deposition of the PE multilayers must also be carried out at reduced pH in order that the hydrogen bonds are not prematurely broken. Exposure to a solution of gold nanoparticles serves two purposes. Firstly the nanoparticles adsorb at the surface of the PE thin film, creating a nanoparticle array at the surface similar to those presented in Section 4.1.2. Simultaneously, the nanoparticle solution, whose pH is above the critical pH of the PAA / PEG system, slowly induces the breakdown of the hydrogen bonds contained within these layers and releases the PE / gold nanoparticle thin film. Examples of these self-standing films can be seen in Figure 41 with the pink colour originating from the LSPR of the gold nanoparticles clearly visible in the inset image.

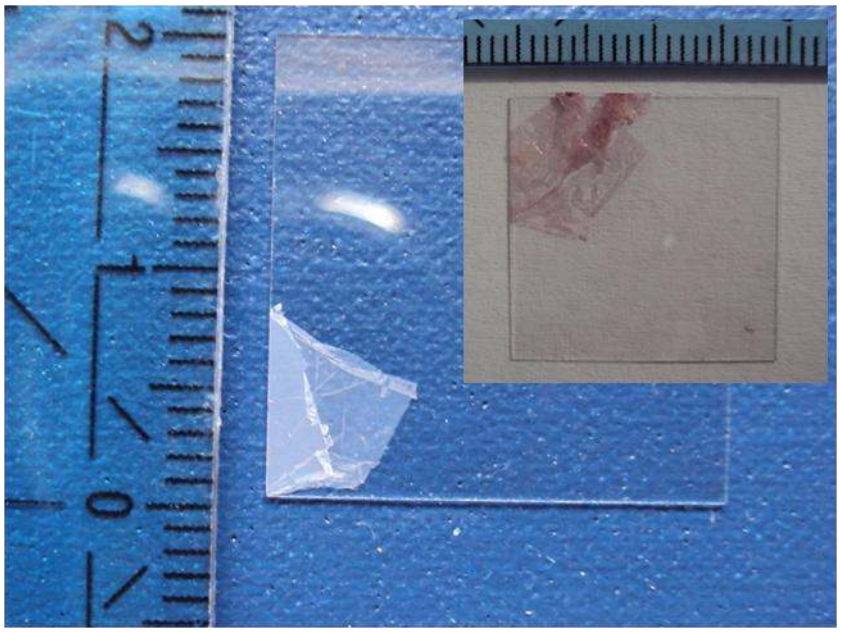

Figure 41 - Photograph of a stand alone PAH / PSS multilayer film with gold nanoparticles (~20 nm diameter) incorporated.

4.1.9. Arrays of rods

As was outlined in Section 2.2 spherical nanoparticles, while perhaps the most commonly used, are by no means the only form available. In certain cases, depending on the application or the desired effect, other forms such as nanorods provide considerable advantages over the more basic spherical particles. The introduction of anisotropy, the enhanced extinction coefficients and the wide range of tunability of the longitudinal plasmon resonance are just some of the benefits afforded by the use of nanorods over nanospheres.

While the fabrication of structures such as SRRs through bottom-up techniques is outwith current capabilities, analogous structures, exhibiting similar properties, can be produced using gold nanorods. As with spherical nanoparticles two nanorods, in close proximity, will strongly couple with one another and, following plasmon hybridisation theory, form new modes – one with a symmetric alignment of the two electric dipoles and one with an antisymmetric alignment.[32] Unlike the situation with nanospheres, however, there are a variety of differing geometrical configurations that the two nanorods can adopt and these configurations can drastically affect the coupling properties.[37] The antisymmetric mode of two nanorods in the transverse, i.e. side to side, configuration is also known as the 'magnetic resonance' as the antisymmetric currents in the two particles, when considered in conjunction with the displacement currents between them, can lead to a resonant excitation of a magnetic dipole moment, the consequence of which being the overall system

displaying a magnetic response.[32] As a result, two nanorods stacked together in a transverse manner can be considered as a 'magnetic atom' – one of the fundamental building blocks of metamaterials.[32] Indeed there is no reason why such magnetic atoms are restricted to nanorod dimers and while the plasmon hybridisation diagrams become significantly more complicated for larger structures constructed from trimers, tetramers or higher oligomers these structures also possess modes which can be interpreted as magnetic resonances.[187]

One potential approach to structures such as these would be to deposit an array of nanorods on a functionalised substrate and then induce their reorganisation in much the same manner as that employed in Section 4.1.3.3. In order to use electrostatic forces to deposit an array of gold nanorods on a substrate it is necessary to render that substrate negatively charged. This is due to the positive charge originating from the CTAB bilayer that caps the particles. The substrate can be rendered negatively charged simply by functionalising in the usual manner and then depositing a single layer of negatively charged PE. It was also found that in order to facilitate the adsorption of an array of gold nanorods on these substrates, and increase their density to a sufficient level, it was necessary to add NaCl to the solutions from which they were deposited. This can be seen in Figure 42 with the photograph showing arrays of gold nanorods deposited from solutions made up to a variety of differing concentrations of NaCl. The corresponding extinction spectra are also shown and it can clearly be seen that there is an optimum salt concentration that provides high density arrays of gold nanorods. Both plasmon peaks; the longitudinal, at around 660 nm, and the transverse, at around 520 nm, can be discerned, as well as a third peak in the two more optically dense samples at around 780 nm. This, in all likelihood, originates from coupling between particles in small aggregates or between particles that are simply in close proximity in the higher density arrays.

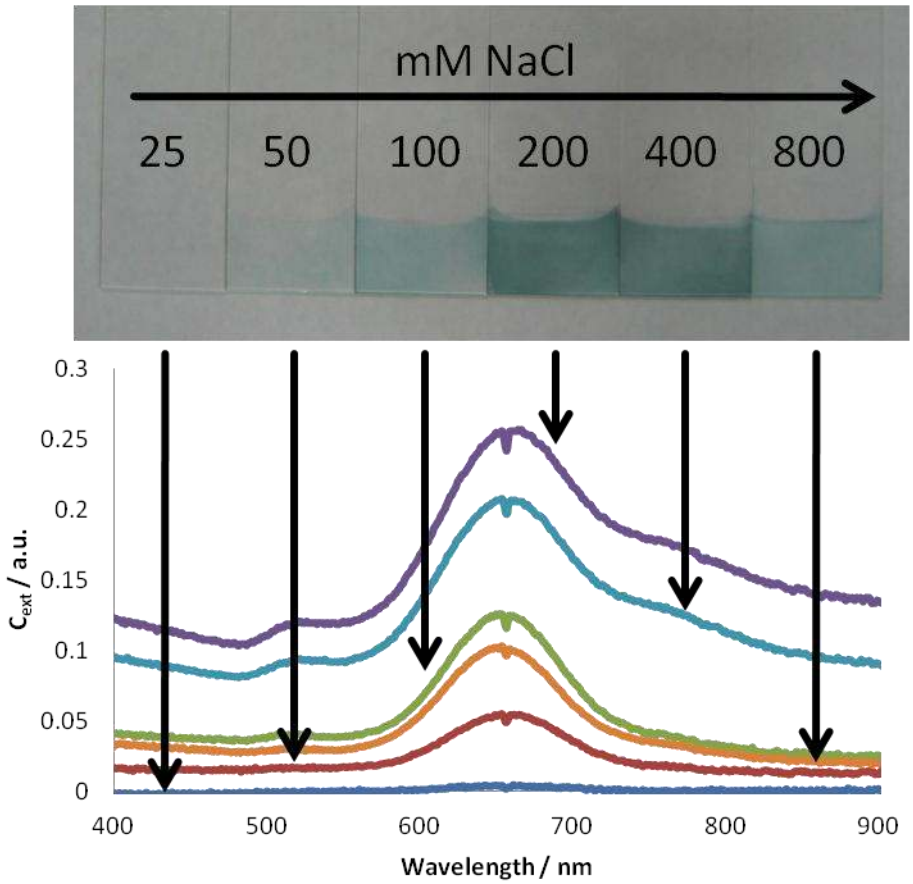

Figure 42 – Photograph showing arrays of gold nanorods deposited from solutions with varying concentrations of NaCl along with the corresponding extinction spectra.

Subjecting arrays such as these to the same repeated reorganisation and deposition process described in Section 4.1.3.3 should also, in principle, form aggregates of the particles. As with previously, the thiol molecules used will exhibit a strong affinity for the gold particles and will, to some extent at least, replace the CTAB molecules that form a capping layer at the surface. This can mobilise the particles and permit their reorganisation at the substrate surface. It is thought that the principle driving force for this reorganisation is the formation of energetically stable bilayers of the long alkyl chains of the thiol molecules. Given that there will be a significantly higher number of interactions between these thiol chains were the nanorods to align side to side rather than end to end it was thought that this would be the more favourable and therefore more likely configuration upon reorganisation. This was, in fact, seen to be the case – as shown in the SEM images in Figure 43. Figure 43a shows a gold nanorod array after the first deposition. All of the nanorods are well spaced out and no dimers or higher order structures can be seen. A number of nanosphere impurities, which originated from the growth process are also present. After exposure to the thiol solution the gold nanorods are seen to reorganise and form some dimers in the transverse configuration (Figure 43b). This deposition and reorganisation process can be repeated several times

and results in the formation of increasingly higher proportions of nanorod aggregates ordered in a transverse fashion. Figure 43c is a typical image of the structures formed after a second reorganisation step. While some individual nanorods can still be detected the majority of particles have reorganised into larger structures composed of two, three or more particles. This is even more evident in Figure 43d which shows the typical structures that could be expected after a fourth deposition step. Here, virtually no solitary nanorods can be seen and the organisation of the particles is overwhelmingly seen to be in the transverse configuration. This strongly supports the hypothesis that the driving force for the formation of the aggregates is the establishment of bilayers of the alkyl chains of the thiol molecules.

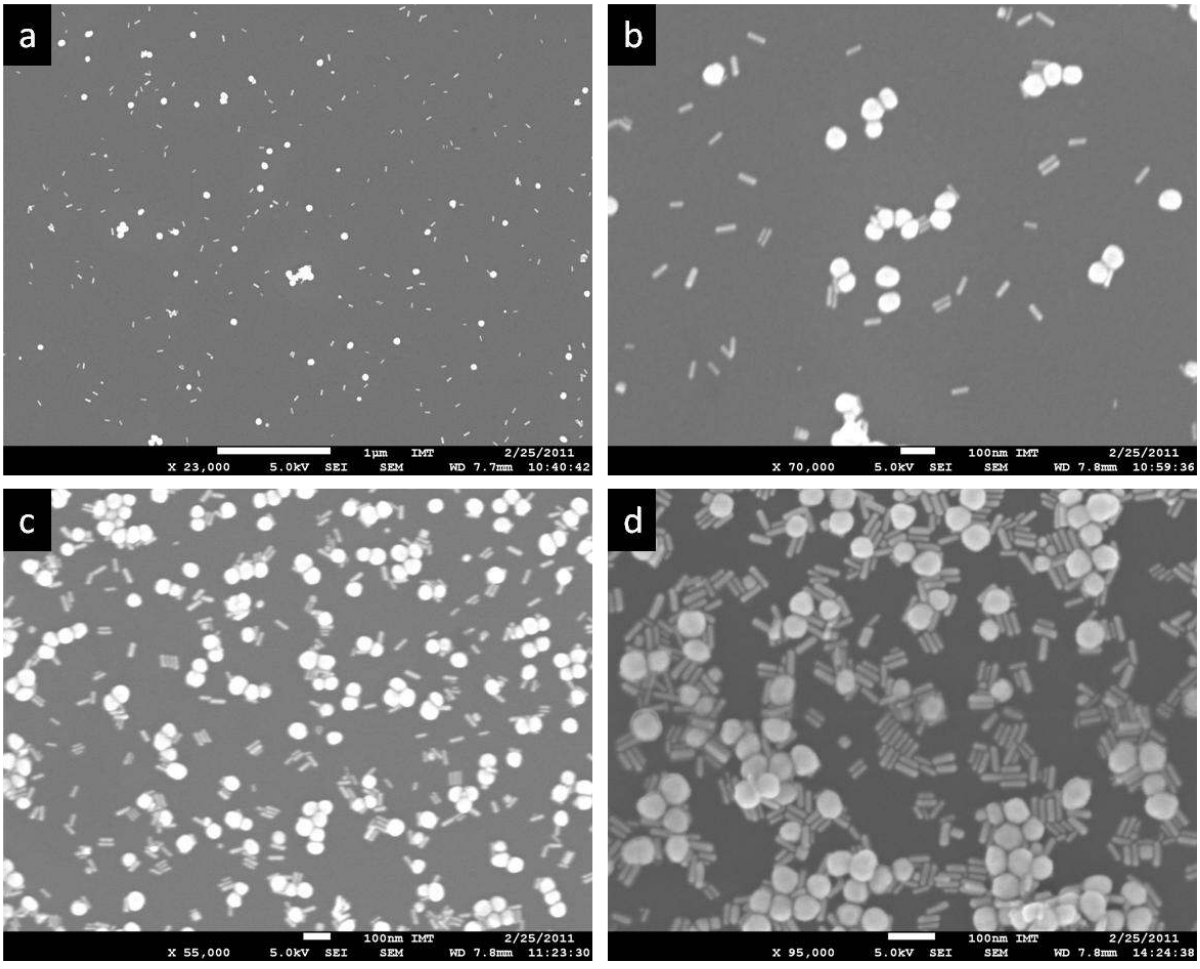

Figure 43 – SEM images of gold nanorods deposited on functionalised substrates depicting various stages of the deposition and reorganisation process as described in the main body of the text. Shown are typical morphologies observed after a) the first deposition, b) the first reorganisation, c) the second reorganisation and d) the fourth deposition. An increase in particle density as well as the lateral organisation of the nanorods can clearly be observed. Gold nanorods were deposited from solutions with an NaCl concentration of 200 mM.

It is also possible to follow this process by UV-vis spectroscopy, as can be seen in Figure 44. Successive deposition (blue traces) and reorganisation (red traces) steps are shown, steadily progressing to higher extinction coefficients. The most important feature of these spectra is that upon each reorganisation step a significant blue shift of the LSPR is perceived. This is indicative of lateral coupling and is further evidence of the preferential organisation of the nanorods in a transverse fashion.

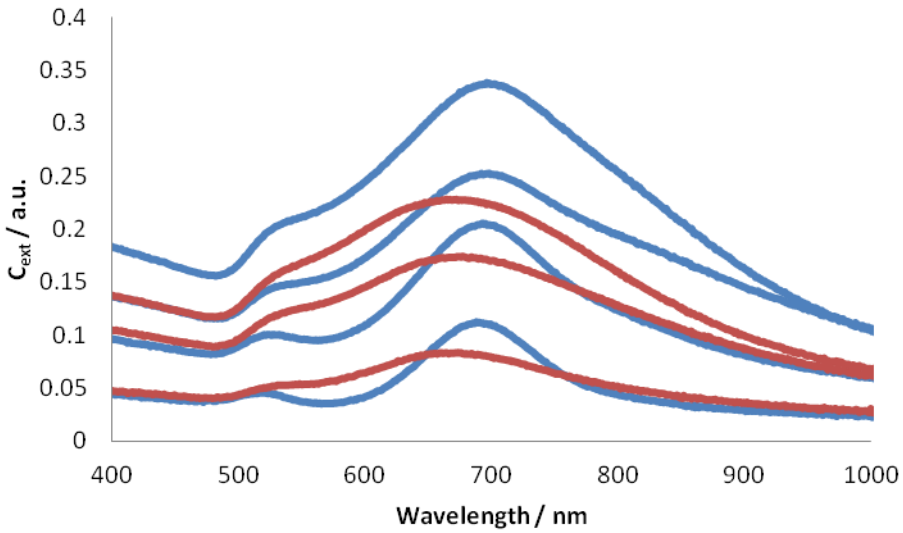

Figure 44 – Extinction spectra of gold nanorod arrays that have undergone several reorganisation and additional deposition steps. Deposition steps are shown as blue traces, progressing from low extinction coefficients to higher extinction coefficients while reorganisation steps are shown as red traces, again progressing from low coefficients to higher extinction coefficients.

Two negative aspects of this work are very clearly observable from the SEM images in Figure 43. Firstly, the nanosphere impurities form an increasingly large proportion of the particles at the substrate surface as successive deposition steps are carried out. These will both affect the optical properties of the samples and could, additionally, hamper the formation of ordered nanorod domains. It would, therefore, be desirable to repeat this work without these nanosphere impurities. Another notable negative point is the fact that while this process is clearly capable of reorganising nanorods into transverse configurations these are limited to relatively small domains. Each organised structure is independent of the next and there is no overall alignment of the nanorods. In such a situation the advantages introduced through the use of anisotropic particles are largely cancelled out unless only these small domains are taken into account. This is particularly disadvantageous when it is considered that one of the major benefits of the bottom-up techniques used is the inexpensive fabrication of large scale samples. As such, if this work is to be further developed it would be of high interest to find a means to not only organise the nanorods

preferentially in a transverse manner but also in terms of their global alignment. This could be carried out, for example, by combining these deposition techniques with the substrate patterning techniques introduced in Section 4.1.2. By confining the nanorods to certain areas which have a width shorter than the nanorod length these rods would, by necessity, adsorb in the direction of the functionalised strip. Another possibility for the alignment of the nanorods would be the application of a strong magnetic field during the deposition process. This technique has been shown as being capable of inducing the lateral organisation of nanorods and polarised optical measurements suggest that this can also impart an overall alignment to the sample.[188] Although the process is not completely understood it is presumed that the induction of the magnetic dipoles present in these transverse arrangements of the particles is the driving force.[188]

4.2.Core-shell nanoclusters

4.2.1. Introduction

As outlined in Section 1.3, it is not only planar organisations of metallic nanoparticles which are of interest to the metamaterials community. Spherical arrangements, otherwise known as core-shell nanoclusters, have also stimulated a great deal of discussion in the literature, both of a theoretical[27,] and experimental nature. Such materials have garnered intense interest as they have highly tunable optical properties and it has been proposed that they will enable advancements towards materials with double negative properties at optical frequencies.[41] While structures showing similar properties can be fabricated by top-down techniques,[40, 189] the disadvantages which this entails, not least of which are the difficulties involved in creating bulk materials and assigning effective material parameters, indicate that bottom-up techniques should be considered as a means more likely to allow progression in the field.

To fully understand the electromagnetic properties that make core-shell nanoclusters of such great interest to metamaterials research it is perhaps beneficial to first consider a simplified version of the structure. It has been shown in simulations that several metallic nanoparticles, organised into the form of a ring, could exhibit a resonant magnetic dipole in the visible region of the electromagnetic spectrum.[43] This magnetic response is an important aspect as far as many further applications are concerned.[190] The same nanoparticles that provide this magnetic response can also exhibit a resonant electric dipole and when these two properties are combined a potential path towards left-handed materials in the optical domain could be created.[43] In the subwavelength ring of nanoparticles the plasmon resonance of each nanoparticle induces a displacement current around the loop.[43] This is in contrast to SRRs where it is the conventional conduction current that produces

the magnetic dipole moment. It was also shown in this theoretical study that, again unlike the SRRs which are used more commonly in the microwave regime, the size of the ring is not the most important factor in determining the frequency of the induced dipole moment but rather the LSPR frequency of the constituent nanoparticles. Core-shell nanoclusters essentially function on the same principal as the rings of metallic nanoparticles discussed above – the prime difference being that the principal is expanded into a third dimension. When the particles are organised around a spherical core many potential rings in which propagating currents exist can generate a magnetic dipole moment can be envisaged – in this case the displacement current circulates in a plane perpendicular to the polarisation of the incident magnetic field.[102] In addition, developing the concept of this planar organisation of metallic nanoparticles into the core-shell nanocluster is sufficient for the fabrication to be considered conceivable using current bottom-up nanochemistry techniques.

Core-shell nanoclusters possess a variety of advantages over other structures that have been proposed as potential metamaterials. The majority of the other structures introduced in Figure 1, such as the fishnets and SRRs, exhibit a high degree of geometrical anisotropy. The strongest magnetic response in these structures exists in one specific direction of propagating light while in certain other directions no magnetic response can be observed at all. Core-shell nanoclusters on the other hand, due to their geometry and small size relative to the wavelengths of light of interest, are completely isotropic and any magnetic response observed should exist in all directions. In theoretical studies of these structures it has been reported that in order to obtain the strongest electromagnetic response, and achieve negative permeabilities, the number of nanoparticles per structure should be as high as possible while still ensuring no contact between them.[41] This number can be calculated, assuming knowledge of certain geometrical material parameters, according to Equation 9:[41]

$$N_{tot} = \left[\frac{\left(a+a_p+\frac{d}{2}\right)^2}{\left(2a_p+d\right)^2}\right] \qquad [9]$$

where N_{tot} = number of metallic nanoparticles on core sphere

a = radius of sphere

a_p = radius of metallic nanoparticle

d = edge to edge distance between nanoparticles on core sphere

In order to control the filling fraction of nanoparticles at the surface of the core spheres it is possible to apply the same manipulations introduced in Section 4.1.3. In principal, as the fabrication process employed is essentially analogous to that used for the planar arrays, simply replacing the large planar substrates with smaller scale spherical ones, these procedures should function equally well when applied to these very similar structures.

Depending on the orientation of the electric field of linearly polarised incident light with respect to the polarisation of the nanoparticles either the electric dipole or the magnetic dipole of the nanocluster will dominate. These processes occur at different frequencies. While it is the magnetic resonance that is primarily of interest, both originate from the plasmonic resonance of an individual nanoparticle. As described above, the many rings of nanoparticles, which form around the circumference of the sphere, facilitate the formation of a magnetic dipole moment - much like the effect observed for the single ring in Reference 43. The wavelength of this magnetic resonance should be strongly red-shifted compared to the frequency of the plasmon resonance of a single metallic nanoparticle. This is as a result of the strong coupling between the ensemble of nanoparticles at the surface of the dielectric sphere. That such a strong red-shift is observed originates from the multiple possibilities of rings of nanoparticles, in each direction, around the core sphere.[41] Other factors, such as the presence of the dielectric core, can also contribute to the overall magnitude of this red-shift.

There are several methods available to form spherical assemblies of metallic nanoparticles, each with their own advantages and disadvantages. For example, microfluidic techniques can be employed to prepare ‘nanoislands’, of metals, which can be grown to different sizes, on colloidal silica particles.[72] This technique allows precise control over reagent mixing and dispensing as well as ensuring reproducibility and straightforward upscaling. However, the dominant presence of microchannel walls which can lead to rapid and irreversible particle deposition can cause the quality of the products to degrade over time.[72]

An alternative method, exploiting electrostatic interactions, involves the self-assembly of silica-encapsulated gold nanoparticles on polystyrene core spheres coated in poly(diallyldimethylammonium chloride).[191] As with the work introduced in Section 4.1.4, this assembly process can be conducted in a layer-by-layer manner – allowing potentially very high packing densities. In addition, if the samples are calcined the silica shells can form a solid network while at the same time the polystyrene cores thermally degrade - permitting hollow spherical metallic nanoparticle structures to be formed and the optical properties to be further tuned.[191]

Rather than core-shell clusters, where the metallic inclusions encase a dielectric sphere, other approaches result in complete spherical assemblies of nanoparticles. However these structures have been shown to interact with electromagnetic radiation in a very similar manner.[42] One preparative route entails the confinement of metallic nanoparticles to oil droplets in an oil in water emulsion.[102] It can, however, be challenging to control the size of such assemblies. A similar approach, although achieved entirely in aqueous solution, entails the use of a flocculation process involving PEs and multivalent ions to form 'nano-bags' and 'micro-pouches' of nanoparticle assemblies.[192] Magnetic resonances were also measured in smaller nanoparticle assemblies prepared by Fan et al.[193] Here the gold nanoparticles were protected by thiolated polymers which define the separation between nanoparticles in the clusters and in turn establishes the magnitude of interparticle electromagnetic coupling. The optical properties of the clusters, prepared by simply drying droplets of the particles, were then measured by dark-field spectroscopy.[193]

As shown above, several bottom-up methods are available to fabricate spherical assemblies of metallic nanoparticles. Given all of the advantages related to electrostatic self-assembly outlined in previous sections, perhaps the most facile and flexible method is an extension of that used to construct planar arrays of gold nanoparticles.[194, 195] By simply replacing the large-scale planar substrates with smaller scale spherical ones it is possible to create solutions of such core-shell nanoclusters. It is also possible to apply the principles described in these syntheses to other systems, for example those including semiconductor and magnetic nanoparticles thus adding to the flexibility offered by this method. As with the research shown in the previous section, the only prerequisite to self-assembly is that the species in question exhibit a charge.

In order to induce this electrostatic attraction between substrate and particle it is first necessary, as before, to functionalise the surface of the substrate. It is possible to carry this out using the same reaction as was described in previous sections for planar glass or silicon substrates, albeit under slightly different conditions.[196] This colloidal nanochemistry approach requires additional purification steps, such as centrifugation, however large parallels remain between the two methods.

4.2.2. Optical properties[6]

Figure 45 shows an SEM image of a core-shell nanocluster that has been fabricated by such a method.[196] It can be seen that the dielectric sphere is decorated with a large number of isolated, non-touching gold nanoparticles. As described above, the organisation of the gold nanoparticles

[6] Much of the work presented in this section appeared in: Mühlig, S.; Cunningham, A.; Scheeler, S.; Pacholski, C; Bürgi, T; Rockstuhl, C.; Lederer, F: Self-Assembled Plasmonic Core–Shell Clusters with an Isotropic Magnetic Dipole Response in the Visible Range. *ACS Nano* **2011**, *5* (8), 6586-6592.

results in large changes in the optical properties when compared to isolated units which are uncoupled to others.

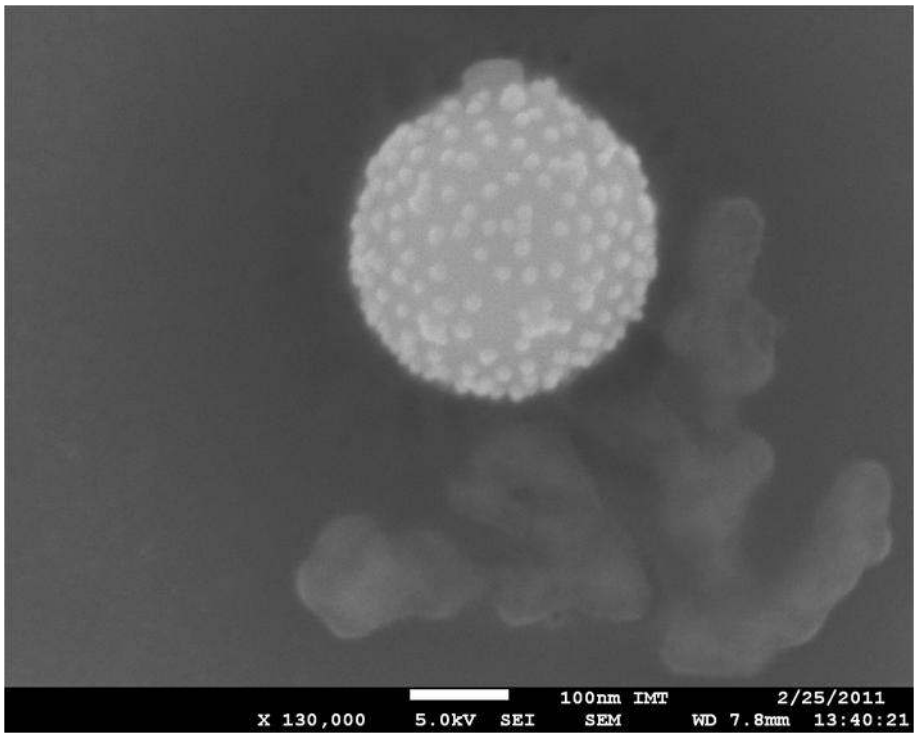

Figure 45 – SEM image of an isolated SiO_2 microsphere (~270 nm diameter) decorated with an array of gold nanoparticles (~20 nm diameter), also known as a core-shell nanocluster.

The changes in optical properties are shown in Figure 46 which highlights both experimental (a) and simulated (b) results.[196] Simulations were carried out by Stefan Mühlig and Carsten Rockstuhl of the Friedrich-Schiller-Universität Jena. All traces in Figure 46 are normalised to their respective maxima in the region under study.

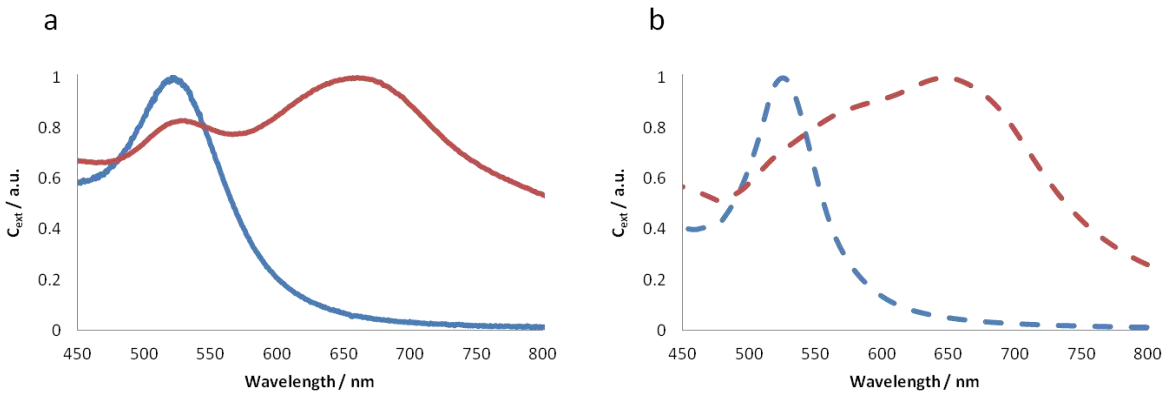

Figure 46 - a) Measured extinction spectrum of fabricated core-shell clusters in solution (red trace). For comparison, the extinction spectrum of a solution of gold nanospheres is shown (blue trace). b) Simulated extinction spectra of core-shell clusters in solution (red dashed trace) and a single gold nanosphere (blue dashed trace).

Immediately apparent in the experimental spectra shown in Figure 46a is the large red-shift, from around 520 nm to around 670 nm, of the LSPR that is induced upon the organisation of the gold nanoparticles (solid blue trace) into a spherical geometry (solid red trace). This is in excellent agreement with the simulated spectra shown in Figure 46b where the extent of the red-shift from a single gold nanoparticle (blue dashed trace) to a spherical organisation (red dashed trace) is reproduced almost exactly. Any slight deviations could be explained by the fact that in the simulations only a single core-shell nanocluster is considered, compared to the situation in the case of the experimental work where a large ensemble in solution are measured spectroscopically. Here, there will be a certain degree of polydispersity in relation to both the dielectric core and metallic shell spheres. Additionally the organisation of the metallic nanoparticles, while to a large extent comparable, is not identical on each of the individual structures. These slight differences in geometrical parameters can clearly not be taken into account in a simulation of a solitary core-shell nanocluster. Despite any discrepancy between the experimental and simulated spectra, with respect to the strongly red-shifted resonance, the agreement is convincing. However, one major difference between the two traces can be discerned. A peak in the experimental spectra at the same wavelength as the LSPR of an isolated particle is not reproduced in the simulations. This is caused by excess gold nanoparticles in solution which result from the fabrication process. In order to ensure the cores remain covered it is thought that an excess of ‘free’ gold nanoparticles must be present. This could be as a result of an equilibrium existing between the gold nanoparticles at the surface of the dielectric cores and those in solution. These particles are not considered in the simulations and account for this difference between the experimental and simulated data.

As explained in the introduction to this section, such structures exhibit a strong isotropic magnetic response.[41] This magnetism can be explained by assuming that the shell of metallic nanospheres acts, in effect, as a medium with an extremely high permittivity at wavelengths slightly above the collective plasmonic resonance. The large permittivity in turn evokes Mie resonances. For the lowest order one, the electric displacement field rotates in a plane perpendicular to the polarisation of the incident magnetic field, meaning that this mode can be associated with a magnetic dipole contribution. That the core-shell nanoclusters exhibit artificial isotropic magnetism was confirmed through simulations, again carried out by Stefan Mühlig and Carsten Rockstuhl of the Friedrich-Schiller-Universität Jena. These simulations, shown in Figure 47, decompose the extinction spectra into its respective multipole moments and examine the contribution of each to the total scattered field of the structures. These simulated spectra were normalised such that their sum is equal to the total scattering cross-section, thus allowing their relative contribution to be quantitatively analysed. Higher order multipoles, while present, do not appreciably affect the overall outcome and as such were not considered in Figure 47. While this quadrupole moment only weakly influences the scattering cross-section it does, however, result in increased absorption at slightly higher frequencies than the scattering cross-section peak. This explains the small difference between the peak position observed in Figure 46 and Figure 47.

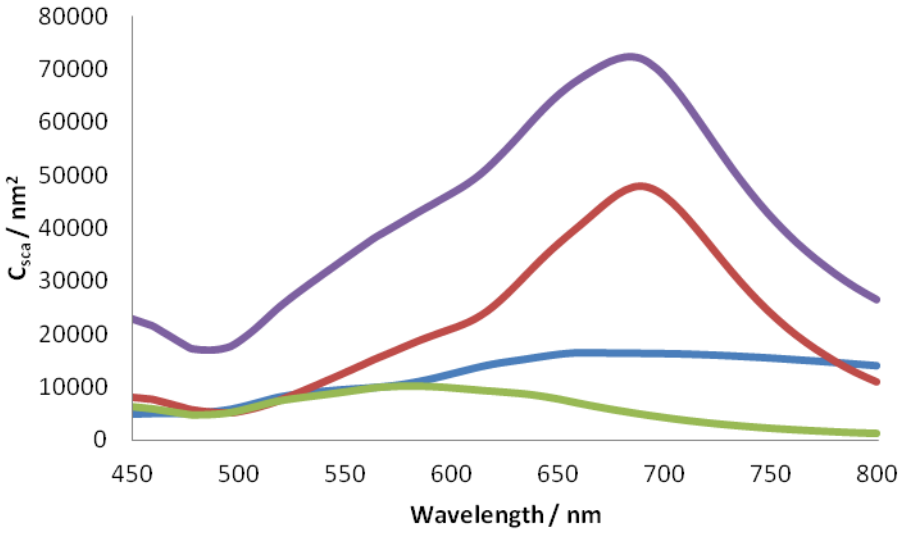

Figure 47 – Simulated contributions of the relevant multipole moments to the scattering cross section of a core-shell nanocluster. Purple trace – total scattering cross section, red trace – magnetic dipole contribution, blue trace – electric dipole contribution and green trace – electric quadrupole contribution.

It is clear from Figure 47 that the most significant contribution to the red-shifted peak of the total scattering cross-section (purple trace) comes from a resonant magnetic dipole moment (red trace) which dominates in the relevant spectral region.

The fabrication of these structures is extremely flexible and a number of possibilities to fine tune the architecture, and therefore the optical properties, are available. For instance, a wide range of sizes of both the dielectric core and the surrounding gold nanoparticles can be accessed. Additionally, while the fabrication above relates to a coating of gold nanoparticles on a SiO_2 core sphere different elements can be brought together in a similar manner. Structures using polymer, or metallic, core spheres coated with nanoparticles of a variety of different materials and functionalities can be envisaged. The only prerequisite for their fabrication is that an attraction, of either a physical or chemical nature, exists between the two. In this work the widespread applicability of electrostatic interactions has been highlighted.

4.2.3. Large scale arrays

This electrostatic approach can also be used to produce large-scale arrays of core-shell nanoclusters deposited on planar substrates. Such a step is required if systems like this are to be incorporated into functional optical devices. In addition, pre-depositing functionalised SiO_2 cores on a planar substrate prior to their coating with metallic nanoparticles could prove to be a promising route to reducing or eliminating the excess particles in solution which existed in the previous fabrication

approach. Shown in Figure 48a are the extinction spectra of an array of silica microspheres on a glass substrate before (blue trace) and after (red trace) the deposition of gold nanoparticles at their surfaces. The deposition of the spheres, which are charged positively after a functionalisation step, self-assemble at the glass substrate surface which has itself been coated in a negatively charged polymer. The arguments, given previously, for the exhibition of a strong isotropic magnetic response and for the large red-shift of the LSPR, when compared to that of an isolated particle, remain unchanged. However, the large step that has been taken, from structures that exist purely in colloidal form to the formation of large scale single layers show the versatility and applicability of the bottom-up techniques used. The two SEM images shown in Figure 48b give an impression of what is achievable. The larger image shows that arrays can be created on a suitably large scale while the image in the inset shows that, at least in small domains, a degree of order can be achieved. Additionally, it should also be possible to combine such methods with the layer by layer assembly outlined previously, allowing the construction of truly bulk optical materials. In this case, due to the large size of the core spheres bulk materials could be achieved after a relatively small number (2 – 3) of layers of the core-shell nanoclusters.

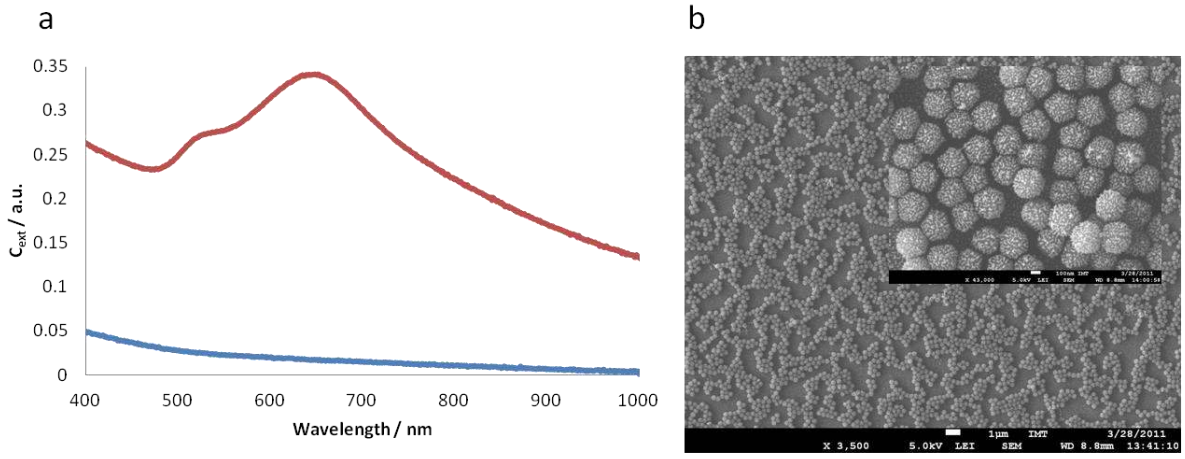

Figure 48 - a) Extinction spectra showing an array of SiO_2 microspheres deposited on a charged glass substrate both pre- (blue trace) and post- (red trace) functionalisation with gold nanoparticles. b) SEM micrographs of an array of core-shell nanoclusters deposited on a charged silicon substrate.

4.2.4. Cloaking device

Cloaking, along with negative refractive indices and perfect lensing, is often used as one of the achievable goals that is used to promote metamaterials research. Rather than merely camouflaging – a 'technology' that certain plants and animals have evolved over thousands of years in order to hide them from predators or, alternatively, their prey, metamaterials could be used to actually make objects invisible. To this end, several approaches have been adopted. One of the more lauded

theoretical means is known as transformation optics[197] which involves the redirection of electromagnetic fields. It essentially results in the 'bending' of rays of light around an object in such a manner that on the far side of the object the rays will appear as if no object is present. The method can be simply summed up by two steps; the deformation of space around an object by coordinate transformation and then finding a medium with the correct properties and structure to mimic this curved space. The second step, although considerably more challenging, remains one possible means of achieving cloaking. Such theory has been applied to cloak objects in the microwave regime.[198] However, it must be stated that while the object being cloaked would appear invisible to an observer on the outside, no light can either pass in or out of the object and an observer on the inside would perceive everything as black. Other structures, known as carpet cloaks, have been both theoretically proposed[199] and experimentally demonstrated[200] at optical frequencies. The prime disadvantage of this approach is that it is limited to cloaking objects on flat substrates.

An alternative route to cloaking involves the use of plasmonic materials, such as nanoparticles, to render small dielectric objects nearly invisible.[201] As with many metamaterials applications, experimental studies of these effects have been conducted at longer wavelengths,[202] however the real challenges lie in adapting the technology for optical frequencies. One approach designed to achieve this involves coating small dielectric spheres in a shell of silver nanoparticles. Such a structure has been shown by simulations to drastically reduce (by around 70%) the scattering response of the core spheres. [27] The mechanism involves tuning the scattering response of the shell to be 180° out of phase with that of the core, effectively cancelling out any scattering from the core itself. The simulations conducted showed that the structure is relatively robust to changes in geometry – such changes resulting primarily in slight shifts in the frequency of operation.[27] By treating the shell as an effective medium it is possible to select at which wavelength the cloaking device operates simply by tuning the relative sizes of the core and shell and / or the density of the nanoparticle array. Another advantage of this approach, evident from the discussions in Section 4.2.2, is that such structures should be readily accessible using bottom-up fabrication methods. There are, however, some challenges common to all cloaking applications. These chiefly include difficulties faced when trying to prepare broadband and low loss cloaks.

As can be seen from the SEM image in Figure 49 such structures were successfully fabricated. This was significantly more challenging than the structures discussed in Section 4.2.2, primarily due to the requirement that silver nanoparticles be used rather than gold. While silver nanoparticles have superior optical properties fabricating monodisperse solutions is not a trivial process, as can be seen

in Figure 31. In addition due to their relative reactivity, their handling is more complicated than in the case of the gold particles.

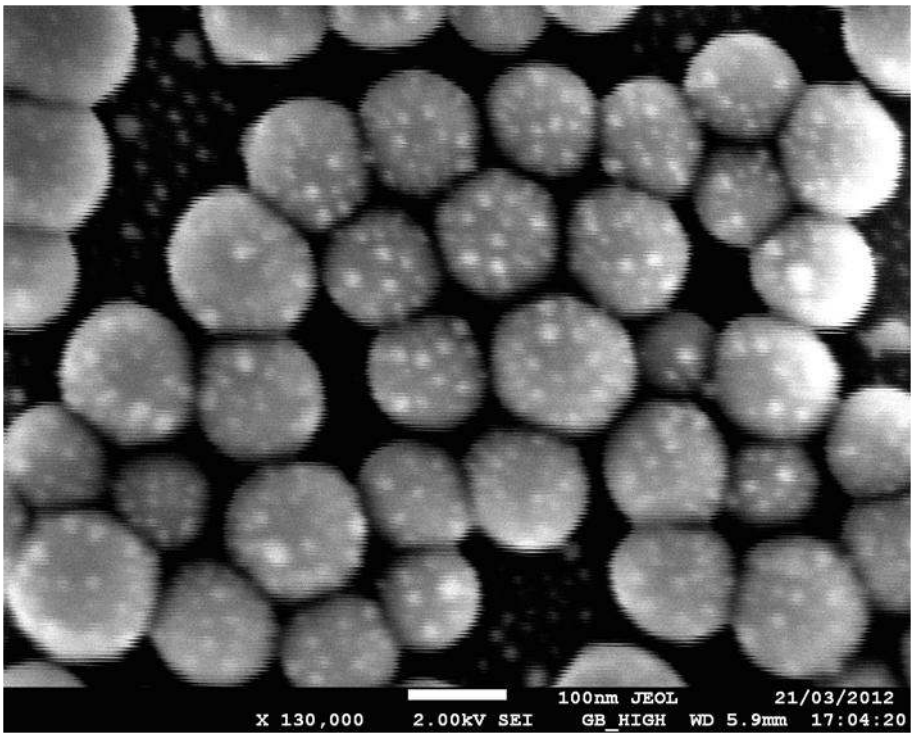

Figure 49 – SEM image showing an array of core-shell nanoclusters composed of SiO_2 cores and a shell of silver nanoparticles.

It can be seen from this image that the nanoparticles form a complete array at the surface of each of the silica core spheres. They are reasonably equally spaced and do not form aggregates or leave any areas bare. While, due to the slightly different fabrication technique, the silver nanoparticles used in this work are far more monodisperse than those used in Section 4.1.5 the silica core spheres are significantly more polydisperse than the core-shell work presented in Section 4.2.2. To ensure any potential cloaking effect observed occurred at optical frequencies, and to accurately construct the structure proposed in Reference 27, the core-shell clusters must remain under a certain size. While SiO_2 microspheres can be synthesised with very high levels of monodispersity this becomes increasingly difficult as the size regime is reduced and explains the range of sizes seen in the structures in Figure 49. While the majority of the structures seen in Figure 49 lay well within a narrower range structures from 115 to 165 nm in diameter can be discerned. In addition, an array of silver nanoparticles can be observed at the surface of the substrate. Despite repeated attempts using a number of strategies this base array of nanoparticles was found to be unavoidable. It was thought that these particles could potentially interfere with any measurements conducted to verify the existence of a cloaking effect. However additional simulations, supplementary to those seen in

Reference 27, were carried out by Stefan Mühlig and Carsten Rockstuhl of the Friedrich-Schiller-Universität Jena and were able to confirm that the effect was robust against both the polydispersity of the structures and the presence of the background silver nanoparticle array.

As the structure prepared is designed to cloak exclusively the scattering response of the central dielectric core, optical measurements were conducted on samples using a setup including an integrating sphere used to capture diffuse light. This allows each component of the overall extinction (total transmission, diffuse transmission, total reflectance and diffuse reflectance) to be measured and in turn means that both the scattering and the absorption of the samples can be determined. A sketch of the experimental setup used for measurements is shown in Figure 50.

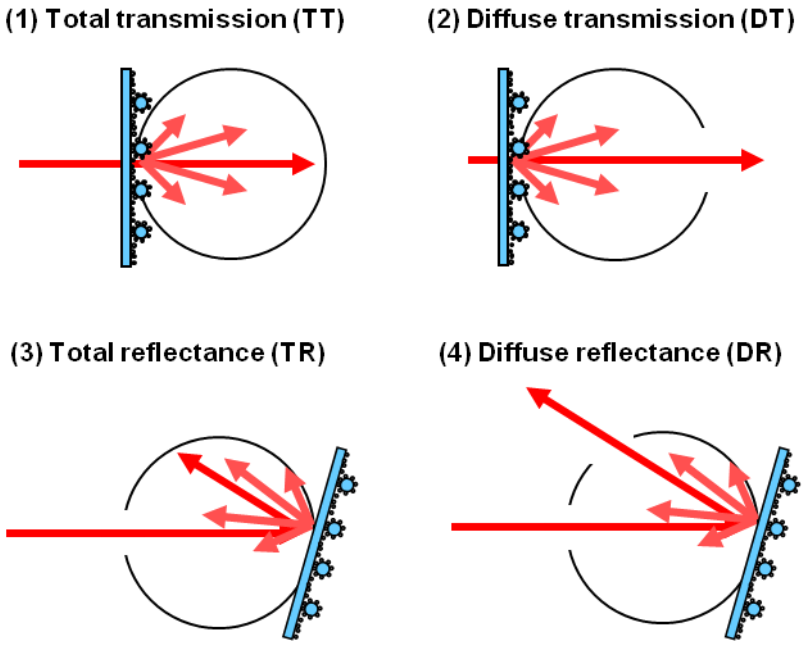

Figure 50 – Experimental setup showing the position of the sample relative to the integrating sphere required to measure each of the properties defined. Figure supplied by José Dintinger of the École Polytechnique Fédérale de Lausanne.

Total scattering (including specular reflection) is calculated through the addition of the diffuse transmission and the total reflectance. The direct transmission is calculated through the subtraction of the diffuse transmission from the total transmission. As it is impossible to tell from the SEM image (Figure 49) whether or not the reverse side of the silica cores are coated with silver nanoparticles or not it was chosen to orientate the samples as is shown in Figure 50, with the incident light impinging on the uncovered side of the glass plate. In the case where only the upper hemisphere is covered with nanoparticles simulations have shown that the cloaking effect should still be in place if the propagation of the incident light is in this direction relative to the sample.

As can be seen in Figure 51a a dip in the scattering of the core-shell structure (blue trace) when compared to an array of the undecorated core spheres (red trace) was indeed observed. However, as is shown in Figure 51b, the core-shell cluster (blue trace) also displays an absorption peak which is not present in the sample prior to silver nanoparticle deposition (red trace). This peak occurs at the same wavelength as the scattering dip whereas in the simulations these two features were well separated. It is therefore impossible to unambiguously relate any measured reduction in scattering to the cloaking effect that had been proposed. Any effect observed is significantly less than that predicted by the simulations. Initially it was thought that the nanoparticles used to create the shell were too small and were therefore not efficient scatterers of light. However the experiments were repeated with larger silver nanoparticles and similar results were found. Another possible reason for the discrepancy between the measured and simulated spectra is that the substrate, a standard microscope slide, is not considered in the simulations and could possibly result in such deviations. This theory is currently being tested by more rigorous simulations carried out by Vassilis Yannopapas of the University of Patras.

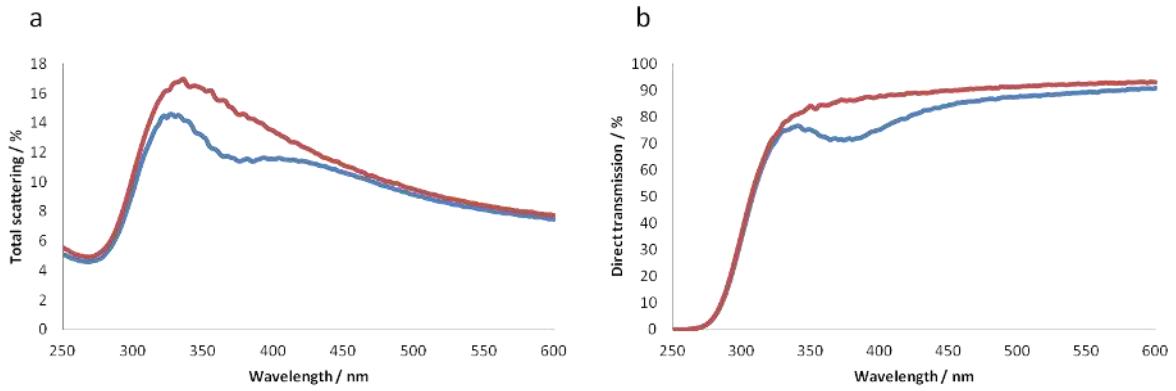

Figure 51 – a) Total scattering (including specular reflection) for an array of silica spheres (red trace) and an array of core-shell nanoclusters constructed with silver nanoparticles (blue trace). b) Direct transmission of an array of silica spheres (red trace) and an array of core-shell nanoclusters constructed with silver nanoparticles (blue trace).

5. Conclusions

As outlined in the Introduction, the stated aim of the Nanogold project was to investigate methods that permit the fabrication and application of bulk electromagnetic metamaterials at optical frequencies using bottom-up techniques.

Despite the concept of metamaterials research being relatively new, it has rapidly grown in importance and has attracted interest from a variety of differing fields. However, prior to the start of the investigation, which began at the same time as three other similar projects also funded primarily by the 7th Framework Programme for Research, very little literature existed specifically detailing attempts to fabricate metamaterials using bottom-up approaches. This can be considered as being simultaneously advantageous and disadvantageous since whilst progress can be more difficult when starting from scratch a wider variety of paths can be taken in order to achieve the goals established at the outset. Throughout the duration of the project the domain of bottom-up metamaterials rapidly grew. Presentations at conferences and workshops, outlining the latest advances made, became increasingly prevalent and fruitful discussions could be had on a more regular basis with fellow researchers working towards similar objectives. Growth in the field can be expected to continue as it firmly establishes itself under the umbrella of metamaterials research in general. The publishing of studies will also serve a variety of purposes. In addition to disseminating current research to a wider audience it will also encourage others to further develop concepts, identify new avenues for research and generally stimulate interest in the field.

The research undertaken as part of this thesis has contributed to the advancement of knowledge in the field in a variety of manners. An in-depth study of the deposition of metallic nanoparticles on planar substrates such as glass and silicon was conducted. Substrates were suitably functionalised and homogeneous arrays of metallic nanoparticles, over several square centimetres, were fabricated by exploiting electrostatic interactions between them. It was shown that both the density and the organisation of these particles could be controlled through a variety of techniques. By replacing the capping agent at the surface of the nanoparticles, for example, it was shown that high density arrays of gold particles with small ordered domains could be produced. The optical characteristics of these assemblies were studied throughout and were shown to exhibit a significant degree of tunability, allowing particular geometrical arrangements coupled with specific optical properties to be fabricated. The deposition of metallic nanoparticles was not limited to glass or silicon substrates with adapted techniques being used to create similar structures on PDMS and ITO-coated glass. This gave access to a wider variety of potential studies allowing the effects of substrate stretching or the

application of potentials to nanoparticle coated substrates to be studied. It was also shown that arrays of nanoparticles could be produced using stand alone polymer films as substrates. These structures, which have a thickness in the sub-micron range, can also be prepared over relatively large areas. In a world where several technologies are driven by constant pressure to reduce device weight, thickness and cost, the development of these techniques has obvious advantages.

This initial work was also used as the base upon which to build up structures into the third dimension. This was achieved largely through the application of the layer by layer assembly of charged polymer layers, or PEs. This process allows the cyclic deposition of oppositely charged polymer layers, each with a thickness on the order of 2 nm. As with the deposition of the nanoparticles described above, the build-up of the polymer layers takes advantage of electrostatic attractions. It is this synergy between the two methods that enables a powerful means of creating nanoparticle assemblies with a great degree of control over a number of geometrical parameters to be realised. This in turn affords the same degree of control over the optical properties of the structures. Distinct nanoparticle arrays, separated by tunable distances that are dependent solely on the number of polymer layers employed, can be assembled. Regulation of the distance between two distinct nanoparticle arrays is naturally accompanied with variations in the electromagnetic coupling between individual particle pairings within each array resulting in shifts of the plasmon resonance. It was shown that, depending on the size of the nanoparticles and on their filling fraction, the shifts in optical properties observed could be attributed uniquely to interactions between particles within individual arrays and that no appreciable coupling between particles within a single array contribute. In line with well established theory, a red-shift of the LSPR was observed as two metallic nanoparticle arrays were brought closer together. This effect became more pronounced at both shorter separations and when larger nanoparticles were used. This work was supported by rigorous simulations conducted by colleagues within the framework of the Nanogold project. The research outlined here is, of course, not limited to studies pertaining to two distinct gold nanoparticle arrays. One of the challenges facing the metamaterials community at large is the fabrication of three dimensional materials. The technique described above, assembling nanoparticle / polymer composite structures, lends itself particularly well to this goal. No limits, other than practical ones, inhibit the construction of multiple stratified nanoparticle arrays and as such studies of these multilayered structures were also conducted.

Similar structures were also investigated with a view to probing the nature of asymmetric coupling between metallic nanoparticles. Here, planar arrays of both silver and gold nanoparticles were again separated by discrete numbers of PE layers and an in-depth study of symmetry breaking in complex

nanoparticle structures was conducted. It was found that all four hybridised eigenmodes, according to the plasmon hybridisation scheme, were observable and that they could be selectively excited, altering their relative magnitudes, simply by varying the angle of incidence of the probing beam.

The application of these structures as potential SERS substrates was also investigated. While relatively modest enhancements were observed the flexibility of geometrical and compositional parameters allows a wide range of theoretical aspects to be probed. It was found, for the analyte and excitation wavelength used, that higher degrees of separation between two gold nanoparticle arrays leads to lower enhancements of Raman signals.

Analogous techniques to those described above were used to prepare spherical assemblies of metallic nanoparticles. The large scale planar substrates were replaced with micro-scale spherical ones to allow the nanoparticles to be organised in this manner. Such structures are of intense interest to the metamaterials community, largely due to the isotropic magnetic response that they exhibit in the visible region of the electromagnetic spectrum. This, it is hoped, could lead to greater control over the permeability of matter and open up a route towards negative refractive index materials at optical frequencies. Such structures were prepared and their optical properties analysed both experimentally and, by colleagues, theoretically. The existence of an artificial isotropic magnetic dipole moment in the visible spectral domain was thus discerned.

Similar structures were proposed as potential cloaking devices at the frequencies where the scattering response of the nanoparticle shell is 180° out of phase with that of the core. Several factors, including reduced size, the requisite use of silver nanoparticles rather than gold, and the need to prepare samples on substrates suitable for subsequent analyses, made the fabrication of these structures more challenging. However these challenges were largely overcome and investigations, the results of which are at this time inconclusive, were carried out to probe any potential cloaking properties present.

A wide variety of clearly identifiable advancements summarised above and laid out in more detail in the main body of the thesis, have been made throughout the course of this work. As a result of the work carried out many questions have been answered and it is hoped that a greater understanding of a small section of an ever expanding field has been achieved. It is also hoped that some of the work contained in this thesis may form a base upon which others can build to one day realise true bottom-up metamaterials that have practical applications and can benefit everyday lives.

6. Outlook

While much was achieved during the course of this research it became clear that similar techniques could be applied to such a wide variety of systems and that, due to time constraints, many potential avenues would have to remain unexplored. The systems developed in this thesis readily lend themselves to characterisation by standard spectroscopic techniques and an extensive range of prospective applications and potential areas for further development can be foreseen.

For example, one possible application of the stratified metallic nanoparticle arrays would be the exploitation of the hotspots that exist between them to investigate enhanced fluorescence. By incorporating fluorescent units into the dielectric spacer, either as part of the polymers themselves or as separate charged entities, an enhancement of the fluorescence can be measured.[203, 204] The magnitude of this enhancement is dependent on a number of factors such as the size and composition of the nanoparticles and the separation distance between them and the chromophores. The structures developed in this thesis provide the perfect platform from which to perform an in-depth study of all of these factors. The expansion of these concepts into non planar systems, in much the same manner to that seen with the core-shell nanoclusters, could also be envisaged. Fluorescent spheres of a range of sizes and absorption / emission wavelengths are commercially available. Decorating these in a shell of metallic nanoparticles could result in the enhancement of the fluorescence as well as the induction of an isotropic magnetic response at optical frequencies and potential cloaking properties.

Other interesting applications could also arise from a theoretical study investigating chains of metallic nanospheres. If the particles gradually decrease in size and separation it has been proposed that such structures could act as efficient nanolenses.[205] When the plasmon resonance of the particles in the chain is excited this theoretical study claims that due to the multiplicative, cascade effect of the geometry a 'hottest spot' will develop in the gap between the two smallest particles with local fields enhanced by orders of magnitude.[205] Similar structures could be prepared in an extension of the work conducted on stratified arrays of metallic nanoparticles. It would, of course, be impossible to form precise chains of particles. However, larger scale analogues could be fabricated using the techniques examined and developed in this thesis. A wide range of gold nanosphere diameters are accessible by the Turkevich method and by depositing differing numbers of PE layers between the nanoparticle arrays it would be possible to gradually diminish the distance between them. The theory could then be tested, for example, by incorporating SERS active

compounds or fluorescing molecules in each of the gaps between successive arrays and measuring the extent to which the relevant signals are enhanced.

An additional effect that could possibly be measured from the layered arrays of metallic nanoparticles is Bragg reflection. In principle, the periodic variation of refractive indices, as is seen in these samples, offers the prototypical structure of a Bragg reflector.[206] These structures are widely used in waveguides and the ease with which the distance between subsequent nanoparticle arrays can be controlled allows for either constructive or destructive interference to be achieved. While waveguide technology is relatively mature, plasmonic structures that can be tuned to determine both the extent to which incident light is reflected and the range of wavelengths that are efficiently reflected, also known as the photonic stopband, could be employed in niche applications.

Lasing effects, proposed theoretically but yet to be fully explored experimentally, would be another potentially exciting application of multiple layered arrays of metallic nanoparticles separated by dielectric slabs.[207] The dielectric cavities were shown to act as resonant cavities where lasing action, dependent on the thickness of the cavities, could occur if there is an introduction of gain.[207] That the separation of the nanoparticle arrays can be tuned with almost nanometre precision using differing numbers of PE layers brings such applications one step closer to realisation.

Recent research describing the plasmoelectronic effect – the influence of macroscopic flows of charge through plasmonic excitation – has opened up an exciting new field which could be, for example, used in energy and sensing applications.[78] While novel prototype devices are already in existence the application of the particle growth, deposition and organisation techniques outlined in this thesis could well provide researchers with the means to fabricate new systems with advantageous properties.

As was described in Section 2.2.3 the supply or removal of electrons from metallic nanoparticles will result in changing optical properties. This could be achieved, for example, through the application of potentials to arrays of nanoparticles deposited on electrically conducting substrates or alternatively by chemical means. Coating arrays of metallic nanoparticles, such as those discussed at length in this thesis, with electroactive compounds like poly(ferrocenyl silane)[208] would allow the simultaneous measurement of both the optical properties of the gold nanoparticles and the redox properties of the system in general. Such structures could prove to have extremely useful sensing applications. Again, these concepts are not limited to planar structures. Poly(ferrocenyl silane) microspheres can be prepared and through chemical oxidation processes can be rendered positively charged.[209] Combination with negatively charged metallic nanoparticles should lead to core-shell clusters with

redox properties. The addition of this functionality to the pre-existing properties of the core-shell clusters discussed at length in Section 4.2 and the ability to organise these spheres using external magnetic fields make such structures of potential interest for a variety of applications.

The particular properties of metallic nanorods were investigated to some extent in this thesis, however many potential avenues remain unexplored. One such avenue would be the selective excitation of different plasmonic bands, using sources of different wavelengths, and of particles with particular orientations, using polarised light, could lead to the performance of chemical reactions at the surface of only specific nanoparticles. This, given that similar techniques to those seen in Section 4.1.4 can readily be used to fabricate layers of nanorods, means that such structures could lead to high density systems for information storage.[210]

It can be seen, by the volume of potential concepts and applications related to similar systems to those described in this thesis that, by no means, has this area of research been fully exhausted. A variety of largely disparate hypothetical applications have been presented in this section and while some of these are not necessarily connected to the field of metamaterials, this only serves to show the versatility of the techniques developed and the wide-ranging applicability of plasmonic nanoparticles organised in specific forms. It is clear that only the surface of what is potentially achievable using these materials has been scratched.

7. Acknowledgements

Many people helped during the course of the work that went into this thesis and I would like to take this opportunity to thank them all.

Firstly I would like to extend my immense gratitude to Professor Thomas Bürgi who supervised my doctoral studies. His unswerving support, from my Masters work in Neuchâtel, through to the commencement of my PhD in Heidelberg and its completion here in Geneva, has made these last years unimaginably easier, extremely educational and, perhaps above all, more enjoyable. I can't thank him enough for all of the help and encouragement he has given me at both a professional and personal level.

I would also like to thank the other members of my jury for taking the time out of their busy schedules to both read this thesis and be present for the examination. Dr. Philippe Barois, of the Centre de Recherche Paul Pascal, CNRS-Bordeaux, is the coordinator of the Metachem project, which has very similar goals to that which the Nanogold project had. As such I believe that he is in a perfect position to judge the merits of this research. I have had the pleasure of being present at several presentations that he has given on his, and his project's, research and have found these to be enjoyable, stimulating and above all of excellent quality. Similarly, the expert knowledge of Dr. Serge Stoll of the Forel Institute, University of Geneva, in the fields of colloidal nanoparticles and polymers, and in particular polyelectrolytes, makes him ideally placed to evaluate the quality of the work carried out. His Masters course entitled 'Colloids and Polymers in the Environment', which I attended earlier this year, was extremely informative, well-taught and introduced me to some concepts which I was able to apply in both the experimental work that I conducted and in understanding some of the theoretical concepts that underpin this research.

The colleagues, both past and present, with whom I have worked also deserve my appreciation. They have helped to make coming to work a pleasurable and rewarding experience. Contributing to the research through discussions of a scientific nature and helping to create a friendly atmosphere around the office and laboratory, carrying out this research would not have been the same without these people around. In particular I have enjoyed the group hikes that we have made, which have also given us the opportunity to see some of the beautiful country in which we have had the good fortune to live.

The collaborative nature of the Nanogold project should be clear from reading this thesis and I would like to give credit to all of colleagues that aided in the realisation of the results presented

here. Toralf Scharf, José Dintinger and Irène Philipoussis Fernandez of the École Polytechnique Fédérale de Lausanne aided in the optical measurements carried out on some of the core-shell nanoclusters and in the optical lithography used in producing the patterned nanoparticle arrays. José also helped enormously with the preparation of the French abstract. Merci beaucoup! Stefan Mühlig and Carsten Rockstuhl of the Friedrich-Schiller-Universität Jena provided a huge amount of theoretical assistance with their simulations and interpretation of results. Xiangbing Zeng and Feng Lui of the University of Sheffield helped in the characterisation of the stratified arrays of metallic nanoparticles by performing GISAXS measurements. Outwith the Nanogold project, Dana Cialla and Karina Weber of the Institute of Photonics in Jena conducted SERS measurements on the samples sent to them while Brittany Cindric of the University of Geneva put in a large amount of work to fabricate and characterise the multiple layers of metallic nanoparticles.

The scientific work was also supported by a number of technicians. I would like to particularly thank Dominique Lovy and Patrick Barman for providing me with an excellent homemade dip-coater which saved me an enormous amount of time as well as Raymond Azoulay for his general assistance around the chemistry lab.

I would also like to thank my family, Mum, Dad and Euan, who couldn't have encouraged me more. Hopefully Dad learned a thing or two about metamaterials and plasmonics while proof reading the thesis and thanks to Mum for helping with the French translation of the abstract as well! Last, but by no means least, I would like to extend my gratitude to Cristina, without whose support I'm convinced none of this would have been possible. I'll always be indebted to you.

8. References

1. Smith, D. R.; Padilla, W. J.; Vier, D. C.; Nemat-Nasser, S. C.; Schultz, S., Composite Medium with Simultaneously Negative Permeability and Permittivity. *Physical Review Letters* **2000,** *84* (18), 4184-4187.

2. Shelby, R. A.; Smith, D. R.; Schultz, S., Experimental Verification of a Negative Index of Refraction. *Science* **2001,** *292* (5514), 77-79.

3. Stavenga, D. G., Invertebrate superposition eyes-structures that behave like metamaterial with negative refractive index. *Journal of the European Optical Society* **2006,** *1*, 06010.

4. Rainwater, D.; Kerkhoff, A.; Melin, K.; Soric, J. C.; Moreno, G.; Alù, A., Experimental verification of three-dimensional plasmonic cloaking in free-space. *New Journal of Physics* **2012,** *14* (1), 013054.

5. Grbic, A.; Eleftheriades, G. V., Overcoming the Diffraction Limit with a Planar Left-Handed Transmission-Line Lens. *Physical Review Letters* **2004,** *92* (11), 117403.

6. Cai, W.; Shalaev, V. M., Optical Metamaterials: Fundamentals and Applications. Springer, New York (2010).

7. Zouhdi, S.; Shivola, A.; Voinogradov, A. P., Metamaterials and Plasmonics: Fundamentals, Modelling and Applications. Springer, Dordrecht (2008).

8. Capolino, F., Theory and Phenomena of Metamaterials. CRC Press, Boca Raton (2009).

9. Palmer, J. (January 26, 2012). BBC News. In 'Cloaking' a 3-D object from all angles demonstrated. Retrieved September 19, 2012, from http://www.bbc.co.uk/news/science-environment-16726609.

10. Tassin, P.; Koschny, T.; Kafesaki, M.; Soukoulis, C. M., A comparison of graphene, superconductors and metals as conductors for metamaterials and plasmonics. *Nat Photon* **2012,** *6* (4), 259-264.

11. Krauss, T. F.; Rue, R. M. D. L.; Brand, S., Two-dimensional photonic-bandgap structures operating at near-infrared wavelengths. *Nature* **1996,** *383* (6602), 699-702.

12. Freestone, I., The Lycurgus Cup - A Roman Nanotechnology. *Gold Bulletin* **2007,** *40* (4), 270-277.

13. Bruggeman, D. A., The calculation of various physical constants of heterogeneous substances. I. The dielectric constants and conductivities of mixtures composed of isotropic substances. *Annalen der Physik* **1935,** *24*, 636.

14. Garnett, J. C. M., Colours in Metal Glasses and in Metallic Films. *Philosophical Transactions of the Royal Society of London. Series A, Containing Papers of a Mathematical or Physical Character* **1904,** *203* (359-371), 385-420.

15. Soukoulis, C. M.; Linden, S.; Wegener, M., Negative Refractive Index at Optical Wavelengths. *Science* **2007,** *315* (5808), 47-49.

16. Lok, C., Nanotechnology: Small wonders. *Nature* **2010,** *467* (7311), 18-21.

17. Feynman, R. P., There's Plenty of Room at the Bottom. *Caltech Engineering and Science* **1960,** *23* (5), 22-36.

18. Thompson, S. E.; Parthasarathy, S., Moore's law: the future of Si microelectronics. *Materials Today* **2006,** *9* (6), 20-25.

19. Li, X.; Jia, Y.; Wei, J.; Zhu, H.; Wang, K.; Wu, D.; Cao, A., Solar Cells and Light Sensors Based on Nanoparticle-Grafted Carbon Nanotube Films. *ACS Nano* **2010,** *4* (4), 2142-2148.

20. Boisselier, E., Gold nanoparticles in nanomedicine - preparations, imaging, diagnostics, therapies and toxicity. *Chem. Soc. Rev.* **2009,** *38*, 1759-1782.

21. Shimomura, M.; Sawadaishi, T., Bottom-up strategy of materials fabrication: a new trend in nanotechnology of soft materials. *Current Opinion in Colloid & Interface Science* **2001,** *6* (1), 11-16.

22. Acikgoz, C.; Hempenius, M. A.; Huskens, J.; Vancso, G. J., Polymers in conventional and alternative lithography for the fabrication of nanostructures. *European Polymer Journal* **2011,** *47* (11), 2033-2052.

23. Zhu, M.; Chen, X.; Wang, Z.; Chen, Y.; Ma, D.; Peng, H.; Zhang, J., Structural and optical characteristics of silicon nanowires fabricated by wet chemical etching. *Chemical Physics Letters* **2011,** *511* (1–3), 106-109.

24. Reyntjens, S.; Puers, R., A review of focused ion beam applications in microsystem technology. *Journal of Micromechanics and Microengineering* **2001,** *11* (4), 287.

25. Zeng, H.; Du, X.-W.; Singh, S. C.; Kulinich, S. A.; Yang, S.; He, J.; Cai, W., Nanomaterials via Laser Ablation/Irradiation in Liquid: A Review. *Advanced Functional Materials* **2012,** *22* (7), 1333-1353.

26. Yao, J.; Liu, Z.; Liu, Y.; Wang, Y.; Sun, C.; Bartal, G.; Stacy, A. M.; Zhang, X., Optical Negative Refraction in Bulk Metamaterials of Nanowires. *Science* **2008,** *321* (5891), 930-.

27. Mühlig, S.; Farhat, M.; Rockstuhl, C.; Lederer, F., Cloaking dielectric spherical objects by a shell of metallic nanoparticles. *Physical Review B* **2011,** *83* (19), 195116.

28. Belov, P. A.; Hao, Y., Subwavelength imaging at optical frequencies using a transmission device formed by a periodic layered metal-dielectric structure operating in the canalization regime. *Physical Review B* **2006,** *73* (11), 113110.

29. Liu, N.; Fu, L.; Kaiser, S.; Schweizer, H.; Giessen, H., Plasmonic Building Blocks for Magnetic Molecules in Three-Dimensional Optical Metamaterials. *Advanced Materials* **2008,** *20* (20), 3859-3865.

30. Pendry, J. B.; Holden, A. J.; Robbins, D. J.; Stewart, W. J., Magnetism from conductors and enhanced nonlinear phenomena. *Microwave Theory and Techniques, IEEE Transactions on* **1999,** *47* (11), 2075-2084.

31. Veselago, V. G., Electrodynamics of Substances with Simultaneously Negative and Magnetic Permeabilities. *Sov. Phys. Usp.* **1968,** *10*, 509.

32. Liu, N.; Giessen, H., Coupling Effects in Optical Metamaterials. *Angewandte Chemie International Edition* **2010,** *49* (51), 9838-9852.

33. Enkrich, C.; Pérez-Willard, F.; Gerthsen, D.; Zhou, J. F.; Koschny, T.; Soukoulis, C. M.; Wegener, M.; Linden, S., Focused-Ion-Beam Nanofabrication of Near-Infrared Magnetic Metamaterials. *Advanced Materials* **2005,** *17* (21), 2547-2549.

34. Murphy, C. J.; Sau, T. K.; Gole, A. M.; Orendorff, C. J.; Gao, J.; Gou, L.; Hunyadi, S. E.; Li, T., Anisotropic Metal Nanoparticles: Synthesis, Assembly, and Optical Applications. *The Journal of Physical Chemistry B* **2005,** *109* (29), 13857-13870.

35. Shalaev, V. M.; Cai, W.; Chettiar, U. K.; Yuan, H.-K.; Sarychev, A. K.; Drachev, V. P.; Kildishev, A. V., Negative index of refraction in optical metamaterials. *Opt. Lett.* **2005,** *30* (24), 3356-3358.

36. Garwe, F.; Rockstuhl, C.; Etrich, C.; Hübner, U.; Bauerschäfer, U.; Setzpfandt, F.; Augustin, M.; Pertsch, T.; Tünnermann, A.; Lederer, F., Evaluation of gold nanowire pairs as a potential negative index material. *Applied Physics B: Lasers and Optics* **2006,** *84* (1), 139-148.

37. Funston, A. M.; Novo, C.; Davis, T. J.; Mulvaney, P., Plasmon Coupling of Gold Nanorods at Short Distances and in Different Geometries. *Nano Letters* **2009,** *9* (4), 1651-1658.

38. Dolling, G.; Enkrich, C.; Wegener, M.; Soukoulis, C. M.; Linden, S., Low-loss negative-index metamaterial at telecommunication wavelengths. *Opt. Lett.* **2006,** *31* (12), 1800-1802.

39. Xiao, S.; Chettiar, U. K.; Kildishev, A. V.; Drachev, V. P.; Shalaev, V. M., Yellow-light negative-index metamaterials. *Opt. Lett.* **2009,** *34* (22), 3478-3480.

40. Valentine, J.; Zhang, S.; Zentgraf, T.; Ulin-Avila, E.; Genov, D. A.; Bartal, G.; Zhang, X., Three-dimensional optical metamaterial with a negative refractive index. *Nature* **2008,** *455* (7211), 376-379.

41. Simovski, C. R.; Tretyakov, S. A., Model of isotropic resonant magnetism in the visible range based on core-shell clusters. *Physical Review B* **2009,** *79* (4), 045111.

42. Rockstuhl, C.; Lederer, F.; Etrich, C.; Pertsch, T.; Scharf, T., Design of an Artificial Three-Dimensional Composite Metamaterial with Magnetic Resonances in the Visible Range of the Electromagnetic Spectrum. *Physical Review Letters* **2007,** *99* (1), 017401.

43. Alù, A.; Salandrino, A.; Engheta, N., Negative effective permeability and left-handed materials at optical frequencies. *Opt. Express* **2006,** *14* (4), 1557-1567.

44. Chiu, J. J.; Kim, B. J.; Yi, G.-R.; Bang, J.; Kramer, E. J.; Pine, D. J., Distribution of Nanoparticles in Lamellar Domains of Block Copolymers. *Macromolecules* **2007,** *40* (9), 3361-3365.

45. Schmitt, J.; Decher, G.; Dressick, W. J.; Brandow, S. L.; Geer, R. E.; Shashidhar, R.; Calvert, J. M., Metal nanoparticle/polymer superlattice films: Fabrication and control of layer structure. *Advanced Materials* **1997,** *9* (1), 61-65.

46. Liu, Z.; Lee, H.; Xiong, Y.; Sun, C.; Zhang, X., Far-Field Optical Hyperlens Magnifying Sub-Diffraction-Limited Objects. *Science* **2007,** *315* (5819), 1686.

47. Choi, S. Y.; Mamak, M.; von Freymann, G.; Chopra, N.; Ozin, G. A., Mesoporous Bragg Stack Color Tunable Sensors. *Nano Letters* **2006,** *6* (11), 2456-2461.

48. Sánchez-Sobrado, O.; Lozano, G.; Calvo, M. E.; Sánchez-Iglesias, A.; Liz-Marzán, L. M.; Míguez, H., Interplay of Resonant Cavity Modes with Localized Surface Plasmons: Optical Absorption Properties of Bragg Stacks Integrating Gold Nanoparticles. *Advanced Materials* **2011,** *23* (18), 2108-2112.

49. Simovski, C. R.; Viitanen, A. J.; Tretyakov, S. A., Sub-wavelength resolution in linear arrays of plasmonic particles. *Journal of Applied Physics* **2007,** *101* (12), 123102.

50. Nie; Fava, D.; Rubinstein, M.; Kumacheva, E., "Supramolecular" Assembly of Gold Nanorods End-Terminated with Polymer "Pom-Poms": Effect of Pom-Pom Structure on the Association Modes. *Journal of the American Chemical Society* **2008,** *130* (11), 3683-3689.

51. Nahin, P. J., Maxwell's grand unification. *Spectrum, IEEE* **1992,** *29* (3), 45.

52. Silveirinha, M.; Engheta, N., Design of matched zero-index metamaterials using nonmagnetic inclusions in epsilon-near-zero media. *Physical Review B* **2007,** *75* (7), 075119.

53. Mossotti, O. F., Discussione analitica sull'influenza che l'azione di un mezzo dielettrico ha sulla distribuzione dell'elettricita alla superficie di piu corpi elettrici disseminati in esso. *Memorie di Matematica e di Fisica della Societa Italiana delle Scienze* **1850,** *24* (11).

54. Forfar, D. O., James Clerk Maxwell: his qualities of mind and personality as judged by his contemporaries. *Mathematics Today* **2002,** *38* (3), 20.

55. Bruggeman, D. A., The calculation of various physical constants of heterogeneous substances. I. The dielectric constants and conductivities of mixtures composed of isotropic substances. *Annalen der Physik* **1935,** *24*, 665.

56. Black, M. R.; Lin, Y. M.; Cronin, S. B.; Rabin, O.; Dresselhaus, M. S., Infrared absorption in bismuth nanowires resulting from quantum confinement. *Physical Review B* **2002,** *65* (19), 195417.

57. Bruchez, M.; Moronne, M.; Gin, P.; Weiss, S.; Alivisatos, A. P., Semiconductor Nanocrystals as Fluorescent Biological Labels. *Science* **1998,** *281* (5385), 2013-2016.

58. Hong, S.; Myung, S., Nanotube Electronics: A flexible approach to mobility. *Nat Nano* **2007,** *2* (4), 207-208.

59. Sun, J.; Simon, S. L., The melting behavior of aluminum nanoparticles. *Thermochimica Acta* **2007,** *463* (1–2), 32-40.

60. Chen, M.; Goodman, D. W., Catalytically active gold on ordered titania supports. *Chemical Society Reviews* **2008,** *37* (9), 1860-1870.

61. Yu, H.; Li, J.; Loomis, R. A.; Wang, L.-W.; Buhro, W. E., Two- versus three-dimensional quantum confinement in indium phosphide wires and dots. *Nat Mater* **2003,** *2* (8), 517-520.

62. Ozin, G. A.; Arsenault, A. C., Nanochemistry - A Chemical Approach to Nanomaterials. RSC Publishing, Cambridge (2005).

63. Derjaguin, B. V.; Landau, L., Theory of the Stability of Strongly Charged Lyophobic Sols and of the Adhesion of Strongly Charged Particles in Solutions of Electrolytes. *Acta Phys. Chim. URSS* **1941,** *14*, 633-662.

64. Verwey, E. J. W.; Overbeek, J. T. G., Theory of the stability of lyophobic colloids. Elsevier, Amsterdam (1948).

65. Walker, D. A.; Kowalczyk, B.; de la Cruz, M. O.; Grzybowski, B. A., Electrostatics at the nanoscale. *Nanoscale* **2011,** *3* (4), 1316-1344.

66. Halas, N. J.; Lal, S.; Chang, W.-S.; Link, S.; Nordlander, P., Plasmons in Strongly Coupled Metallic Nanostructures. *Chemical Reviews* **2011,** *111* (6), 3913-3961.

67. Halas, N. J., Plasmonics: An Emerging Field Fostered by Nano Letters. *Nano Letters* **2010,** *10* (10), 3816-3822.

68. Enustun, B. V.; Turkevich, J., Coagulation of Colloidal Gold. *Journal of the American Chemical Society* **1963,** *85* (21), 3317-3328.

69. Kimling, J.; Maier, M.; Okenve, B.; Kotaidis, V.; Ballot, H.; Plech, A., Turkevich Method for Gold Nanoparticle Synthesis Revisited. *The Journal of Physical Chemistry B* **2006,** *110* (32), 15700-15707.

70. P. C. Lee, D. M., Adsorption and Surface-Enhnaced Raman of Dyes on Silver and Gold Sols. *J. Phys. Chem.* **1982,** *86*, 3391-3395.

71. Goulet, P. J. G.; Lennox, R. B., New Insights into Brust−Schiffrin Metal Nanoparticle Synthesis. *Journal of the American Chemical Society* **2010,** *132* (28), 9582-9584.

72. Duraiswamy, S.; Khan, S. A., Plasmonic Nanoshell Synthesis in Microfluidic Composite Foams. *Nano Letters* **2010,** *10* (9), 3757-3763.

73. Sau, T. K.; Murphy, C. J., Room Temperature, High-Yield Synthesis of Multiple Shapes of Gold Nanoparticles in Aqueous Solution. *Journal of the American Chemical Society* **2004,** *126* (28), 8648-8649.

74. Pastoriza-Santos, I.; Liz-Marzán, L. M., Synthesis of Silver Nanoprisms in DMF. *Nano Letters* **2002,** *2* (8), 903-905.

75. Rycenga, M.; Cobley, C. M.; Zeng, J.; Li, W.; Moran, C. H.; Zhang, Q.; Qin, D.; Xia, Y., Controlling the Synthesis and Assembly of Silver Nanostructures for Plasmonic Applications. *Chemical Reviews* **2011,** *111* (6), 3669-3712.

76. Stockman, M. I., Nanoplasmonics: The Physics behind the applications. *Physics Today* **2011,** *64* (2), 39.

77. Kelly, K. L.; Coronado, E.; Zhao, L. L.; Schatz, G. C., The Optical Properties of Metal Nanoparticles: The Influence of Size, Shape, and Dielectric Environment. *The Journal of Physical Chemistry B* **2002,** *107* (3), 668-677.

78. Warren, S. C.; Walker, D. A.; Grzybowski, B. A., Plasmoelectronics: Coupling Plasmonic Excitation with Electron Flow. *Langmuir* **2012**.

79. Gans, R., The shape of ultramicroscopic gold particles. *Ann. Phys.* **1912,** *37*, 881.

80. Wilson, R., The use of gold nanoparticles in diagnostics and detection. *Chemical Society Reviews* **2008,** *37* (9), 2028-2045.

81. Stewart, M. E.; Anderton, C. R.; Thompson, L. B.; Maria, J.; Gray, S. K.; Rogers, J. A.; Nuzzo, R. G., Nanostructured plasmonic sensors. *Chemical Reviews* **2008,** *108* (2), 494-521.

82. Gou, L.; Murphy, C. J., Fine-Tuning the Shape of Gold Nanorods. *Chemistry of Materials* **2005,** *17* (14), 3668-3672.

83. Brioude, A.; Jiang, X. C.; Pileni, M. P., Optical Properties of Gold Nanorods: DDA Simulations Supported by Experiments. *The Journal of Physical Chemistry B* **2005,** *109* (27), 13138-13142.

84. Wu, H.-Y.; Huang, W.-L.; Huang, M. H., Direct High-Yield Synthesis of High Aspect Ratio Gold Nanorods. *Crystal Growth & Design* **2007,** *7* (4), 831-835.

85. Garcia, G.; Buonsanti, R.; Runnerstrom, E. L.; Mendelsberg, R. J.; Llordes, A.; Anders, A.; Richardson, T. J.; Milliron, D. J., Dynamically Modulating the Surface Plasmon Resonance of Doped Semiconductor Nanocrystals. *Nano Letters* **2011,** *11* (10), 4415-4420.

86. Gai, P. L.; Harmer, M. A., Surface Atomic Defect Structures and Growth of Gold Nanorods. *Nano Letters* **2002,** *2* (7), 771-774.

87. Pecharroman, C.; Perez-Juste, J.; Mata-Osoro, G.; Liz-Marzan, L. M.; Mulvaney, P., Redshift of surface plasmon modes of small gold rods due to their atomic roughness and end-cap geometry. *Physical Review B (Condensed Matter and Materials Physics)* **2008,** *77* (3), 035418.

88. Nie, S.; Emory, S. R., Probing Single Molecules and Single Nanoparticles by Surface-Enhanced Raman Scattering. *Science* **1997,** *275* (5303), 1102-1106.

89. Chang, W.-S.; Willingham, B.; Slaughter, L. S.; Dominguez-Medina, S.; Swanglap, P.; Link, S., Radiative and Nonradiative Properties of Single Plasmonic Nanoparticles and Their Assemblies. *Accounts of Chemical Research* **2012**.

90. Dreaden, E. C.; Mackey, M. A.; Huang, X.; Kang, B.; El-Sayed, M. A., Beating cancer in multiple ways using nanogold. *Chemical Society Reviews* **2011,** *40* (7), 3391-3404.

91. Prodan, E.; Radloff, C.; Halas, N. J.; Nordlander, P., A Hybridization Model for the Plasmon Response of Complex Nanostructures. *Science* **2003,** *302* (5644), 419-422.

92. Zeng, X., 3D Ordered Gold Strings by Coating Nanoparticles with Mesogens. *Adv. Mater.* **2009,** *21*, 1746.

93. Qi, H.; Lepp, A.; Heiney, P. A.; Hegmann, T., Effects of hydrophilic and hydrophobic gold nanoclusters on the stability and ordering of bolaamphiphilic liquid crystals. *Journal of Materials Chemistry* **2007,** *17* (20), 2139-2144.

94. Pratibha, R.; Park, W.; Smalyukh, I. I., Colloidal gold nanosphere dispersions in smectic liquid crystals and thin nanoparticle-decorated smectic films. *Journal of Applied Physics* **2010,** *107* (6), 063511.

95. Alivisatos, A. P.; Johnsson, K. P.; Peng, X.; Wilson, T. E.; Loweth, C. J.; Bruchez, M. P.; Schultz, P. G., Organization of 'nanocrystal molecules' using DNA. *Nature* **1996,** *382* (6592), 609-611.

96. Chen, C.-L.; Zhang, P.; Rosi, N. L., A New Peptide-Based Method for the Design and Synthesis of Nanoparticle Superstructures: Construction of Highly Ordered Gold Nanoparticle Double Helices. *Journal of the American Chemical Society* **2008,** *130* (41), 13555-13557.

97. Lim, D. D.-K., Nanogap-engineerable Raman-active nanodumbbells for single-molecule detection. *Nature Materials* **2010,** *9* (1), 60.

98. Jain, P. K.; Eustis, S.; El-Sayed, M. A., Plasmon Coupling in Nanorod Assemblies:â€‰ Optical Absorption, Discrete Dipole Approximation Simulation, and Exciton-Coupling Model. *The Journal of Physical Chemistry B* **2006,** *110* (37), 18243-18253.

99. Shevchenko, E. V.; Talapin, D. V.; Kotov, N. A.; O'Brien, S.; Murray, C. B., Structural diversity in binary nanoparticle superlattices. Nature Publishing Group: 2006; Vol. 439, pp 55-59.

100. Wang, X.; Li, G.; Chen, T.; Yang, M.; Zhang, Z.; Wu, T.; Chen, H., Polymer-Encapsulated Gold-Nanoparticle Dimers: Facile Preparation and Catalytical Application in Guided Growth of Dimeric ZnO-Nanowires. *Nano Letters* **2008,** *8* (9), 2643-2647.

101. Shalkevich, N.; Shalkevich, A.; Si-Ahmed, L.; Burgi, T., Reversible formation of gold nanoparticle-surfactant composite assemblies for the preparation of concentrated colloidal solutions. *Physical Chemistry Chemical Physics* **2009,** *11* (43), 10175-10179.

102. Dintinger, J.; Mühlig, S.; Rockstuhl, C.; Scharf, T., A bottom-up approach to fabricate optical metamaterials by self-assembled metallic nanoparticles. *Opt. Mater. Express* **2012,** *2* (3), 269-278.

103. Lee, J. H.; Wu, Q.; Park, W., Metal nanocluster metamaterial fabricated by the colloidal self-assembly. *Opt. Lett.* **2009,** *34* (4), 443-445.

104. Fleischmann, M.; Hendra, P. J.; McQuillan, A. J., Raman spectra of pyridine adsorbed at a silver electrode. *Chemical Physics Letters* **1974,** *26* (2), 163-166.

105. Souza, G. R.; Levin, C. S.; Hajitou, A.; Pasqualini, R.; Arap, W.; Miller, J. H., In Vivo Detection of Gold−Imidazole Self-Assembly Complexes: NIR-SERS Signal Reporters. *Analytical Chemistry* **2006,** *78* (17), 6232-6237.

106. Romo-Herrera, J. M.; Alvarez-Puebla, R. A.; Liz-Marzan, L. M., Controlled assembly of plasmonic colloidal nanoparticle clusters. *Nanoscale* **2011**.

107. Jin, R., Nanoparticle Clusters Light Up in SERS. *Angewandte Chemie International Edition 49* (16), 2826-2829.

108. Yan, B.; Boriskina, S. V.; Reinhard, B. M., Design and Implementation of Noble Metal Nanoparticle Cluster Arrays for Plasmon Enhanced Biosensing. *The Journal of Physical Chemistry C* **2011,** *115* (50), 24437-24453.

109. Page Faulk, W.; Malcolm Taylor, G., Communication to the editors: An immunocolloid method for the electron microscope. *Immunochemistry* **1971,** *8* (11), 1081-1083.

110. Boisselier, E.; Salmon, L.; Ruiz, J.; Astruc, D., How to very efficiently functionalize gold nanoparticles by "click" chemistry. *Chemical Communications* **2008,** (44), 5788-5790.

111. Sperling, R. A.; Gil, P. R.; Zhang, F.; Zanella, M.; Parak, W. J., Biological applications of gold nanoparticles. *Chemical Society Reviews* **2008,** *37* (9), 1896-1908.

112. Wei, Q.; Ji, J.; Shen, J., Synthesis of Near-Infrared Responsive Gold Nanorod/PNIPAAm Core/Shell Nanohybrids via Surface Initiated ATRP for Smart Drug Delivery. *Macromolecular Rapid Communications* **2008,** *29*, 645-650.

113. Giljohann, D. A.; Seferos, D. S.; Daniel, W. L.; Massich, M. D.; Patel, P. C.; Mirkin, C. A., Gold Nanoparticles for Biology and Medicine. *Angewandte Chemie International Edition* **2010,** *49* (19), 3280-3294.

114. Sonnichsen, C.; Reinhard, B. M.; Liphardt, J.; Alivisatos, A. P., A molecular ruler based on plasmon coupling of single gold and silver nanoparticles. *Nat Biotech* **2005,** *23* (6), 741-745.

115. Adleman, J. R.; Boyd, D. A.; Goodwin, D. G.; Psaltis, D., Heterogenous Catalysis Mediated by Plasmon Heating. *Nano Letters* **2009,** *9* (12), 4417-4423.

116. Nabika, H.; Takase, M.; Nagasawa, F.; Murakoshi, K., Toward Plasmon-Induced Photoexcitation of Molecules. *The Journal of Physical Chemistry Letters* **2010,** *1* (16), 2470-2487.

117. Chen, C. J.; Osgood, R. M., Direct Observation of the Local-Field-Enhanced Surface Photochemical Reactions. *Physical Review Letters* **1983,** *50* (21), 1705-1708.

118. Arakawa, T.; Munaoka, T.; Akiyama, T.; Yamada, S., Effects of Silver Nanoparticles on Photoelectrochemical Responses of Organic Dyes†. *The Journal of Physical Chemistry C* **2009,** *113* (27), 11830-11835.

119. Leroueil, P. R.; Hong, S.; Mecke, A.; Baker, J. R.; Orr, B. G.; Banaszak Holl, M. M., Nanoparticle Interaction with Biological Membranes: Does Nanotechnology Present a Janus Face? *Accounts of Chemical Research* **2007,** *40* (5), 335-342.

120. Gill, S.; benberg, R.; Ku, T.; Azarmi, S.; Roa, W.; Prenner, E. J., Nanoparticles: Characteristics, Mechanisms of Action, and Toxicity in Pulmonary Drug DeliveryA Review. *Journal of Biomedical Nanotechnology* **2007,** *3* (2), 107-119.

121. Fiorito, S.; Serafino, A.; Andreola, F.; Togna, A.; Togna, G., Toxicity and Biocompatibility of Carbon Nanoparticles. *Journal of Nanoscience and Nanotechnology* **2006,** *6* (3), 591-599.

122. Lewinski, N.; Colvin, V.; Drezek, R., Cytotoxicity of Nanoparticles. *Small* **2008,** *4* (1), 26-49.

123. Decher, G., Fuzzy Nanoassemblies: Toward Layered Polymeric Multicomposites. *Science* **1997,** *277* (5330), 1232-1237.

124. Yu, J.; Rance, G. A.; Khlobystov, A. N., Electrostatic interactions for directed assembly of nanostructured materials: composites of titanium dioxide nanotubes with gold nanoparticles. *Journal of Materials Chemistry* **2009,** *19* (47), 8928-8935.

125. Iler, R. K., Multilayers of colloidal particles. *Journal of Colloid and Interface Science* **1966,** *21* (6), 569-594.

126. Chen, X.; Lenhert, S.; Hirtz, M.; Lu, N.; Fuchs, H.; Chi, L., Langmuir–Blodgett Patterning: A Bottom–Up Way To Build Mesostructures over Large Areas. *Accounts of Chemical Research* **2007,** *40* (6), 393-401.

127. Lavalle, P.; Voegel, J.-C.; Vautier, D.; Senger, B.; Schaaf, P.; Ball, V., Dynamic Aspects of Films Prepared by a Sequential Deposition of Species: Perspectives for Smart and Responsive Materials. *Advanced Materials* **2011,** *23* (10), 1191-1221.

128. Tronin, A., Ellipsometry and x-ray reflectometry characterization of self-assembly process of polystyrensulfonate and polyallylamine. *Colloid Polym. Sci.* **1994,** *272*, 1317-1321.

129. Elbert, D. L.; Herbert, C. B.; Hubbell, J. A., Thin Polymer Layers Formed by Polyelectrolyte Multilayer Techniques on Biological Surfaces. *Langmuir* **1999,** *15* (16), 5355-5362.

130. Iler, R. K., The Chemistry of Silica: Solubility, Polymerization, Colloid and Surfae Properties and the Biochemistry. John Wiley and Sons, Inc., New York (1979).

131. Serizawa, T.; Yamaguchi, M.; Matsuyama, T.; Akashi, M., Alternating Bioactivity of Polymeric Layer-by-Layer Assemblies: Anti- vs Procoagulation of Human Blood on Chitosan and Dextran Sulfate Layers. *Biomacromolecules* **2000,** *1* (3), 306-309.

132. Lvov, Y.; Ariga, K.; Onda, M.; Ichinose, I.; Kunitake, T., A careful examination of the adsorption step in the alternate layer-by-layer assembly of linear polyanion and polycation. *Colloids and Surfaces A: Physicochemical and Engineering Aspects* **1999,** *146* (1–3), 337-346.

133. Nolte, A. J.; Takane, N.; Hindman, E.; Gaynor, W.; Rubner, M. F.; Cohen, R. E., Thin Film Thickness Gradients and Spatial Patterning via Salt Etching of Polyelectrolyte Multilayers. *Macromolecules* **2007,** *40* (15), 5479-5486.

134. Harris, J. J.; DeRose, P. M.; Bruening, M. L., Synthesis of Passivating, Nylon-Like Coatings through Cross-Linking of Ultrathin Polyelectrolyte Films. *Journal of the American Chemical Society* **1999,** *121* (9), 1978-1979.

135. Richert, L.; Boulmedais, F.; Lavalle, P.; Mutterer, J.; Ferreux, E.; Decher, G.; Schaaf, P.; Voegel, J.-C.; Picart, C., Improvement of Stability and Cell Adhesion Properties of Polyelectrolyte Multilayer Films by Chemical Cross-Linking. *Biomacromolecules* **2003,** *5* (2), 284-294.

136. Chiarelli, P. A.; Johal, M. S.; Holmes, D. J.; Casson, J. L.; Robinson, J. M.; Wang, H.-L., Polyelectrolyte Spin-Assembly. *Langmuir* **2001,** *18* (1), 168-173.

137. Izquierdo, A.; Ono, S. S.; Voegel, J. C.; Schaaf, P.; Decher, G., Dipping versus Spraying: Exploring the Deposition Conditions for Speeding Up Layer-by-Layer Assembly. *Langmuir* **2005,** *21* (16), 7558-7567.

138. Kharlampieva, E.; Kozlovskaya, V.; Chan, J.; Ankner, J. F.; Tsukruk, V. V., Spin-Assisted Layer-by-Layer Assembly: Variation of Stratification as Studied with Neutron Reflectivity†. *Langmuir* **2009,** *25* (24), 14017-14024.

139. Félix, O.; Zheng, Z.; Cousin, F.; Decher, G., Are sprayed LbL-films stratified? A first assessment of the nanostructure of spray-assembled multilayers by neutron reflectometry. *Comptes Rendus Chimie* **2009,** *12* (1–2), 225-234.

140. Wang, X.; Kim, H. J.; Xu, P.; Matsumoto, A.; Kaplan, D. L., Biomaterial Coatings by Stepwise Deposition of Silk Fibroin. *Langmuir* **2005,** *21* (24), 11335-11341.

141. Schmitt, J.; Gruenewald, T.; Decher, G.; Pershan, P. S.; Kjaer, K.; Loesche, M., Internal structure of layer-by-layer adsorbed polyelectrolyte films: a neutron and x-ray reflectivity study. *Macromolecules* **1993,** *26* (25), 7058-7063.

142. Sukhorukov, G. B.; Rogach, A. L.; Zebli, B.; Liedl, T.; Skirtach, A. G.; Köhler, K.; Antipov, A. A.; Gaponik, N.; Susha, A. S.; Winterhalter, M.; Parak, W. J., Nanoengineered Polymer Capsules: Tools for Detection, Controlled Delivery, and Site-Specific Manipulation. *Small* **2005,** *1* (2), 194-200.

143. Eckle, M.; Decher, G., Tuning the Performance of Layer-by-Layer Assembled Organic Light Emitting Diodes by Controlling the Position of Isolating Clay Barrier Sheets. *Nano Letters* **2001,** *1* (1), 45-49.

144. Agrios, A. G.; Cesar, I.; Comte, P.; Nazeeruddin, M. K.; Grätzel, M., Nanostructured Composite Films for Dye-Sensitized Solar Cells by Electrostatic Layer-by-Layer Deposition. *Chemistry of Materials* **2006,** *18* (23), 5395-5397.

145. Adusumilli, M.; Bruening, M. L., Variation of Ion-Exchange Capacity, ζ Potential, and Ion-Transport Selectivities with the Number of Layers in a Multilayer Polyelectrolyte Film. *Langmuir* **2009,** *25* (13), 7478-7485.

146. Podsiadlo, P.; Shim, B. S.; Kotov, N. A., Polymer/clay and polymer/carbon nanotube hybrid organic–inorganic multilayered composites made by sequential layering of nanometer scale films. *Coordination Chemistry Reviews* **2009,** *253* (23–24), 2835-2851.

147. Koenig, J.-F.; Martel, D., Applying UV–Vis spectroscopy to step-by-step molecular self assembly on surface: Does it bring pertinent information? *Thin Solid Films* **2008,** *516* (12), 3865-3872.

148. Castelnovo, M.; Joanny, J.-F., Formation of Polyelectrolyte Multilayers. *Langmuir* **2000,** *16* (19), 7524-7532.

149. Shafir, A.; Andelman, D., Polyelectrolyte multilayer formation: Electrostatics and short-range interactions. *The European Physical Journal E: Soft Matter and Biological Physics* **2006,** *19* (2), 155-162.

150. de Paula, A. L.; Barroso, J. J.; Rezende, M. C. In *Modified Nicolson-Ross-Weir (NRW) method to retrieve the constitutive parameters of low-loss materials*, Microwave & Optoelectronics Conference (IMOC), 2011 SBMO/IEEE MTT-S International, Oct. 29 2011-Nov. 1 2011; 2011; pp 488-492.

151. Smith, D. R.; Schultz, S.; Markoš, P.; Soukoulis, C. M., Determination of effective permittivity and permeability of metamaterials from reflection and transmission coefficients. *Physical Review B* **2002,** *65* (19), 195104.

152. Cunningham, A.; Mühlig, S.; Rockstuhl, C.; Bürgi, T., Exciting Bright and Dark Eigenmodes in Strongly Coupled Asymmetric Metallic Nanoparticle Arrays. *The Journal of Physical Chemistry C* **2012,** *116* (33), 17746-17752.

153. Huang, X.; Neretina, S.; El-Sayed, M. A., Gold Nanorods: From Synthesis and Properties to Biological and Biomedical Applications. *Advanced Materials* **2009,** *21* (48), 4880-4910.

154. Nikoobakht, B.; El-Sayed, M. A., Preparation and Growth Mechanism of Gold Nanorods (NRs) Using Seed-Mediated Growth Method. *Chemistry of Materials* **2003,** *15* (10), 1957-1962.

155. Ono, S. S.; Decher, G., Preparation of Ultrathin Self-Standing Polyelectrolyte Multilayer Membranes at Physiological Conditions Using pH-Responsive Film Segments as Sacrificial Layers. *Nano Letters* **2006,** *6* (4), 592-598.

156. Helgert, C.; Rockstuhl, C.; Etrich, C.; Menzel, C.; Kley, E. B.; Tünnermann, A.; Lederer, F.; Pertsch, T., Effective properties of amorphous metamaterials. *Physical Review B* **2009,** *79* (23), 233107.

157. Kao, J.; Bai, P.; Chuang, V. P.; Jiang, Z.; Ercius, P.; Xu, T., Nanoparticle Assemblies in Thin Films of Supramolecular Nanocomposites. *Nano Letters* **2012**.

158. Feng, Z.; Yan, F., Preparation and tribological studies of nanocomposite films fabricated using spin-assisted layer-by-layer assembly. *Surface and Coatings Technology* **2008,** *202* (14), 3290-3297.

159. Feng, Z.; Yan, F., Preparation and resistivity study of silver nanocomposite films using spin-assisted layer-by-layer assembly. *Surface and Interface Analysis* **2008,** *40* (12), 1523-1528.

160. Cunningham, A.; Mühlig, S.; Rockstuhl, C.; Bürgi, T., Coupling of Plasmon Resonances in Tunable Layered Arrays of Gold Nanoparticles. *The Journal of Physical Chemistry C* **2011,** *115* (18), 8955-8960.

161. Talbot, J.; Tarjus, G.; Van Tassel, P. R.; Viot, P., From car parking to protein adsorption: an overview of sequential adsorption processes. *Colloids and Surfaces A: Physicochemical and Engineering Aspects* **2000,** *165* (1–3), 287-324.

162. Ulrich, S.; Stoll, S.; Pefferkorn, E., Computer Simulations of Homogeneous Deposition of Liquid Droplets. *Langmuir* **2004,** *20* (5), 1763-1771.

163. Tarjus, G.; Schaaf, P.; Talbot, J., Generalized random sequential adsorption. *The Journal of Chemical Physics* **1990,** *93* (11), 8352-8360.

164. Carl, P.; Schaaf, P.; Voegel, J. C.; Stoltz, J. F.; Adamczyk, Z.; Senger, B., Deposition Kinetics of Particles at a Solid Surface Governed by the Ballistic Deposition Model. *Langmuir* **1998,** *14* (25), 7267-7270.

165. Abràmoff, M. D.; Magalhães, P. J.; Ram, S. J., Image Processing with ImageJ. *Biophotonics International* **2004,** *7*, 7.

166. Jiang, L.; Sun, Y.; Nowak, C.; Kibrom, A.; Zou, C.; Ma, J.; Fuchs, H.; Li, S.; Chi, L.; Chen, X., Patterning of Plasmonic Nanoparticles into Multiplexed One-Dimensional Arrays Based on Spatially Modulated Electrostatic Potential. *ACS Nano* **2011,** *5* (10), 8288-8294.

167. Love, J. C.; Estroff, L. A.; Kriebel, J. K.; Nuzzo, R. G.; Whitesides, G. M., Self-Assembled Monolayers of Thiolates on Metals as a Form of Nanotechnology. *Chemical Reviews* **2005,** *105* (4), 1103-1170.

168. Sato David Brown, T.; F. G. Johnson, B., Nucleation and growth of nano-gold colloidal lattices. *Chemical Communications* **1997,** (11), 1007-1008.

169. Schauer, C. L.; Chen, M.-S.; Chatterley, M.; Eisemann, K.; Welsh, E. R.; Price, R. R.; Schoen, P. E.; Ligler, F. S., Color changes in chitosan and poly(allyl amine) films upon metal binding. *Thin Solid Films* **2003,** *434* (1–2), 250-257.

170. www.lookchem.com/SODIUM-POLYSTYRENE-SULFONATE/#Chemistry, 4th October 2012.

171. Okamoto, T. (2001). Near-Field Spectral Analysis of Metallic Beads. In S. Kawata, *Near-Field Optics and Surface Plasmon Polaritons* (pp. 97-123). Heidelberg: Springer-Verlag Berlin Heidelberg New York.

172. Christ, A.; Martin, O. J. F.; Ekinci, Y.; Gippius, N. A.; Tikhodeev, S. G., Symmetry Breaking in a Plasmonic Metamaterial at Optical Wavelength. *Nano Letters* **2008,** *8* (8), 2171-2175.

173. Peña-Rodríguez, O.; Pal, U.; Campoy-Quiles, M.; Rodríguez-Fernández, L.; Garriga, M.; Alonso, M. I., Enhanced Fano Resonance in Asymmetrical Au:Ag Heterodimers. *The Journal of Physical Chemistry C* **2011**, null-null.

174. Bachelier, G.; Russier-Antoine, I.; Benichou, E.; Jonin, C.; Del Fatti, N.; Vallée, F.; Brevet, P. F., Fano Profiles Induced by Near-Field Coupling in Heterogeneous Dimers of Gold and Silver Nanoparticles. *Physical Review Letters* **2008,** *101* (19), 197401.

175. Encina, E. R.; Coronado, E. A., On the Far Field Optical Properties of Ag−Au Nanosphere Pairs. *The Journal of Physical Chemistry C* **2010,** *114* (39), 16278-16284.

176. Brown, L. V.; Sobhani, H.; Lassiter, J. B.; Nordlander, P.; Halas, N. J., Heterodimers: Plasmonic Properties of Mismatched Nanoparticle Pairs. *ACS Nano* **2010,** *4* (2), 819-832.

177. Sheikholeslami, S.; Jun, Y.-w.; Jain, P. K.; Alivisatos, A. P., Coupling of Optical Resonances in a Compositionally Asymmetric Plasmonic Nanoparticle Dimer. *Nano Letters 10* (7), 2655-2660.

178. Shegai, T.; Chen, S.; Miljkovic, V. D.; Zengin, G.; Johansson, P.; Kall, M., A bimetallic nanoantenna for directional colour routing. *Nat Commun* **2011,** *2*, 481.

179. Bidault, S.; García de Abajo, F. J.; Polman, A., Plasmon-Based Nanolenses Assembled on a Well-Defined DNA Template. *Journal of the American Chemical Society* **2008,** *130* (9), 2750-2751.

180. Joseph, V.; Gensler, M.; Seifert, S.; Gernert, U.; Rabe, J. P.; Kneipp, J., Nanoscopic Properties and Application of Mix-and-Match Plasmonic Surfaces for Microscopic SERS. *The Journal of Physical Chemistry C* **2012,** *116* (12), 6859-6865.

181. Zhou, J.; Ellis, A. V.; Voelcker, N. H., Recent developments in PDMS surface modification for microfluidic devices. *ELECTROPHORESIS* **2010,** *31* (1), 2-16.

182. Correa-Duarte, M.; Salgueiriño-Maceira, V.; Rinaldi, A.; Sieradzki, K.; Giersig, M.; Liz-Marzán, L., Optical strain detectors based on gold/elastomer nanoparticulated films. *Gold Bulletin* **2007,** *40* (1), 6-14.

183. Lu, G.; Li, H.; Zhang, H., Nanoparticle-coated PDMS elastomers for enhancement of Raman scattering. *Chemical Communications* **2011,** *47* (30), 8560-8562.

184. Wang, A.-J.; Xu, J.-J.; Zhang, Q.; Chen, H.-Y., The use of poly(dimethylsiloxane) surface modification with gold nanoparticles for the microchip electrophoresis. *Talanta* **2006,** *69* (1), 210-215.

185. Qing, Z. Z.; Zhang Qing, Z. Z., In-situ synthesis of poly(dimethylsiloxane)-gold nanoparticles composite films and its application in microfluidic systems. *Lab on a chip* **2008,** *8* (2), 352.

186. Antipov, A. A.; Sukhorukov, G. B.; Leporatti, S.; Radtchenko, I. L.; Donath, E.; Möhwald, H., Polyelectrolyte multilayer capsule permeability control. *Colloids and Surfaces A: Physicochemical and Engineering Aspects* **2002,** *198–200* (0), 535-541.

187. Liu, N.; Guo, H.; Fu, L.; Kaiser, S.; Schweizer, H.; Giessen, H., Plasmon Hybridization in Stacked Cut-Wire Metamaterials. *Advanced Materials* **2007,** *19* (21), 3628-3632.

188. Yonemura, H.; Suyama, J.; Arakawa, T.; Yamada, S., Organization of gold nanorods on a substrate using a strong magnetic field. *Thin Solid Films* **2009,** *518* (2), 668-673.

189. Enkrich, C.; Wegener, M.; Linden, S.; Burger, S.; Zschiedrich, L.; Schmidt, F.; Zhou, J. F.; Koschny, T.; Soukoulis, C. M., Magnetic Metamaterials at Telecommunication and Visible Frequencies. *Physical Review Letters* **2005,** *95* (20), 203901.

190. (a) Pendry, J. B., Negative Refraction Makes a Perfect Lens. *Physical Review Letters* **2000,** *85* (18), 3966-3969; (b) Leonhardt, U.; Philbin, T. G., Transformation Optics and the Geometry of Light. In Wolf E. (ed) Progress in Optics, 1st edn. Elsevier, Amsterdam (2009).

191. Caruso, F.; Spasova, M.; Salgueiriño-Maceira, V.; Liz-Marzán, L. M., Multilayer Assemblies of Silica-Encapsulated Gold Nanoparticles on Decomposable Colloid Templates. *Advanced Materials* **2001,** *13* (14), 1090-1094.

192. Schneider, G. g. F.; Decher, G., From “Nano-bags” to “Micro-pouches”. Understanding and Tweaking Flocculation-based Processes for the Preparation of New Nanoparticle-Composites. *Nano Letters* **2008,** *8* (11), 3598-3604.

193. Fan, J. A.; Wu, C.; Bao, K.; Bao, J.; Bardhan, R.; Halas, N. J.; Manoharan, V. N.; Nordlander, P.; Shvets, G.; Capasso, F., Self-Assembled Plasmonic Nanoparticle Clusters. *Science* **2010,** *328* (5982), 1135-1138.

194. Sadtler, B.; Wei, A., Spherical ensembles of gold nanoparticles on silica: electrostatic and size effects. *Chemical Communications* **2002,** (15), 1604-1605.

195. Pastoriza-Santos, I.; Gomez, D.; Perez-Juste, J.; Liz-Marzan, L. M.; Mulvaney, P., Optical properties of metal nanoparticle coated silica spheres: a simple effective medium approach. *Physical Chemistry Chemical Physics* **2004,** *6* (21), 5056-5060.

196. Mühlig, S.; Cunningham, A.; Scheeler, S.; Pacholski, C.; Bürgi, T.; Rockstuhl, C.; Lederer, F., Self-Assembled Plasmonic Core–Shell Clusters with an Isotropic Magnetic Dipole Response in the Visible Range. *ACS Nano* **2011,** *5* (8), 6586-6592.

197. Pendry, J. B.; Schurig, D.; Smith, D. R., Controlling Electromagnetic Fields. *Science* **2006,** *312* (5781), 1780-1782.

198. Schurig, D.; Mock, J. J.; Justice, B. J.; Cummer, S. A.; Pendry, J. B.; Starr, A. F.; Smith, D. R., Metamaterial Electromagnetic Cloak at Microwave Frequencies. *Science* **2006,** *314* (5801), 977-980.

199. Li, J.; Pendry, J. B., Hiding under the Carpet: A New Strategy for Cloaking. *Physical Review Letters* **2008,** *101* (20), 203901.

200. Fischer, J.; Ergin, T.; Wegener, M., Three-dimensional polarization-independent visible-frequency carpet invisibility cloak. *Opt. Lett.* **2011,** *36* (11), 2059-2061.

201. Alù, A.; Engheta, N., Achieving transparency with plasmonic and metamaterial coatings. *Physical Review E* **2005,** *72* (1), 016623.

202. Edwards, B.; Alù, A.; Silveirinha, M. G.; Engheta, N., Experimental Verification of Plasmonic Cloaking at Microwave Frequencies with Metamaterials. *Physical Review Letters* **2009,** *103* (15), 153901.

203. Guzatov, D. V.; Vaschenko, S. V.; Stankevich, V. V.; Lunevich, A. Y.; Glukhov, Y. F.; Gaponenko, S. V., Plasmonic Enhancement of Molecular Fluorescence near Silver Nanoparticles: Theory, Modeling, and Experiment. *The Journal of Physical Chemistry C* **2012,** *116* (19), 10723-10733.

204. Zhang, R. R.; Wang, Z. Z.; Song, C. C.; Yang, J. J.; Sadaf, A. A.; Cui, Y. Y.; Zhang Ruohu, Y. Y., Immunoassays Based on Surface-Enhanced Fluorescence using Gap-Plasmon-Tunable Ag Bilayer Nanoparticle Films. *Journal of fluorescence* **2012**.

205. Li, K.; Stockman, M. I.; Bergman, D. J., Self-Similar Chain of Metal Nanospheres as an Efficient Nanolens. *Physical Review Letters* **2003,** *91* (22), 227402.

206. Lidorikis, E.; Egusa, S.; Joannopoulos, J. D., Effective medium properties and photonic crystal superstructures of metallic nanoparticle arrays. *Journal of Applied Physics* **2007,** *101* (5), 054304.

207. Yannopapas, V.; Psarobas, I. E., Lasing action in multilayers of alternating monolayers of metallic nanoparticles and dielectric slabs with gain. *Journal of Optics* **2012,** *14* (3), 035101.

208. Manners, I., Poly(ferrocenylsilanes): novel organometallic plastics. *Chemical Communications* **1999,** (10), 857-865.

209. Kulbaba, K.; Cheng, A.; Bartole, A.; Greenberg, S.; Resendes, R.; Coombs, N.; Safa-Sefat, A.; Greedan, J. E.; Stöver, H. D. H.; Ozin, G. A.; Manners, I., Polyferrocenylsilane Microspheres: Synthesis, Mechanism of Formation, Size and Charge Tunability, Electrostatic Self-Assembly, and Pyrolysis to Spherical Magnetic Ceramic Particles. *Journal of the American Chemical Society* **2002,** *124* (42), 12522-12534.

210. Zijlstra, P.; Chon, J. W. M.; Gu, M., Five-dimensional optical recording mediated by surface plasmons in gold nanorods. *Nature* **2009,** *459* (7245), 410-413.